EFFECTS OF PARTICLE SIZE, SHAPE AND DENSITY ON THE PERFORMANCE OF AN AIR FLUIDIZED BED IN DRY COAL BENEFECIATION

Pheneas Chikerema

A dissertation submitted to the Faculty of Engineering and the Built Environment, University of the Witwatersrand, in fulfillment of the requirements for the Master of Science degree in Engineering.

Johannesburg, 2011

Statement of Originality

I hereby certify that the work embodied in this thesis is the result of original research and has not been submitted for another degree at any other university or institution.

Signed: ………………….

Pheneas Chikerema

Date .... the day of ………………… 2011

Abstract

Most of the remaining coalfields in South Africa are found in arid areas where process water is scarce and given the need to fully exploit all the coal reserves in the country, this presents a great challenge to the coal processing industry. Hence, the need to consider the implementation of dry coal beneficiation methods as the industry cannot continue relying on the conventional wet processing methods such as heavy medium separation. Dry coal beneficiation with an air dense-medium fluidized bed is one of the dry coal processing methods that have proved to be an efficient separation method with separation efficiencies comparable those of the wet heavy medium separation process.

Although the applications of the fluidized bed dry coal separator have been done successfully on an industrial scale, the process has been characterized by relatively poor (Ecart Probable Moyen), Ep values owing to complex hydrodynamics of these systems. Hence, the main objectives of this study is to develop a sound understanding of the key process parameters which govern the kinetics of coal and shale separation in an air fluidized bed focusing on the effect of the particle size, shape and density on the performance of the fluidized separator as well as developing a simple rise/settling velocity empirical model which can be used to predict the quality of separation.

As part of this study, a (40 x 40x 60) cm air fluidized bed was designed and constructed for the laboratory tests. A relatively uniform and stable average bed density of 1.64 with STDEV < 0.01 g/cm^3 was achieved using a mixture of silica and magnetite as the fluidizing media. Different particle size ranges which varied from (+9.5 -16mm), (+16 -22mm), (+22 -31.5mm) and (+37 -53mm) were used for the detailed separation tests. In order to investigate the effect of the particle shape, only three different particle shapes were used namely blockish (+16 -22mm Blk), flat (+16 -22mm FB) and sharp pointed prism particles (+16 – 22mm SR).Different techniques were developed for measuring the rise and settling velocities of the particles in the bed.

The Klima and Luckie partition model (1989) was used to analyze the partition data for the different particles and high R^2 values ranging from (0.9210 - 0.9992) were recorded. Average Ep

values as low as 0.05 were recorded for the separation of (+37 -53mm) and (+22 -31.5mm) particles under steady state conditions with minimum fluctuation of the cut density. On the other hand, the separation of the (+16 -22mm) and (+9.5 – 16mm) particles was characterized by relatively high average Ep values of 0.07 and 0.11 respectively. However the continuous fluctuation or shift of the cut density for the (+9.5 -16mm) made it difficult to efficiently separate the particles. Although, particle shape is a difficult parameter to control, the different separation trends that were observed for the (+16 -22mm) particles of different shapes indicate that particle shape has got a significant effect on the separation performance of the particles in the air fluidized bed.

A simple empirical model which can be used to predict the rise/settling velocities or respective positions of the different particles in the air fluidized bed was developed based on the Stokes' law. The proposed empirical model fitted the rise/settling data for the different particle size ranges very well with R^2 values varying from 0.8672 to 0.9935. Validation of the empirical model indicate that the model can be used to accurately predict the rise/settling velocities or respective positions for all the other particles sizes ranges except for the (+9.5 – 16mm) particles where a relatively high average % error of (21.37%) was recorded.

The (+37 -53mm) and (+22 -31.5mm) particles separated faster and more efficiently than the (+16 -22mm) and (+9.5 -16mm) particles. However, the separation efficiency of the particles can be further improved by using deeper beds (bed height > 40cm) with relatively uniform and stable bed densities. Prescreening of the coal particles into relatively narrow ranges is important in the optimization of dry coal beneficiation using an air fluidized bed since different optimum operating conditions are required for the efficient separation of the different particle size ranges and shapes. The accuracy and the practical applicability of the proposed empirical model can be further improved by carrying out some detailed rise/settling tests using more accurate and precise equipment such as the gamma camera to track the motion of the particles in the fluidized bed as well as measuring the actual bed viscosity and incorporate it in the model.

Acknowledgements

Firstly, I would like to express my sincere gratitude to my project supervisor, Professor M. H. Moys for his inspired supervision and guidance in the project, a big thank you.

I would also like to thank CoalTech Research Association for the financial support and taking me on the trip to China, that was an eye opener and it will certainly go a long way both in my professional development and the implementation of dry coal beneficiation systems in South Africa.

To all the members of Prof Moys' Mineral Processing Research group, thank you for always being cheerful! It has been a great fun having you around. Meanwhile, a special mention goes to Dr Murray Bwayla for his helpful suggestions and numerous corrections which helped to shape up this thesis report, thank you so much.

Most importantly, to my parents and other family members, thank you so much for the patience and understanding, you have always been there for me.

Last but not least, I would like to thank all my friends Clayton, Taona, Gwiranai, Murehwa and Tirivaviri for the emotional and moral support you gave me throughout this project.

Table of Contents

Table of Figures

List of Tables

“Relatively small velocities were recorded during the rise/settling tests, hence the results were expressed in cm/s instead of the SI units.”

Chapter 1

Introduction

1.1 Background of dry coal beneficiation in South Africa

In recent years, South Africa, one of the top coal producers in the world has witnessed a significant increase in the demand for coal mainly due to the expansion of the country's economy and export markets, thereby raising alarms on the need to expand both the coal mining and processing operations in line with the market developments and trends. The South African coal ranges from low rank bituminous coal to anthracite and the utilization or potential markets include power generation, export, domestic, metallurgical, liquefaction and chemical sectors.

Most of the remaining coalfields in South Africa are found in arid areas where process water is scarce and given the need to fully exploit all the coal reserves in the country, this presents a great challenge to the coal processing industry. This is in addition to environmental related challenges and the need to reduce carbon footprint and the increasing burden of processing residual slurries. This makes it difficult for the industry to continue relying on the conventional wet processing methods such as wet jigging, heavy medium separation etc. Hence, the need to consider the implementation of dry coal beneficiation methods such as air jig, magnetic separation, electrostatic separation, pneumatic oscillating table, and air-dense medium fluidized bed beneficiation etc.

1.2 Advantages and disadvantages of dry coal beneficiation

Dry coal beneficiation presents numerous advantages to the coal processing industry in South Africa *(Lockhart, 1984)* and these include:

- Dust control and the disposal of dry tailings should be easier than the handling and treatment of large quantities of aqueous slurries with the attendant water pollution and recovery problems.

- While partial drying of feed material may often be needed for dry beneficiation, this could be more than compensated by not having to dewater and dry wet products and tailings. In any event, run-of-mine material, especially in arid areas and from open cuts, may be dry enough or may possibly be air-dried during storage and transportation. It must be pointed out that dried tailings make good fuel for fluidized bed combustion that could dry the feed coal and provide heat for other purposes, thus making the whole process cost effective.

- There are few of the high-cost ancillary operations associated with dry processes, since items like thickeners, flotation reagents ,flocculants ,cyclones, filter machines and media, centrifuges, etc., are largely eliminated.

The perceived shortcomings of dry coal beneficiation include inferior separation, non-routine operation, lack of adjustability and high sensitivity to changes in feed (rate, size, moisture), the need for drying and greater attention to dust control and safety, necessity for prescreening into narrow size fractions, and low capacities. However some of these criticisms apply at least to a certain extent to wet methods as well and besides, some 'shortcomings' can be the result of poor practice, insufficient knowledge, or factors that are not intrinsic deficiencies of any dry separation process. For example, poor separation or inefficiency is often a consequence of inadequate liberation of the components and/or of dampness that causes sticking and aggregation of particles *(Lockhart, 1984)*.

1.3 Comparison of the various dry coal beneficiation methods

The air jig, magnetic separation, electrostatic separation, vibrating table, FGX machine and air-dense medium fluidized bed separator are some of the dry coal beneficiation methods that have been studied in the past. All these methods are carried out by exploiting some of the differentiating properties between coals and refuse such as density, size, shape, magnetic conductivity, electric conductivity, radioactivity, frictional coefficient and so on. Meanwhile, substantial research and development work has been done on the dry beneficiation of coal with an air dense-medium fluidized bed. It has proved to be an efficient coal separation method, which uses a gas-solid fluidized bed as the separating medium, contrasting with the conventional methods of coal preparation using water as medium as in jigs. The fundamentals behind the operation of this system are quite similar to that of the wet dense medium separators. The table below compares the efficiencies of the various coal cleaning methods.

Table 1.1: Comparison of the various coal cleaning methods

Various coal cleaning methods				
	Air dense fluidized bed	**Air Jig**	**FGX Coal Separator**	**Wet dense medium separation**
(Ecart Probable Moyen), Ep	0.04 – 0.12	0.23 – 0.30	0.20 – 0.30	0.015 – 0.12

From the above table, it can be seen that the separation inefficiency, Ep of the air dense fluidized bed is quite comparable to that of the wet dense medium separation.

1.4 Thesis Objectives

Although considerable literature survey suggests that applications of the fluidized bed dry coal separator can been done successfully on an industrial scale as demonstrated in other countries such as China and Germany, there is still need to understand how various factors interact and develop models that would lead to better control and optimization. Hence, as part of this project, we are going to investigate the effect of particle size, shape and density on the performance of an air fluidized bed in dry coal beneficiation. The objectives of this study are as outlined below:

- Develop a sound understanding of the key process parameters which govern the kinetics of coal and shale separation in an air fluidized bed focusing on the effect of the particle size, shape and density on the performance of the fluidized separator. This understanding will be applied in the analysis and possibly further development of the continuous process.

- To integrate coal comminution and preparation with end uses so as to ensure adequate liberation and to optimize the use of the air fluidized bed through the manipulation of the particle size, shape and density. This is in the hope that coal comminution can be optimally controlled in relation to the mechanism of fracture, resulting in the production of particles of optimal shape and size.
- To develop and validate an empirical model that can be used to predict the quality of separation to be expected from an "ideal" continuous separation process and thus evaluate the short – comings of existing industrial scale processes.

1.5 Summary of the Thesis

The scope of work in this thesis involves investigating the effect of particle size, shape and density on the performance of an air fluidized bed in dry coal beneficiation. The first chapter gives a brief overview on the background of dry coal beneficiation in South Africa. Various dry coal beneficiation methods as well as their advantages and disadvantages are also outlined under this chapter. The research problem and objectives are clearly discussed in this chapter.

The second chapter reviews the basic principles and theory behind dry coal beneficiation using air dense medium fluidized beds. Characterization of fluids and fluid systems is also covered under this section. The various theoretical and empirical correlations or models that have been proposed for settling velocities in a fluidized bed are also briefly discussed here. The research problem and objectives are further discussed at the end of this chapter.

The third chapter outlines the design considerations and theory for the 3D fluidized bed. Some of the aspects covered include the types of distributors, optimum pressure drop across the distributor, minimum fluidizing velocities (magnetite, silica) and the air supply requirements (gas flow rate). The experimental equipment specifications and set up are all discussed under this chapter. The procedures followed to carry out the various laboratory tests and the calibrations that were done are all clearly outlined.

The fourth chapter discusses all the tests that were carried out to characterize the silica, magnetite and silica – magnetite beds. Some of the parameters incorporated in this discussion include particle size analysis of the medium particles (magnetite, silica) and bed density distributions in the silica – magnetite beds.

The fifth chapter involves the analysis and discussion of the rise/settling tests as well as the dynamic and steady state separation tests (5s, 10s, 15s, 30s, 60s, 90s, 600s, 1200s). The settling velocity versus particle density graphs together with the dynamic and steady state partition curves for the different particle size ranges and shapes were used as the basic tools for the analysis. A simple rise/settling velocity empirical model for predicting the performance of the ideal continuous separation process is proposed and analyzed in this chapter. The development of the empirical model is based on the Stokes' law and the basic equations, assumptions and parameters that were incorporated in the empirical model are all discussed in this chapter.

Chapter six summarizes the conclusions and recommendations from all the findings of this study. After this chapter, all the references used in this study are outlined. An appendix of all the experimental and calibration of equipment data is included at the end of this thesis report.

Chapter 2

Literature Review

<u>2.1 Brief history of dry coal beneficiation using air – dense medium fluidized beds</u>

Research on dry beneficiation technology with fluidization in coal preparation started more than 50 years ago (*Beeckmans etal., 1982; Leonard, 1979).* Different research groups in the United States, Netherlands, China, Canada and South Africa have contributed in various ways in the development of this technology.

The following three dry fluidized bed separators have been studied in the past:

- The Yancey and Frazer separator *(Chapman, 1928)*.
- Two separators developed by Warren Spring Laboratories: an inclined bed separator and a sluice box *(Douglas, 1966)*,
- The rectangular trough separator *(Eveson, 1968; Jong, 1999)* and the circular trough separator *(Lupton, 1989)*.

In 2003, researchers from Delft University of Technology in Netherlands constructed a pilot sized separator similar to the design of Eveson (1968) and used it to carry out some detailed experiments. The separator consists of a horizontal rectangular vibrating box; 160 cm long, 20 cm deep and 15 cm wide. The coal/shale mixture (F) is added at one end (b) and the separated fractions leave at the other end of the box passing a splitter (d) via extracting openings (e and f) as shown in Figure 2.1 below *(Jong, Houwelingen, Kuilman, Mesina and Reuter 2003).*

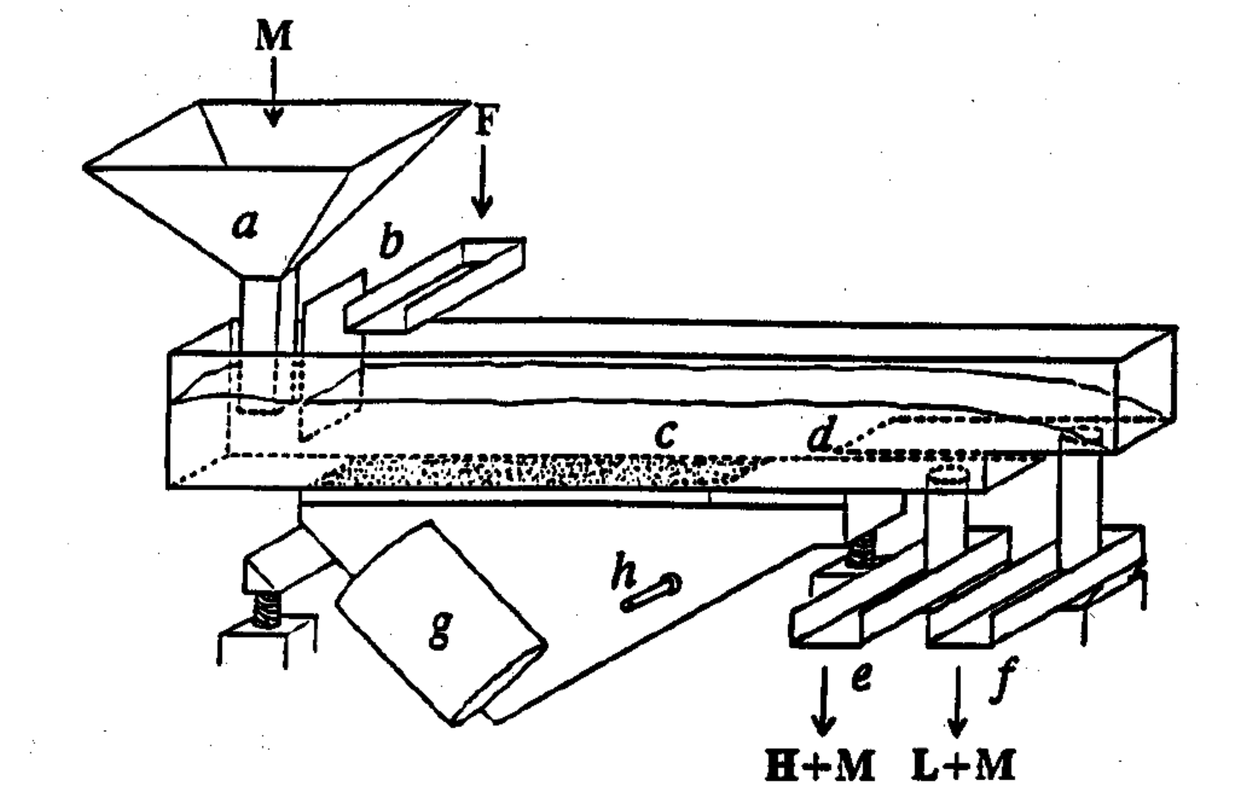

F=feed inlet, **a**=feed bin of sand medium, **b**=feed vibrator of coal/shale mixture, **c**=porous bottom, **d**=splitter of sink and float, **h**=pressurized air inlet, **g**=vibration motor, **e**=sink fraction

Figure 2.1: Delft University of Technology pilot scale fluidized bed separator.

The researchers from Delft University of Technology concluded that the performance of the fluidized bed was quite comparable to the conventional wet jigging process with an average Ep of 0.1 being obtained.

In China, the first dry coal beneficiation plant with an air-dense medium fluidized bed was established by the Mineral Processing Research Center of China University of Mining and Technology (CUMT).The plant was commissioned in June, 1994 and since then, new applications have been found. A 50ton/hr dry coal beneficiation plant with air-dense medium fluidized bed has been put into commercial testing in China *(Chen etal., 1991; 1994).*Figures 2.2 and 2.3 illustrate the 50ton /hr dry air dense separator and the principle of operation respectively.

Figure 2.2: The 50ton/hr dry air dense separator in China

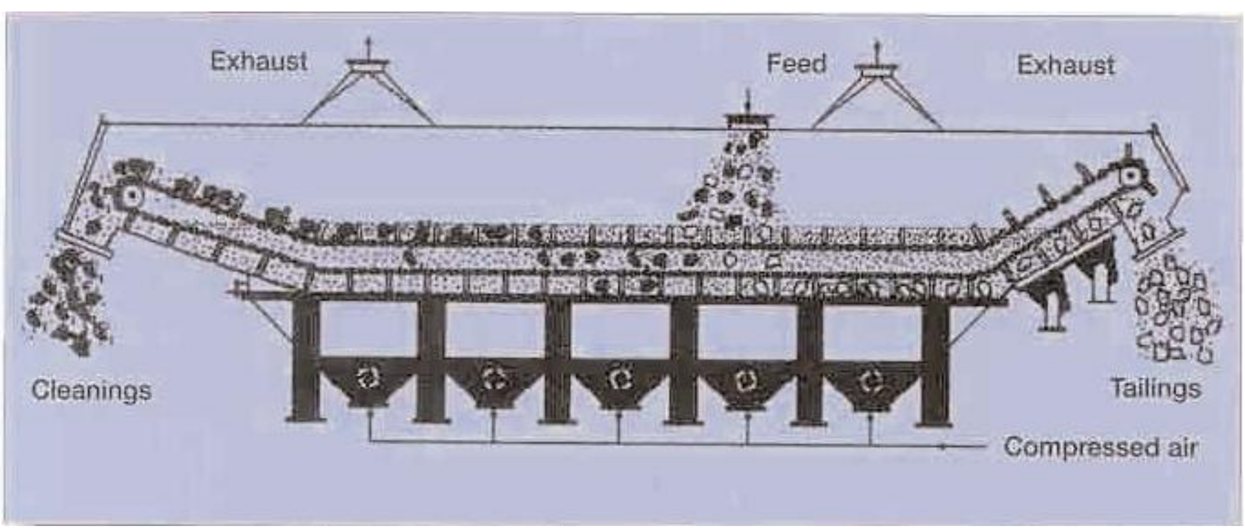

Figure 2.3: Principle of the 50ton /hr dry air dense separator

Dry beneficiation of coal with an air dense-medium fluidized bed is an efficient coal separation method characterized by an average industrial Ep of 0.05. It utilizes an air-solid suspension as beneficiating medium whose density can be maintained with consistency, similar in principle to the wet dense medium beneficiation using liquid-solid suspension as separating medium.

The air-dense medium fluidized bed used in dry coal beneficiation is not only pseudo fluid in nature, but also has a stable and uniform density. The heavy particles in feedstock whose density is higher than the density of the fluidized bed will sink, whereas the lighter particles will float, thus stratifying the feed materials according to their density *(Blagov, 1974; Beeckmans & Grayson, 1982; Leonard, 1979)*.This technique introduces a new method of coal beneficiation for the regions where water resources are in short supply and for the coals which tend to slime with wet separation processes.

In South Africa, some researchers from the University of Kwazulu Natal, Minerals Processing Research group have done some considerable work aimed at developing this novel dry coal processing system. Initially semi-batch tests were conducted using density tracers followed by batch separation of discard coal which varied in size between 1.5 –3.5cm. A novel collecting mechanism was also constructed to aid in the removal of the materials from the bed. At optimum conditions, separation inefficiency (Ep) of 0.0458 was obtained when separating the high ash Waterberg coal at an approximate average separation density of about 1996 kg/m3. Continuous test work at a flow rate of 18 kg/hr yielded an Ep of 0.0462 at the same density. The experimental data demonstrated that dry separation can be as efficient as the corresponding wet processes *(Kretzschmar, Pocock J., Loveday B. etal,. 2008)*.

2.2 Basic principles and characteristics of air dense – medium fluidized beds

In order to obtain an efficient dry separation condition in an air-dense medium fluidized bed, stable dispersion fluidization and micro bubbles must be achieved. The main requirements are that the bed density is well distributed in the three-dimensional space, not changing with time, and that the bed medium is of low viscosity and high fluidity *(Qingru Chen, Lubin Wei etal., 2007)*. The bed density can be calculated using equation (2.1) below.

$$\rho_{bed} = (1-\varepsilon)\rho_s + \varepsilon\rho_a \approx \rho_{50} \qquad (2.1)$$

Where ρ_s is the density of the solid particle, g/cm3; ρ_a is the density of the air, g/cm3; ρ^- is the average density of the fluidized bed, g/cm^3; ρ_{50} is the separation density of the fluidized bed, g/cm^3; and ε is the bed porosity, %.

When air flow velocity is in a suitable range above the minimum fluidization velocity (U_{mf}; m/s), ε is constant. Then,

$$\rho_{bed} = (1-\varepsilon)\rho_s \approx k\rho_s \approx W/LAg \qquad (2.2)$$

where W is the total weight of medium solids, kg; L is the depth of the bed, m; A is the cross-section area of bed, m^2; g is the gravitational acceleration m/s^2.

When a homogeneous and stable level of bed density with air-dense medium fluidized bed is established, a dispersion fluidized bed with dense-phase, high density, and micro bubbles is formed. The pure buoyancy of beneficiation materials plays a major role in maintaining the fluidized bed density, and the displaced distribution effect should be restrained. The displaced distribution effects include viscosity-displaced distribution effect and movement-displaced distribution effect. The former mostly affects fine materials occurring when the fluidized bed has high viscosity. It reduces with increased air flow velocity. The value of the latter will be large when air flow rate is much lower or higher than the optimum required to maintain a stable fluidized bed. If medium particle size distribution and air flow are well controlled, both displaced distribution effects will be restrained effectively *(Qingru Chen, Lubin Wei etal., 2007)*.

Mixtures of magnetite powder and fine coal can be used as dense medium in a fluidized bed to produce a stable and uniform beneficiation density ranging from 1.3 to 2.2 g/cm3. Therefore, this technology can meet the needs of beneficiating different coals for various products. It can either be used to remove gangues at high density or to produce clean coal at low density. By the Archimedes Law, light and heavy particles separate from each other by the bed density with the light particles floating and the heavy particles sinking.

2.3 Theory of the gas- solid fluidized bed used in dry coal beneficiation

In dry dense medium separation, the size of separated materials is much larger than that of the fluidized particles, which can be treated as a continuum. The drag force on a spherical object moving in a fluidized bed can be expressed as follows *(Yaomin Zhao, Lubin Wei etal., 2000)*:

$$F_d = C_D \pi \left({d_o}/{2} \right)^2 \left({\rho_{bed} u_r^2}/{2} \right) \tag{2.3}$$

where F_d is the drag force, C_D is the drag coefficient, d_0 is the diameter of object, u_r is the relative velocity of an object and the fluidized particles, and ρ_{bed} is the bed density given by equation bed. Calculation of drag force on the object in a Bingham fluid involves modifying Reynolds number of drag formula for Newtonian fluids. At low Reynolds number, *(Cai, 1981)* obtained the drag formula based on the velocity distribution of Stokes' solution:

$$F_d = 3\pi \mu d_0 u_r + \pi d_0^{\,2} \tau_0 \tag{2.4}$$

where μ is the plastic viscosity and τ_0 is the yield stress. The first term on the right side of the above equation is Stokes' drag formula for Newtonian fluid and the second term represents the influence of yield stress on drag force *(Yaomin Zhao, Lubin Wei etal., 2000)*.

Yaomin Zhao and Lubin Wei (2000) found that the drag coefficient formula for the Newtonian fluids can be represented by the drag coefficient associated formulae of Schiller and Nauman. This formula is valid for Re< 800, and the Reynolds number should be replaced by the modified Reynolds number as illustrated in equation (2.6) *(Yaomin Zhao, Lubin Wei etal., 2000).*

$$C_D = \frac{24}{\mathrm{Re}_m} \left(1 + 0.15 \mathrm{Re}_m^{\,0.687}\right) \tag{2.5}$$

where Re_m is the modified Reynolds number defined by equation (2.7)

$$\mathrm{Re}_m = \frac{d_0 u_r \rho_{bed}}{\mu_e} \tag{2.6}$$

$$\mu_e = \mu + \tau_0 d_0 \Big/ 3u_r \tag{2.7}$$

μ_e is the effective viscosity

A spherical particle immersed in a fluidized bed is subjected to the following forces which include gravity, effective buoyancy due to hydrostatic pressure distribution, and drag forces. The drag forces are contributed by the relative motion of the particle and gas, and of the spherical particle and fluidized particles. Drag forces contributed by the relative motion of the particle and gas can be neglected. The effective buoyancy force on the spherical particle can be calculated by Archimedes' principle, as it is immersed in real fluid with the density equal to the bulk density of fluidized bed. The motion equation of a particle falling through the fluidized bed can be written as:

$$\frac{\pi}{6} d_o^{\ 3} \rho_0 g - \frac{\pi}{6} d_o^{\ 3} \rho_{bed}\, g - C_D \pi \left(d_0 \Big/ 2 \right)^2 \left(\rho_{bed} u_r^{\ 2} \Big/ 2 \right) = \frac{\pi}{6} d_o^{\ 3} \rho_0 \frac{du_o}{dt} \tag{2.8}$$

where ρ_0 is the density of spherical particle and u_o is the falling velocity of spherical particle. When the falling velocity u_o reaches the terminal settling velocity u_t , $\frac{du_o}{dt}$ = 0. As u_t is much larger than the flow rate of fluidized particles under close to minimum fluidization conditions, $u_r \cong u_t$ .The above equation can be simplified as:

$$C_D = \frac{4 d_o g (\rho_0 - \rho_{bed})}{3 \rho_{bed} u_t^{\ 2}} \tag{2.9}$$

<u>2.3.1 Dense Bed Viscosity</u>

The bed viscosity of an air fluidized bed decreases as gas flow rate increases. The rate of decrease of viscosity is greatest near incipient fluidization, there after the rate of decrease lessens. Matheson found that bed viscosity increases with particle size and solids density in gas fluidized beds. The particle size distribution, shape and fines content have a significant effect on the viscosity. A number of expressions have been proposed for correlating air fluidized bed viscosity with bed voidage. These have been reviewed by Johnson, who proposed that the fluidized bed viscosity is related to bed voidage by:

$$\mu_a = \mu \frac{1+0.5(1-\varepsilon)}{\varepsilon^4}\left(\frac{1-\varepsilon}{\varepsilon}\right)^9 \tag{2.10}$$

where all the terms have the same meanings as defined before.

2.4 Density stability of the air dense – medium fluidized bed

The bed density stability and uniformity is very important for the efficient operation of the air fluidized bed coal separator. Several parameters such as the bed pressure drop, bed height, expansion ratio of bed, gas flow rate, bed porosity, and particle movement behavior, properties of the feed and medium particles all affect the bed density stability. The various ways in which the above parameters can be manipulated to ensure a stable and uniform bed density are discussed below.

2.4.1 Mean bed density and mean diameter of particles

In order to assess the uniformity of the bed, pressure measurements are made at the various points in the bed. The arithmetic mean density of all measurements at each bed pressure measuring point is defined as

$$\rho_{bed} = \frac{1}{N}\sum_{i=1}^{N}\rho_{bed\ (i)} \tag{2.11}$$

where N is the number of the pressure measuring points in the bed, and $\rho_{bed\ (i)}$ is the density recorded at each pressure measuring point. A sample standard deviation can be used to assess the homogeneity of the density distribution in the bed *(Luo Zhenfu, Chen Qingru etal., 2002).*

$$\sigma = \sqrt{\frac{1}{N-1}\sum_{i=1}^{N}(\rho_{bed\ (i)} - \rho_{bed})^2} \tag{2.12}$$

where σ is the standard deviation. A small standard deviation $(\sigma \approx 0)$ indicates that the bed density is homogeneous throughout the three dimensional space. On the other hand, the higher the standard deviation then the less homogenous is the bed density.

The mean diameter d_p of medium solids can be calculated using the following Sauter mean diameter formula:

$$d_p = \frac{1}{\sum_{i=1}^{M} \frac{X_i}{d_{pi}}} \tag{2.13}$$

Where X_i the weight % of the particles in a size is range, and d_{pi} is the mean diameter of this group, M is the number of size ranges. The Sauter diameter is a common measure used in fluid dynamics to estimate the average particle size and it is defined as the diameter of a sphere that has the same (volume/surface area) ratio as a particle of interest. The Sauter diameter is usually used where the active surface area is important like fluidization.

2.4.2 The static stability of bed density

The fluidizing gas velocity u is a very important parameter on the performance of an air fluidized bed used in dry coal beneficiation. It may have some effects on bed pressure drop, expansion ratio of bed, bed porosity and particle movement behavior. So, it should also be closely controlled in order to reach a good fluidizing condition of the bed. The fluidizing gas velocity can be adjusted over a wide range with the stability of the bed being maintained, but it is always fixed at an optimal value, in order not to result in fluctuation of the bed density *(Luo Zhenfu, Chen Qingru etal., 2002)*.

2.4.3 The dynamic stability of the bed density during separating

During separation, some fine coal will continuously accumulate in the fluidized bed and eventually affect the separation efficiency. The fine coal content in the bed is too high for coal beneficiation when the mean bed density becomes lower than a critical value of permitted separation density *(Luo Zhenfu, Chen Qingru etal., 2002)*.

2.5 Characterization of fluid systems and particles

A fluidized bed is formed by passing a fluid, in this case a gas upwards through a bed of particles supported on a distributor. Although, it is now known that even above the minimum fluidization velocity the particles are touching each other most of the time, with the exception of cohesive solids, the interparticle friction is so small that the fluid / solid assembly behaves like a liquid having a density equal to the bulk density of the powder, pressure increases linearly with distance below the surface, denser objects sink, lighter ones float, and wave motion is observed.

The behavior of particulate solids in a fluidized bed depends largely on a combination of their mean size and density *(Geldart etal., 1973)* and it has become increasingly common to discuss fluidized systems in relation to the so – called Geldart fluidization diagram. This is used to identify the package of fluidization characteristics associated with fluidization of any particular powder at ambient conditions.

2.5.1 Geldart classification of powders

According to Geldart, the major hydrodynamic characteristics of a fluidized bed are determined by particle size and superficial gas velocity. Figure 2.4 below illustrates the Geldart Particle classification diagram, which relates particle size (d_p) and the difference between particle and gas density ($\rho_p - \rho_g$) to general behavior. In the order of increasing particle size, the groups are designated as Group C, A, B and D.

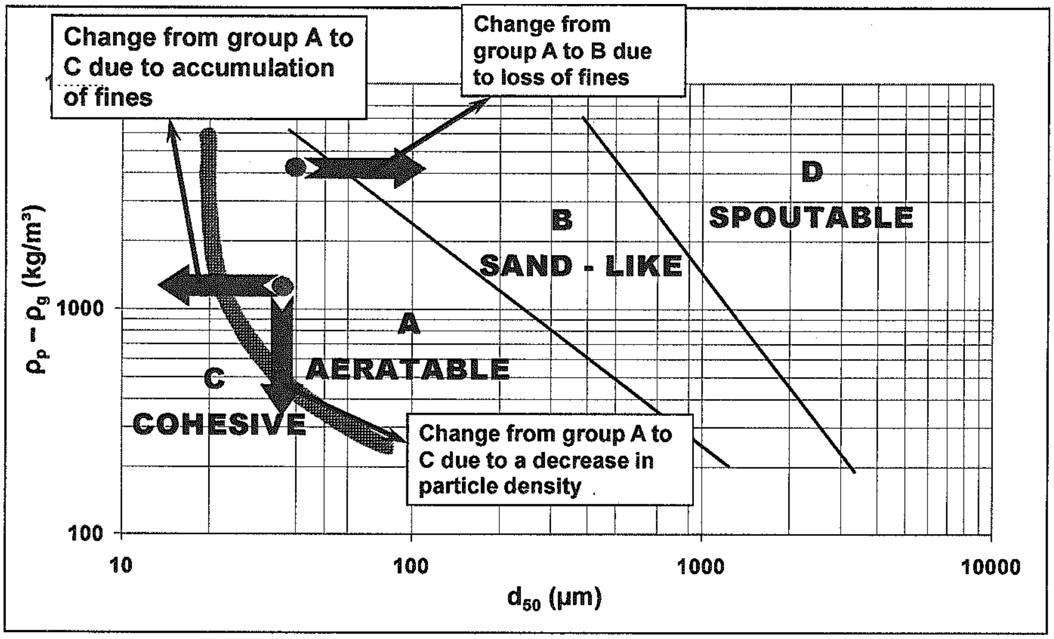

Figure 2.4: Geldart Classification diagram.Knowlton (2002)

Group C particles: Cohesive or very fine powders belong to this group. Normal fluidization of these solids is extremely difficult mainly because the interparticle forces are greater than those resulting from the action of gas.

Group A particles: This group consists of aeratable, or materials having a small mean particle size and /or low particle density (< ~ 1400 kg/m^3). The particle size is generally between 30 and 100 μm. These solids fluidize easily, with smooth fluidization at low gas velocities and controlled bubbling with small bubbles at higher velocities. Beds of these solids do not form bubbles immediately after the incipient fluidization and all bubbles rise faster than the interstitial gas velocity.

Group B Particles*:* The group B is made up of sand -like particles of size 40µm < d_p < 500 µm and 1400 < ρ_p <4000 kg/m^3. In contrast with Group A powders, interparticle forces are negligible and bubbles form as soon as the gas velocity exceeds U_{mf}. Bed expansion is small and the bed collapses very rapidly when the gas supply is cut off. Most bubbles rise more quickly than the interstitial gas velocity and bubble size increases roughly linearly with bed height and excess gas velocity U-U_{mf}

Group D Particles: Spoutable, or large and or dense particles Group D particles are generally considered to have a size greater than 1000 µm. All but the largest bubbles rise more slowly than the interstitial fluidizing gas, so that the gas flows into the base of the bubble and out of the top, providing a mode of gas exchange and by – passing which is different from that observed with group A or B powders. Bubbles coalesce rapidly and grow to a large size.

Geldart (1986) gives the numerical criteria for groups. The criteria are used to describe the group boundaries without the diagram.

2.5.2 Characterization of particle shape

Although little quantitative work has been carried out on the characterization of the particle shape, it is known that it influences such properties as flowability of powders, packing and interaction with fluids. Qualitative terms may be used to give some indication of the nature of particle shape and some of these extracted from the British standard 2955 are given in the Table 2.1 below *(Terrance etal., 1991)*.

Table 2.1: Definitions of particle shape (Terrance etal., 1991)

Qualitative term	Shape definition
Acicular	needle Shaped
Angular	sharp – edged or having roughly polyhedral shape
Crystalline	freely developed in a fluid medium of geometric shape
Dentritic	having a branched crystalline shape
Fibrous	regularly or irregularly thread - like
Flaky	plate - like
Granular	having approximately an equidimensional irregular shape
Irregular	lacking any symmetry
Modular	having rounded, irregular shape
Spherical	global shape

General qualitative terms outlined in Table 2.1 are inadequate for the determination of shape factors that can be incorporated as parameters into equations concerning particle properties where particle shape is involved as a factor. Given the fundamental importance of particle shape in fluid dynamics, it is therefore necessary to be able to measure and define shape quantitatively.

Terrance (1991) stated that there are two points of view that have been raised regarding the assessment of particle shape. One is that the actual shape is unimportant and all that is required is a number for comparison purposes. The other is that it should be possible to regenerate the original particle shape from the measurement data *(Terrance etal., 1991).*The numerical relations between the different sizes of a particle depend on the particle shape, and the dimensionless combinations of the sizes are called shape factors. The relations between measured sizes and particle volume or surface are called shape coefficients.

2.5.2.1 Shape coefficients

One of the commonly used approaches, which involve the use of shape coefficients, was given by Heywood who recognized that the word ‘shape’ in common usage refers to two distinct characteristics of a particle. These two characteristics should be defined separately, one by the degree to which the particle approaches a definite form such as a cube, tetrahedron or sphere, and the second by the relative ratio of the particle’s dimensions which distinguish one cuboid, tetrahedron, or spheroid from one of the same class . The Heywood’s dimensions are illustrated in Figure 2.5 below.

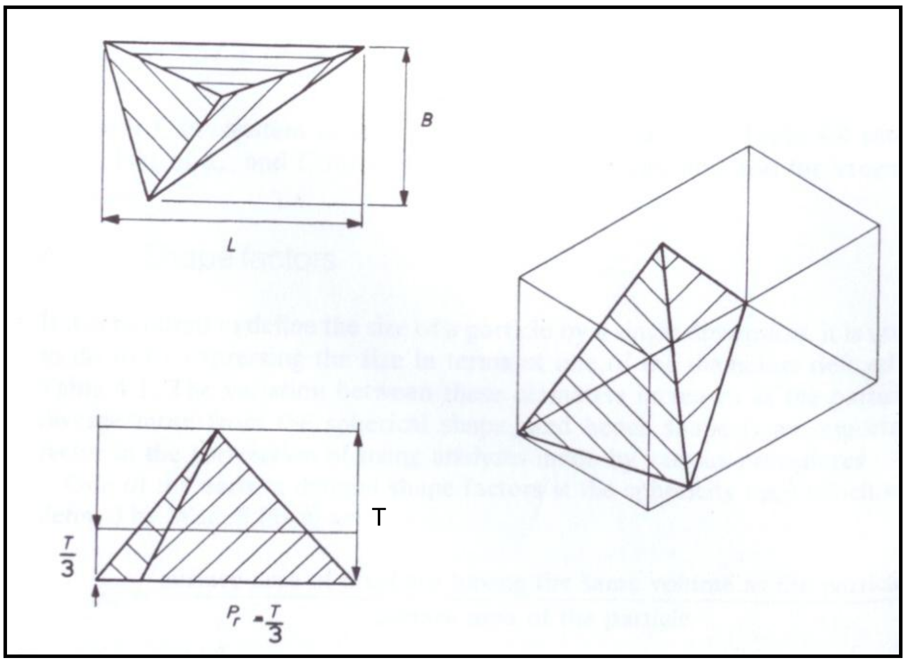

Figure 2.5: Heywood’s dimensions

If three mutually perpendicular dimensions of a particle may be determined, then the following Heywood’s ratios may be used:

Elongation ration $n = L / B$ (2.14)

Flakiness ratio $m = B/ T$ (2.15 a)

Where

(a) The thickness T is the minimum distance between two parallel planes which are tangential to opposite surfaces of the particle, one plane being the plane of maximum stability.

(b) The breadth B is the minimum distance between two parallel planes which are perpendicular to the planes defining the thickness and are tangential to opposite sides of the particle.

(c) The length L is the distance between two parallel planes which are perpendicular to the planes defining thickness and breadth and are tangential opposite sides of the particle.

Heywood classified particles into tetrahedral, prismoidal, sub – angular and rounded. Values of α and p_r for these classes are given in the table below:

$$p_r = \frac{T}{3} \tag{2.15 b}$$

$$\alpha_a = \frac{\pi {d_a}^2}{4BL} \tag{2.15 c}$$

Table 2.2: Values of α and pr for particles of various shapes

Shape group	α_a	p_r
Angular Tetrahedral	0.50 – 0.80	0.40 – 0.53
Angular Prismoidal	0.50 – 0.90	0.53 – 0.90
Sub - angular	0.65 – 0.85	0.55 – 0.80
Rounded	0.72 – 0.82	0.62 – 0.75

2.5.3 Bed voidage

The bed voidage is one of the parameters which have got a significant effect on the bed density and it is defined as:

$$\varepsilon = \frac{Volume\ of\ bed - Volume\ of\ particles}{Volume\ of\ bed} \tag{2.16}$$

The bed voidage for an air dense fluidized bed can also be estimated from equation 2.4. The voidage of the packed bed varies from ‘dense’ packing to ‘loose’ packing. The ‘dense’ packing state is independent of particle size, but is dependent on shape. The particle shape is usually characterized in terms of sphericity (ϕ) which is defined as the ratio of the surface area of a given particle to the surface area of a sphere with the same volume. Table 2.6 below summarizes the bed voidage for both loose and dense packing for particles larger than 500μm.

Table 2.3: Voidage versus sphericity for randomly packed beds uniformly sized particles larger than about 500μm (Geldart 1986).

ϕ	ε	
	Loose packing	Dense packing
0.25	0.85	0.8
0.3	0.8	0.75
0.4	0.72	0.67
0.5	0.64	0.59
0.6	0.58	0.51
0.7	0.53	0.45
0.8	0.49	0.4
0.9	0.45	0.36
1	0.41	0.32

2.5.4 Pressure drop through packed beds

A fluidized bed is a packed bed through which a fluid flows at such a high velocity that the bed is loosened and the particle – fluid mixture behaves as if though it’s a liquid. The pressure drop across a fixed bed height H containing a single size of isotropic solids is given by the Ergun equation:

$$\frac{\Delta P}{H} = 150\frac{(1-\varepsilon)(1-\varepsilon)^2}{\varepsilon^3}\frac{\mu U}{{d_p}^2} + 1.75\frac{1-\varepsilon}{\varepsilon^3}\frac{\rho_f U^2}{d_p}$$

(2.17)

Where μ is the viscosity of the fluid, ρ_f is the density of the fluid and U is the superficial velocity. The Ergun equation has been found to represent the data for randomly packed granular materials to within ±25%. The equation does not apply to beds of abnormal void content (e.g. Raschig rings) or to highly porous beds (e.g. fibrous beds where ε = 0.6 to 0.98), *(Kunii, Levenspiel etal., 1991).*

2.5.5 Minimum Fluidizing velocity

The minimum fluidizing velocity is a very important parameter in both the design and operation of fluidization technologies. The basis of the theory for prediction of minimum fluidization velocity is that the pressure drop across the bed must be equal to the effective weight per unit area of the particles at the point of incipient fluidization. Minimum fluidization velocity, U_{mf} is the velocity of the fluid at which the above condition is satisfied. The minimum fluidization velocity can be estimated by either using equation 2.17 or by experiment as illustrated in Figure 2.6 below.

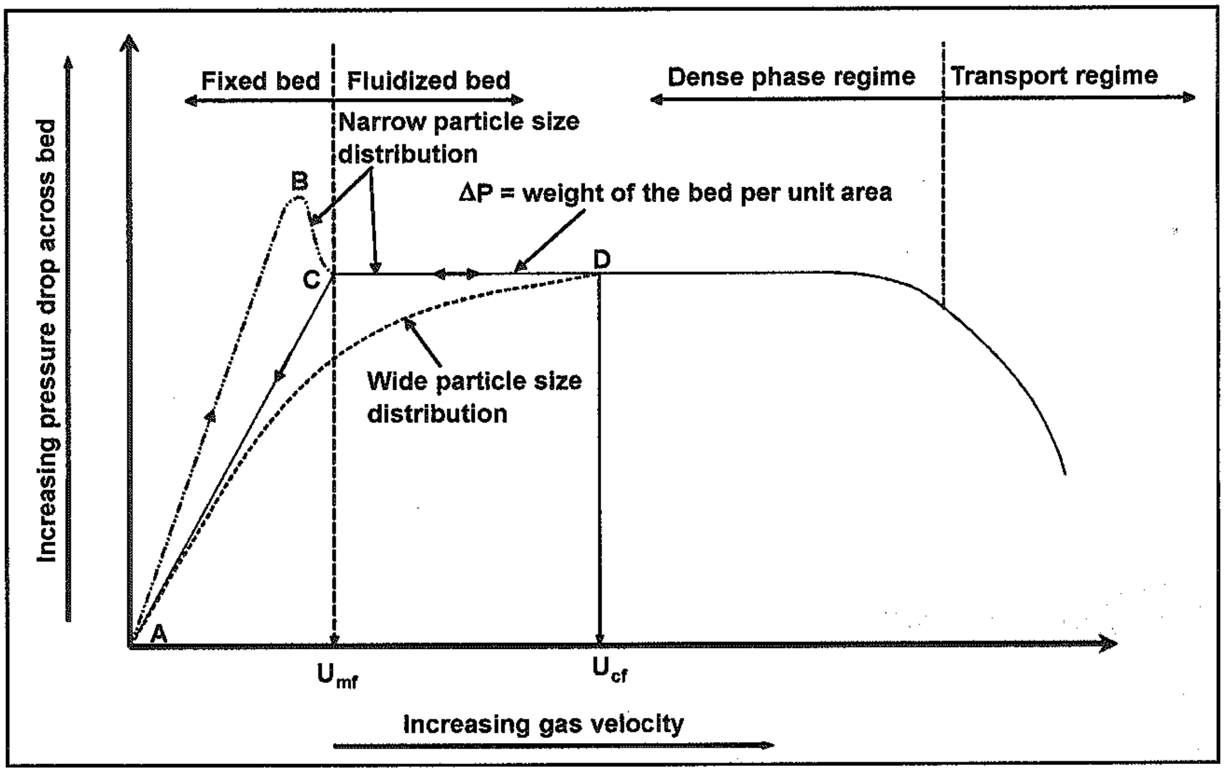

Figure 2.6: Pressure drop versus velocity diagram (IFSA, 2008)

A pressure drop versus velocity diagram such as the one shown in Figure 2.7 can be used to experimentally determine the minimum fluidizing, U_{mf}. The velocity at point C is the minimum fluidization velocity. When the gas velocity is increased from zero, curve ABCD is followed, and this shows that the pressure drop initially increase above that required to fluidize the bed (Point B). This is because the bed is initially compact and an extra force is necessary to' unlock' (increase the bed voidage from ε_m to ε_{mf}) the bed. An increase in the bed voidage results in a decrease in pressure drop to static pressure (equal to weight per unit area) of the bed.

The pressure drop remains constant with an increase in gas velocity beyond minimum fluidization velocity. The reason for this is that the dense gas – solid phase is well aerated and can deform easily without appreciable resistance. When the gas velocity is decreased the fluidized particles settle down and the bed voidage is also reduced to ε_{mf}. The pressure drop versus velocity curve is now ACD and shows a lesser pressure drop in the fixed bed regime.

Once the gas is turned off, a gentle tapping or vibration will reduce its voidage to its stable initial value of ε_m.

2.6 Effect of the gas distributor on the performance of an air fluidized bed

The gas distributor is one of the vital components of a fluidized bed since the satisfactory operation the bed mainly depends on the uniformity of the gas distribution across the bed area. The distributor prevents the bed solids from falling through into the air box and must also be able to support the forces due to pressure drop associated with gas flow during operation and the weight of the bed solids during shutdown.

Apart from the gas velocity and the particle characteristics, the bubbling bed behavior also depends on the type of gas distributor used. Figure 2.7 below shows commonly used distributors and the way in which the bubbles form above the different types of distributors. The distributor determines the extent of gas – particle contacting and the extent of particle mixing.

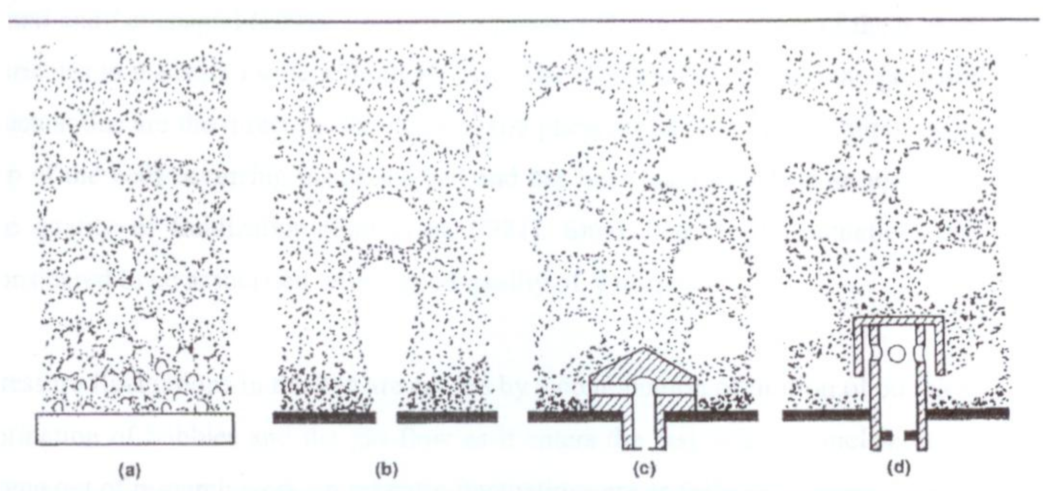

Figure 2.7: Behaviour of bubbles just above the distributor: (a) porous plate; (b) perforated plate; (c) nozzle-type tuyere; (d) bubble cap tuyere. (Kunii and Levenspiel etal 1991)

The porous distributor (Figure 2.7(a)) promotes very good solid gas contacting and solid mixing can be achieved above the distributor and high up the bed. Ceramic or sintered metal porous plate distributors are mostly used in small – scale or laboratory studies of fluidization. This is because they have a sufficiently high flow resistance to give a uniform distribution of gas across the bed. Several disadvantages, including high pressure drop and low construction strength makes the use of this type of distributors for industrial use impractical.

A single orifice – type (Figure 2.7 (b)) distributor do not promote good gas solid contact as most of the gas escape into the bubble as it enters the bed. The other types of distributors (tuyeres, Figure 2.7 (c) and (d) have the same characteristic as the orifice type distributors, except that that the gas can be introduced at different angles. Due to their robustness and ease of construction the nozzle type distributors have a wide industrial application *(Kunii, Levenspiel etal., 1991)*.

2.7 Segregation in gas- solid fluidized beds

Segregation in gas-solid fluidized beds has been found to be stronger for the heterogeneous systems than the homogeneous ones. Density difference of the medium particles is one of the major factors affecting segregation. Some of the system variables or parameters that affect segregation in gas – solid fluidized beds include the initial static bed height, composition of the mixture, superficial velocity of the of the fluidizing medium, the flotsam and jetsam concentration, particle characterization of the material to be separated (i.e. particle density, size and shape), bubble diameter, bubble rise velocity, bed voidage fraction, fraction of bed in bubbles, minimum fluidization velocity. Knowledge of the minimum fluidization velocity and the mechanism of the segregation are crucial to the behavior of the fluidized bed and need to be properly understood as they significantly affect the overall performance of the fluidizing bed. Much work has been devoted to investigating the segregation of particles by size and to a less extent by density and shape *(Gibilaro etal., 1974)*.

2.8 Modeling of dense medium separators (DMS)

Although there is an extensive literature on the performance of dense medium separation (DMS) processes in coal applications, there has been little attention paid to modeling of such kind of processes. DMS separations are conventionally represented by their partition curve. The efficiency of the process is defined by the departure of the curve from a perfect partition represented by a vertical line at the cut point. An empirical measure of the inefficiency is the (Ecart Probable Moyen, or probable error), Ep. The error area represents the material misplaced in the separation over the whole density range, but it does not describe the curve itself.

In one of his publications in 1991, Napier Munn highlighted that in the design and optimization of dense medium separators, we need to know not only what cut point and Ep to target to achieve a given metallurgy but also how to obtain them. This is a difficult objective for any process model, but its attainment is essential to be able to unlock the full power of simulation *(Napier – Munn etal., 1991)*. Knowledge of the size-by-size partition curve partition curves of a given separation, together with the assays associated with each particle size/density interval; permit the complete metallurgy of the separation to be determined, including the yield and assay of the products. Thus, the purpose of any DMS model is to predict the partition curve for a given set of operating conditions *(Napier – Munn etal., 1991)*.

Medium properties have to a certain extent driven the evolution of modeling DMS processes. A particular important property is the viscosity of the medium. The influence of viscosity on the process, in a hydrodynamic sense, has been recognized from the earliest studies, but very few models have been developed in which viscosity is explicitly incorporated (*Napier – Munn etal., 1990).* JKMRC have done some considerable work aimed at quantitatively incorporating the effects of medium viscosity, and decouple this property from the medium density, with which it is strongly correlated *(Napier – Munn etal., 1991).*

2.9 Research Problem & Objectives

Although considerable literature survey suggests that applications of the fluidized bed dry coal separator can been done successfully on an industrial scale as demonstrated in other countries such as China and Germany, there is still need to understand how various factors interact and develop models that would lead to better control and optimization. Hence, as part of this project, we are going to investigate the effect of particle size, shape and density on the performance of an air fluidized bed in dry coal beneficiation. The objectives of this study are as outlined below:

- Develop a sound understanding of the key process parameters which govern the kinetics of coal and shale separation in an air fluidized bed focusing on the effect of the particle size, shape and density on the performance of the fluidized separator. This understanding will be applied in the analysis and possibly further development of the continuous process.
- To integrate coal comminution and preparation with end uses so as to ensure adequate liberation and to optimize the use of the air fluidized bed through the manipulation of the particle size, shape and density. This is in the hope that coal comminution can be optimally controlled in relation to the mechanism of fracture, resulting in the production of particles of optimal shape and size.
- To develop and validate an empirical model that can be used to predict the quality of separation to be expected from an "ideal" continuous separation process and thus evaluate the short – comings of existing industrial scale processes.

Chapter 3

Experimental equipment and Procedures

3.1 Design considerations and theory for the 3D fluidized bed

As part of this research project a (40 x 40 x 60) cm three dimensional (3 D) fluidized bed was designed for the detailed laboratory tests. Particular attention was paid to address some of the following design challenges. Fluidized beds behave quite differently when solid properties, gas velocities or vessel geometries are varied. Some of the variables that directly or indirectly influence the design of a fluidized bed include pressure drop across the distributor, pressure drop across the bed, bed weight, bed height, bed expansion ratio, fluidizing velocity, and particle size, particle size distribution, geometry of the distributor and fraction of the distributor plate area open for gas flow. Many of these variables are interrelated in unknown complex ways and as a result the information available in the literature is often difficult to interpret in terms of general conclusions. A critical component that requires specific attention is the gas distributor at the base of the bed.

3.1.1 Design of the distributors

The gas distributor supports the weight of the defluidized bed during down-time and prevents the flow back of particles both during down-time and also when operating. However, its main function is to distribute the fluidizing gas across the base of the bed so that it is maintained in the fluidized condition over the whole of its cross-section. The distributor also plays a major part in determining the size of the bubbles in the bed which are the major cause of particle circulation and mixing *(Qureshi, Creasy etal., 1978)*. In the present context the usual malfunction of the distributor is that either it does not fluidize the whole of the cross-section of the bed on startup, or during the course of operation a portion of the bed defluidizes, so blocking a proportion of the discharge area. In order to ensure stable operation it is apparent that the pressure drop through the distributor should be sufficiently large so that the flow rate through it is relatively undisturbed by the bed pressure fluctuations above it *(Qureshi, Creasy etal., 1978)*.

Kirwan and Vines (1981), Gregory and Harrison (1987) have reviewed the available literature on distributors and have concluded that the design of gas distributors for fluidized beds is largely empirical and sufficient information does not exist linking the distributor design and fluidized bed behavior. The existing investigations may be related to such areas as pressure drop, grid design, jet behavior, fluidization uniformity, bed density, bubble behavior, and chemical conversions.

3.1.2 Significance of pressure drop through a distributor

Some of the various types of distributors that are commonly used in the construction of fluidized beds have already been discussed in Chapter 2 and these include porous plates, perforated plates, nozzle type tuyere and bubble cap tuyere and bubble cap tuyere. In the design of dense phase gas-solid fluidized beds it is normal to require the distributor plate to have a pressure drop equal to some fraction *f* of the pressure drop across the bed. The choice of this fraction is based upon a compromise between pumping costs and undesirable gas channeling through the bed.

Recommended values of *f* vary from 0.01 to 0.60 *(Kunii, Levenspiel etal., 1991)*, with the higher values preferred for wide, shallow beds. Once *f* has been set and a bed height established, the pumping power required to force the gas through the distributor plate and bed can be calculated readily. It is normal in this design process to assume that the pressure drop across the bed is fixed and equal to the weight of the solids divided by the cross-sectional area of the bed. For dense bubbling beds the analysis outlined above can be used to give reliable estimates of bed and distributor pressure drops and gas pumping power *(Benavides, Turton and Clark etal., 1996)*.

3.1.3 Calculation of a pressure drop through a distributor

The type of gas distributor and the characteristics of the bed material have got a direct influence on the stable and efficient operation of air fluidized beds as they determine the optimum gas distributor to bed pressure drop ratio that should be used. A number of recommendations relating distributor and bed pressure drop have been made for satisfactory operation. D.Kunni and O. Levenspiel (1991) summarized their findings with the following design recommendations:

- For even distribution of fluidizing gas to a bed where the operating velocity, u_o is close to minimum fluidizing velocity, u_{mf} choose

$$\frac{\Delta p_d}{\Delta p_b} \geq 0.15 \qquad (3.1)$$

where Δp_d and Δp_b refers to the pressure drop across the distributor and the bed respectively

- The required $\Delta p_d/\Delta p_b$ decreases as u_o/u_{mf} increases
- $\Delta p_d/\Delta p_b$ is roughly independent of bed height, or Δp_b
- For the same bed, the same u_o and same u_{mf} but different distributors,

$$\left(\frac{\Delta p_d}{\Delta p_b}\right)_{porous\,plate} > \left(\frac{\Delta p_d}{\Delta p_b}\right)_{orifice\,plate} \qquad (3.2)$$

The difference is greater when u_o is close to u_{mf} and decreases to zero for $u_o \gg u_{mf}$

- The original rule of thumb

$$\Delta p_d = (0.2 - 0.4)\Delta p_b \qquad (3.3)$$

"The above relationship has been verified by various analyses and experiments. It represents a reasonable upper bound to the required pressure drop for smooth operations. This value can be made lower in specific cases."*(Kunii, Levenspiel etal., 1991).*

3.1.3 Minimum fluidizing velocities (magnetite, silica)

In the design of fluidized bed systems, it is very important to calculate the minimum fluidizing velocities of all the various medium particles sizes. This will go a long way in the accurate and precise sizing of the air supply requirements. The operating superficial velocity range of a fluidized bed is usually expressed in terms of the minimum fluidizing velocity, u_{mf}. In order to ensure that no elutriation of the medium particles takes place, the superficial gas velocity should be less than $10u_{mf}$.

The minimum fluidizing velocity of the medium particles can be estimated using the Ergun equation given below.

$$\frac{\Delta P}{H} = 150\frac{(1-\varepsilon)(1-\varepsilon)^2}{\varepsilon^3}\frac{\mu U}{{d_p}^2} + 1.75\frac{1-\varepsilon}{\varepsilon^3}\frac{\rho_f U^2}{d_p} \tag{2.17}$$

The pressure drop versus velocity diagram is also another very powerful graphical tool in the estimation of the minimum fluidizing velocity of the medium.

Although there has been an enormous amount of work that has been reported on the design and operation of various types of fluidized bed, there is still lack of simple and clear generalized design and scale up guidelines partly due to the complexity of interactions between fluid and particles in multiphase flow systems.

3.2 Experimental Equipment Specifications

The (40 x 40 x 60) cm rectangular 3 D Fluidized bed was constructed from perspex and reinforced using some steel framework at the edges. The bed is made up of a uniform canvas distributor sandwiched between two pieces of wire mesh. Figure 3.1 below shows the 3 D fluidized bed:

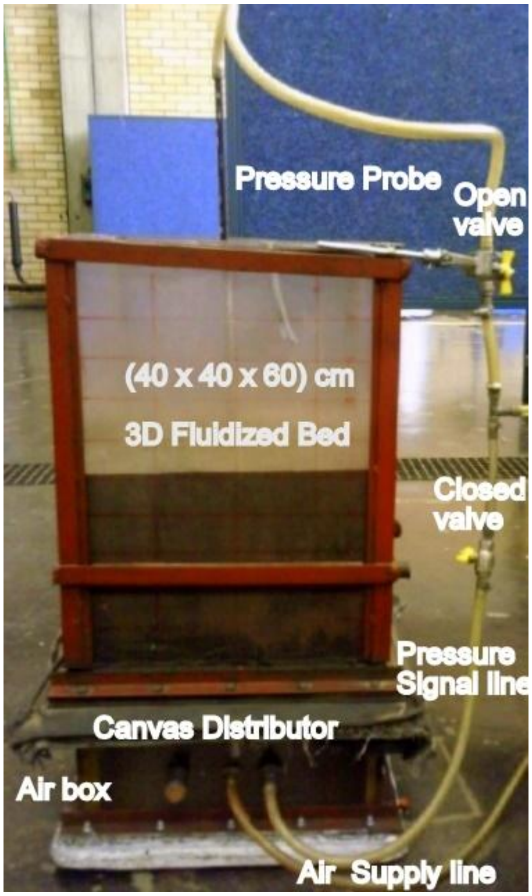

From the top of the bed

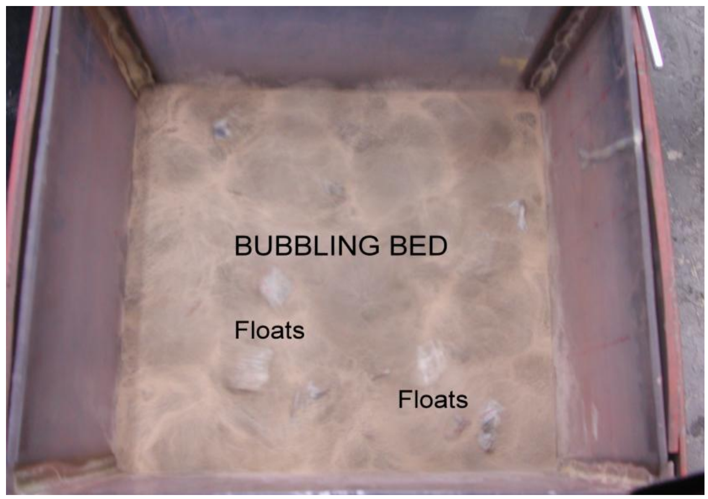

Fig 3.1: A (40 x 40 x 60 cm) 3 D fluidized bed

The bed was graduated in intervals of 1.0 cm from the bottom up to the top 50 cm mark. This was done in preparation of the separation and rise/settling velocity tests.

3.3 Experimental Set up

The experimental set up for the detailed laboratory tests is as shown in the process flow diagram below. In addition to all the equipment shown in the flow diagram, a flat wooden (400 x 150 x 2mm) scraper was used to scrap off some medium from the bed during settling tests. A stop watch was also used to measure the time in both rise and settling velocity tests.

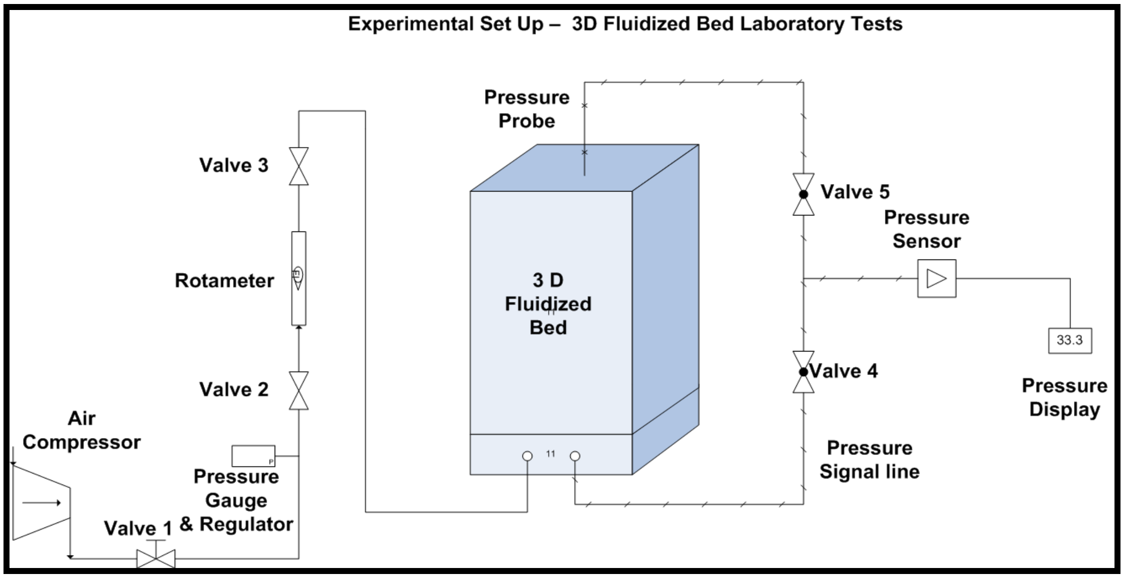

Figure 3.2: Experimental Set up – 3D Fluidized Bed Laboratory Tests

The specifications of some of the equipment used during the tests are discussed below.

3.3.1 Air supply requirements

Compressed air at an average inlet pressure of 320 kPa was used to fluidize the medium particles in the bed.

3.3.2 Bed solids

Preliminary characterization tests were carried out using separate beds of silica and magnetite, but for the detailed laboratory tests, a compound mixture of silica and magnetite was used.

3.3.3 Flow measurements

A rotameter was used to measure the gas flow rate. The rotameter was connected as shown in the experimental set up above. The valve on top of the rotameter was used to control the gas flow rate.

3.3.4 Pressure measurements

A pressure probe connected to a gas sensor was used to measure the pressure drop in the bed. The pressure probe was made from a polythene tube which had graduations ranging from 0mm to 500mm. A pressure gauge was used to measure the inlet air pressure and to ensure a constant air pressure supply, a pressure regulator was used.

3.3.5 Calibration of the pressure sensor

The pressure sensor was calibrated using a 100cm H_2O manometer. A plot of the manometer reading versus the pressure sensor reading was made. The relationship was found to be linear as illustrated by the calibration curve in the Appendix A - 1.

3.3.6 Calibration of the gas rotameter

The calibration curve for the gas rotameter is shown in Appendix A- 2. The rotameter was calibrated at an atmospheric pressure of 0.83 bars and temperature of 298 Kelvins. All the necessary correction calculations were carried out (see Appendix A -2).

3.4 Procedures for characterizing coal and medium particles

Coal particles of different sizes, densities and shapes were used for the detailed separation tests. They were characterized as outlined below:

3.4.1 Particle size

A vibrating screen was used to classify the coal particles into the following particle size ranges:

- (+9.5 – 16mm)
- (+16 – 22mm)
- (+22 – 31.5mm)
- (+37 – 53 mm)

3.4.2 Particle density

The float and sink method was used to determine the density range of the particles whilst the water displacement method was used to determine the specific density of the particles. Carbon tetrachloride and benzene were used as the floating reagents. Determinations of the specific densities of the particles using the water displacement method involved weighing the mass of each particle on a scale and then divide that by the volume of water displaced by the particle. The particles were not weighed together because in order to study the rise and settling behavior of each particle, it is of critical importance that the specific density of the particle is known mainly because the settling /rise velocity is a function of the density. The following particle density ranges were used for the detailed laboratory tests:

- (1.30 – 1.40)
- (1.40 – 1.50)
- (1.50 – 1.60)
- (1.60 – 1.70)
- (1.70 – 1.80)
- (1.80 – 1.90)
- (1.90 – 2.00)
- (2.0 – 2.60)

3.4.3 Particle shape

Particle shape is a difficult parameter to define quantitatively. In the separation tests, the particle shape was only qualitatively described and particles which resemble the following shapes were used:

- Blockish (Blk) particles
- Flat (FB) particles
- Sharp pointed prism (SR) particles

However, shape coefficients of some of the particles that were used for rise / settling tests were calculated using Heywood's approach, refer to Appendix B.

3.4.4 Medium particles

A compound mixture of magnetite and silica was used as the medium for the detailed laboratory tests. Preliminary tests were carried out using separate silica and magnetite beds respectively. Silica with a particle size distribution (PSD) range of (+50 - 300µm) was mixed with magnetite with the following PSD range, (+50 - 150µm) to form a compound medium. Vibrating screens with aperture sizes corresponding to the above PSDs were used to classify the medium. An electronic microscope was used to capture magnified photographs of the above medium particles and their respective shapes were qualitatively analyzed.

3.5 Procedures for characterizing the silica and magnetite beds

Tests aimed at characterizing the silica and magnetite beds were carried following the procedures outlined below:

- The respective medium (silica/magnetite) was added into the bed until a fixed bed height of 35cm was attained. The air supply outlet valve to the bed was slowly opened and the air pressure was measured using a pressure gauge. A pressure regulator was used to ensure a constant air supply pressure. As the gas flow rate was increased, the bed expanded until it reached a stage where small bubbles could be seen on top of the bed. This stage represented the transformation of the bed from a fixed bed to a bubbling stage. Microbubbles are desirable for coal separation. The pressure drop at the various bed levels (0, 5, 10, 15, 20, 25, 30 and 35 cm) was measured at different gas flow rates following the sampling plan shown in the diagram below.

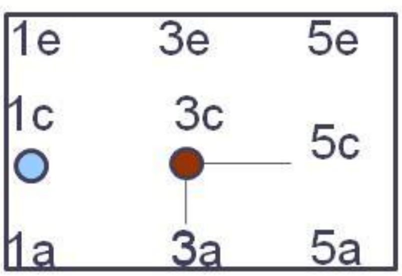

(1e, 1c, 1e, 3a, 3c, 3e, 5a, 5c and 5a represent the respective sampling points at the various bed levels)

Fig 3.3: Sampling plan for pressure drop measurements at various bed levels

- At least seven sets of gas flow rate and pressure drop data were collected before slugging could be observed in the bed. The superficial gas velocity was calculated using the following equation:

$$gas\ superficial\ velocity = \frac{gas\ flowrate\ (m^3/s)}{crossectional\ area\ of\ the\ distributor\ (m^2)} \qquad (3.5)$$

- The bed pressure drop (Pa) was plotted against the superficial velocity (m/s) and the pressure drop – velocity graph was used to determine the minimum fluidizing velocity of the medium.
- On the other hand, the pressure drop data was plotted against the corresponding bed levels and the following equations outlined below were used to determine the distribution of the bed densities at the various bed levels.

$$P = -\rho_{bed}\, g\, (h_{top} - h) \tag{3.6}$$

$$dP = -\rho_{bed}\, g\, dh \tag{3.7}$$

Where P is the pressure drop (Pa)

ρ_{bed} is the bed density (kg/m^3)

g - 9.81 m/s^2

From equation 3.7 above, it can be clearly seen that when the bed pressure drop (dP) is plotted against the bed level (dh) plot, then:

$$-\rho_{bed} g = gradient\ of\ the\ dP\ vs\ dh\ graph \tag{3.8a}$$

Therefore,

$$\rho_{bed} = \frac{-(Gradient\ \times 10000)}{9.81} \tag{3.8b}$$

where 10000 is the conversion factor to SI units.

- Using the above approach, the bed density distribution was established and analyzed respectively.

3.6 Procedures for measuring the settling velocities of the coal particles in the bed

- Six particles were selected from each of the particle density intervals and size ranges outlined above. In order to investigate the effect of the particle shape, six particles approximating the following different shapes (Blockish, Flat and sharp pointed) were selected from the (+16 – 22mm) particle size range. A total of 252 coal particles were used for the detailed settling tests.

- Before any tests could be carried out the bed was allowed to run for at least five minutes so that a stable and uniform bed density could be established. All the experimental set up connections were also checked for leakages.
- The coal particles were then introduced into the bubbling fluidized bed by uniformly spreading them throughout the three dimensional space. The stop watch was also started at the same time.
- After running for a specific time period of e.g. (5s, 10s, 15s, 30s, 60s, 90s, 10 min and 20 min), the air supply and the stop watch were simultaneously stopped. A flat scraper with a length of approximately 40cm was used to gently scrap off the medium in intervals of 1cm. All the particles recovered from the different bed levels are arranged on a (1500 x 1500 x 2mm) metal sheet according to their respective positions in the bed and the recovered medium was put in a bucket. Labels of the bed levels in decreasing intervals of 1cm from top to the bottom of the bed were used to identify the particles found at the different positions in the bed. In order to improve on the precision and accuracy of the results, the above tests were repeated at least three times.
- The instantaneous settling velocities of the particles after different running times were calculated using the equation given below.

$$Settling\ velocity = \frac{B_{t2} - B_{t1}}{t_2 - t_1} \tag{3.9}$$

where B_{t1} is the position of the particle in the bed after time t_1

B_{t2} is the position of the particle in the bed after time t_2, ($t_2 > t_1$)

3.7 Procedures for measuring the rise velocities of the coal particles in the bed

A relatively simple technique was used to measure the rise velocities of the particles in the bed. However this technique could only be used to accurately measure the rise velocities for particles with density less than 1.50 following the procedures outlined below:

- At least two particles were selected from each density interval and particle size ranges stated in section 3.4. Before any rise velocity tests could be carried out, the bed was allowed to reach a stable state as discussed in section 3.8. A 50 cm long tong was used to pick a single particle from the tray and push it right to the bottom centre of the bed. The tong was aligned in such a manner that it did not interfere with the motion of the particle when it was released. The stop watch was started at the same time the particle was released from the bottom of the bed and it was immediately stopped when the particle was seen floating at the top of the bed. The tests were repeated for at least six times so as to improve on the repeatability of the results.

- The rise velocities of the particles were calculated using the equation below;

$$Rise\ velocity = \frac{B_s - B_o}{t} \tag{3.10}$$

where *Bs* is the bed level corresponding to the top surface of the fluidized bed

B_o is the bed level corresponding to the bottom of the bed, $B_o = 0$ at $t = 0$

t is the time taken by the particle to move from B_o to *Bs*

3.8 Procedures for measuring the partition curve of the 3D fluidized bed

In order to assess the performance of the 3D fluidized bed separator, tests aimed at measuring the partition curve of the bed were carried out following the procedures discussed below. The tests were carried out using both density tracers and coal particles.

3.8.1 Procedures for measuring the partition curve of the bed using density tracers

- A total of eighty 20mm diameter disc shaped density tracers were used for the tests and at least ten density tracers with the following specific densities (1.30, 1.40, 1.50, 1.60, 1.70, 1.80, 1.90 and 2.10) were selected for the tests respectively. All the particles were introduced into the bed when the bed density was stable and uniform. Different running times varying from 10s to 10 minutes were used for both dynamic and steady state tests. A static bed of 35 cm was used for the tests and all the particles recovered above 20 cm were regarded as floats whilst all the particles below 10 cm were classified as sinks. On the other hand, particles found between 10cm and 20cm regarded as middlings.

- The number of density tracers that reported to the floats and sinks were counted respectively and the % sinks were then plotted against the relative density a partition curve which could be used to measure the performance of the bed.

- The effective cut density ,ρ_{50} was interpolated from the partition curve whilst the process inefficiency, E_p was calculated using the equation given below:

$$E_p = \frac{\rho_{75} - \rho_{25}}{2} \tag{3.11}$$

where ρ_{75} is the relative density at which 75 % of the particles report to the sinks.

ρ_{25} is the relative density at which 25% of the particles report to the sinks.

3.8.2 Procedures for measuring the partition curve of the bed using coal particles

- Procedures similar those described in section 3.8.1 were followed for the tests. The only difference is that coal particles were used instead of density tracers. The partition data was derived from the following calculations: total mass of the feed particles, total mass of the floats, total mass of the sinks, the yield, % reconstituted feed, % sinks (partition coefficient) and the nominal specific density. All the above data was tabulated as shown in Appendix D.
- The respective Ep values and effective cut densities of the coal particles were determined as discussed above. The Klima and Luckie model was also used to fit the partition data and approximate some of the critical process parameters such the Ep and ρ_{50}.

Chapter 4

Characterization Tests for the fluidized bed media

Dry coal beneficiation using an air fluidized bed has already proved to be a very efficient separation process with encouraging industrial Ep values getting as low as 0.04 in some instances. However, maintaining a stable and uniform bed density throughout the three dimensional space still remains a challenge to the development of the continuous processing system. Moreover, fluidized beds behave differently when the solid properties, gas velocities or vessel geometries are varied. Hence, as part of this project, characterization tests aimed at establishing the optimum media and operating parameters for the 3 D fluidized bed were done before any detailed separation tests could be carried out.

4.1 Characterization of the medium particles – Silica and magnetite

The air fluidized coal separator uses an air – solid suspension as a beneficiating medium whose density is consistent with the beneficiating density. Preliminary tests aimed at establishing the optimum medium properties required for coal separation using the 3D air fluidized bed were carried out using magnetite and silica of different particle size distributions shown in the chart below. Approximate minimum fluidizing velocities of the different medium particles were initially calculated using the Ergun equation (2.17), but the actual U_{mf} values were later on determined using the pressure – velocity graphs plotted using the experimental data.

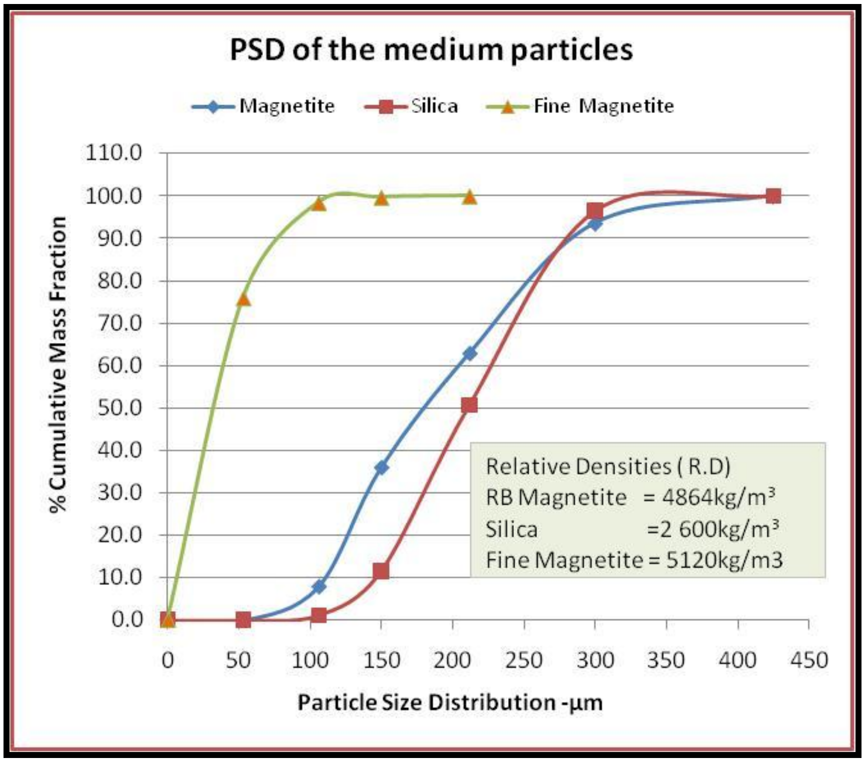

Figure 4.1: Particle size distributions of the different medium particles

4.1.1 Silica

Silica with a specific density of 2600kg/m3 and particle size distribution of (+53 - 450µm) as shown in Figure 4.1 above was initially used to carry out some characterization tests with a fixed bed height of 35 cm. All the 53µm particles were washed off before tests mainly for dust control purposes. According to some previous fluidization studies *(Geldart etal., 1986)*, a powder with a wide particle size distribution can fluidize more satisfactorily than a powder with a narrow size range. Such kind of beds are characterized by smaller wind box fluctuations, less vibration of the bed, and less tendency to slug and this is attributed to a smaller bubble sizes promoted by the wide size distribution. Although a relatively wide particle size distribution was used in this study, it was found that the wider the particle size distribution, the more likely is segregation going to take place as particles of different sizes have got different minimum fluidizing velocities. In order to check if there was any segregation taking place in the bed, random samples were grabbed from the different bed levels and screened off so as to determine the particle distribution of the various samples as illustrated in Figure 4. 2 below.

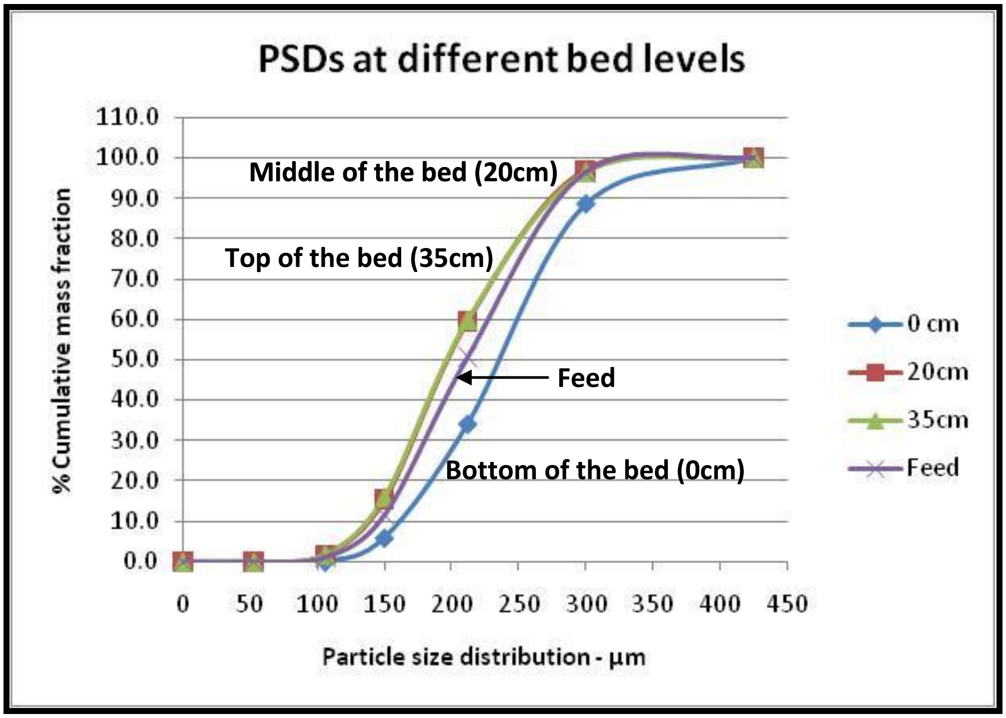

Figure 4.2: Particle size distributions of silica at the different bed levels

From the above plots, it can be seen than there was more coarse material (300 - 450µm) at the bottom of the bed (0cm) than at the middle (20cm) and the top (35cm) bed levels. The particle size distribution curves of both samples collected at the different bed levels slightly deviate from the medium feed PSD curve. This deviation can be attributed to segregation taking place in the bed due to the different minimum fluidizing velocities of the (+53 -300 µm) and the (+300 - 450 µm) particles. The segregation effect is more pronounced at the bottom of the bed where there is a relatively high portion of the (+300 - 450 µm). Otherwise from the intermediate levels of the bed right to the top, the particle size distribution is relatively uniform.

The silica medium particles belong to Geldart's group B powders. The interparticles forces are negligible and bubbles start to form in this type of powder at or only slightly above the minimum fluidization velocity. The bed expansion is very small and the bed collapses very rapidly when the gas supply is cut off. Back mixing of dense phase gas is relatively low, as is gas exchange between bubbles and dense phase. When the gas velocity is so high that slugging commences, the slugs are initially symmetrical about the bed axis, but with a further increase in gas velocity an increasing proportion becomes asymmetric, moving up the bed wall with an enhanced velocity rather than the bed axis.

The shape of the particles has got a significant effect on the quality of fluidization and spherical particles are always associated with good quality fluidization. The picture below shows the microstructure of the silica particles.

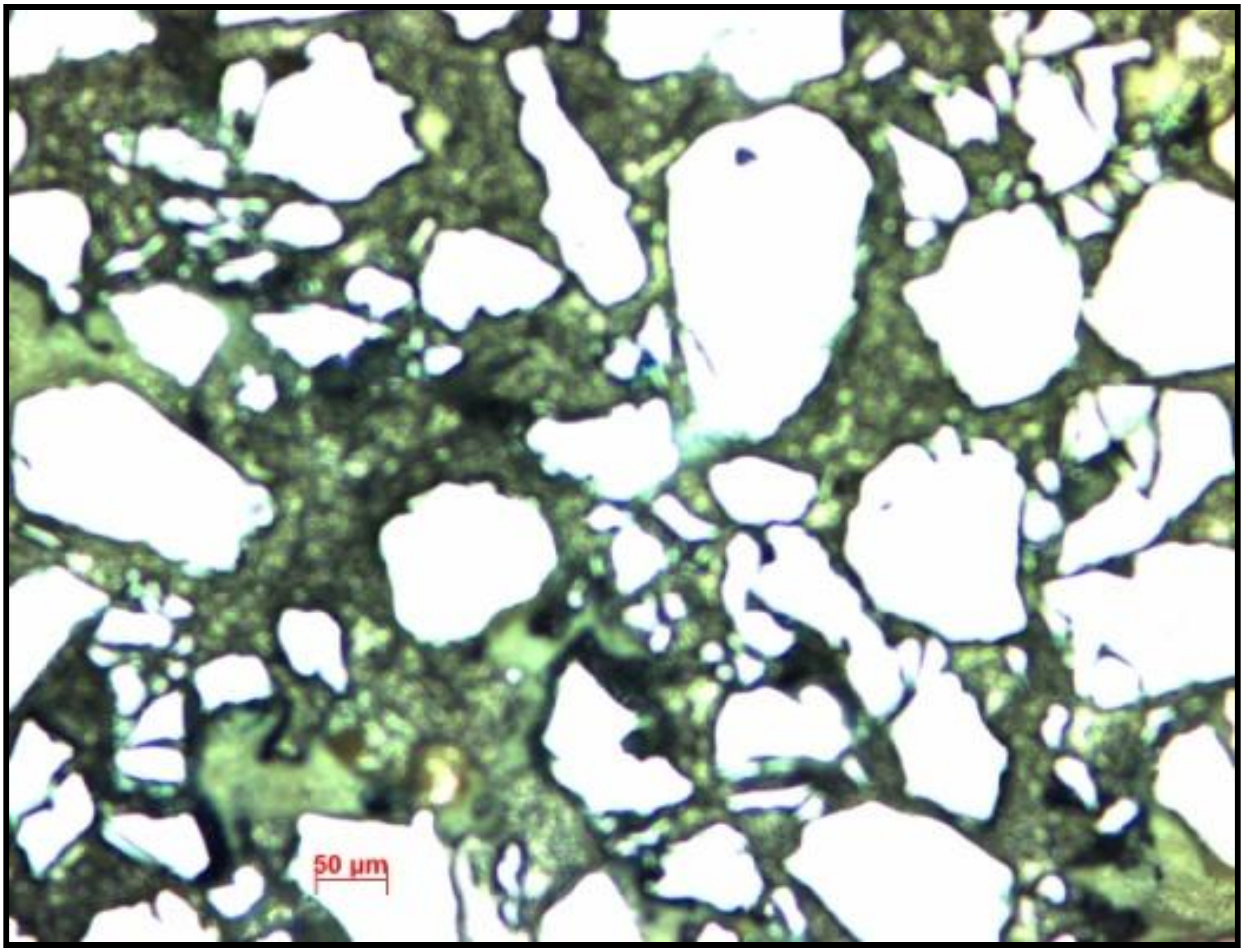

Figure 4.3: Microstructure of the silica medium particles

The silica particles approximate a round shape and tend to fluidize well as they promote the generation of relatively uniform micro bubbles. From the above photograph, it can also be seen that the particle size distribution is wide enough to enhance good quality fluidization.

4.1.2 Magnetite

Magnetite from Richards Bay Minerals with a particle size distribution of (+53 - 450 µm) was used as the medium for some of the preliminary characterization tests that were carried out. The magnetite has got a specific density of 4864kg/m^3 and belongs to Geldart's group A. The magnetite is slightly cohesive and expands considerably at velocities between U_{mf} and the velocity at which bubbling commences, U_{mb}. As the gas velocity is increased above U_{mb}, the bed height becomes smaller because the dense phase voidage is reduced more quickly with increasing gas velocity than the bubble hold up increases. When the gas supply is suddenly cut off, the bed collapses at a rate comparable to the superficial velocity of the gas in the dense phase of the bubbling bed (*Geldart etal., 1986)*.

Random samples were grabbed from the different bed levels and the particle size distribution was found to be relatively uniform throughout the bed, see Figure 4.4 below.

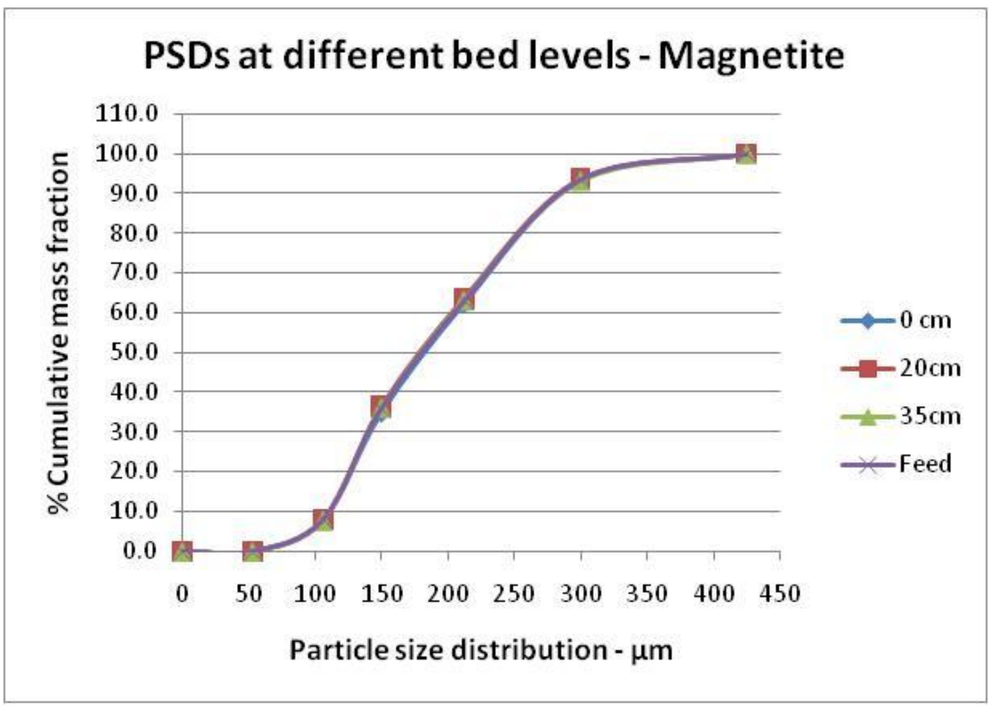

Figure 4.4: Particle size distributions of magnetite at different bed levels

The microstructure of the magnetite medium is shown in Figure 4.5 below. The magnetite is a mixture of small rounded particles and sharp edged big particles whose microstructure resembles that of crushed particles. The medium fluidized uniformly and a relative stable bed density was obtained.

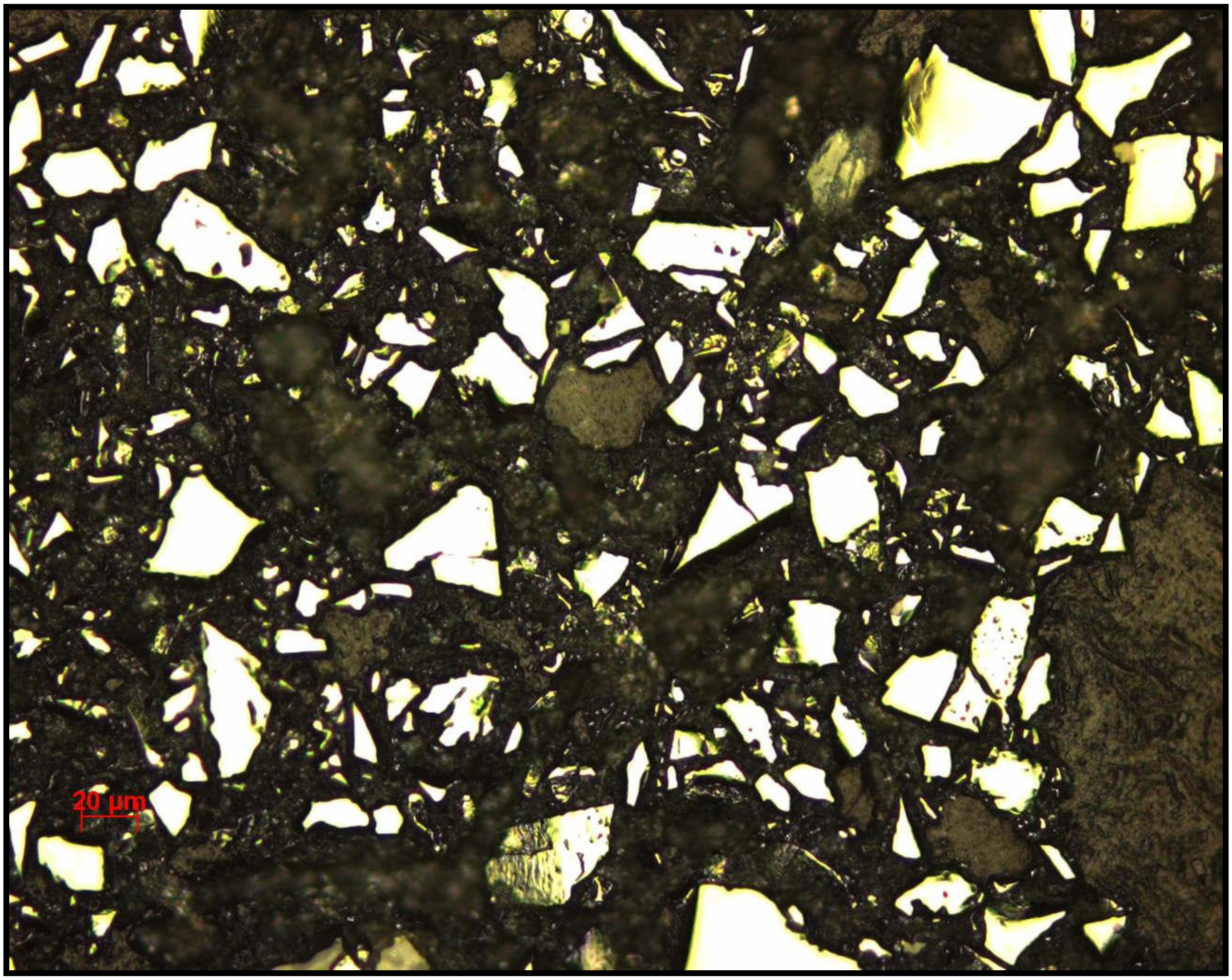

Figure 4.5: microstructure of the magnetite medium

4.1.3 Fine magnetite

Fine magnetite similar to the one used in wet dense medium separation was used as the medium in some of the preliminary characterization tests. The medium had a particle size distribution of (+15 - 150µm) with approximately 75% mass fraction of the medium less than 50 µm (see Figure 4.1). The fine magnetite is cohesive and belongs to Geldart's group C, such kind of material is very difficult to fluidize mainly because of the strong interparticle forces being greater than those which the fluid can exert on the particle. This is probably as a result of the small particle size, strong electrostatic charges, sticky particle surfaces, soft solids having a very irregular shape as shown in the Figure 4.6. Soft solids can easily deform and give a large surface area for interparticle contacts *(Geldart etal., 1986).*

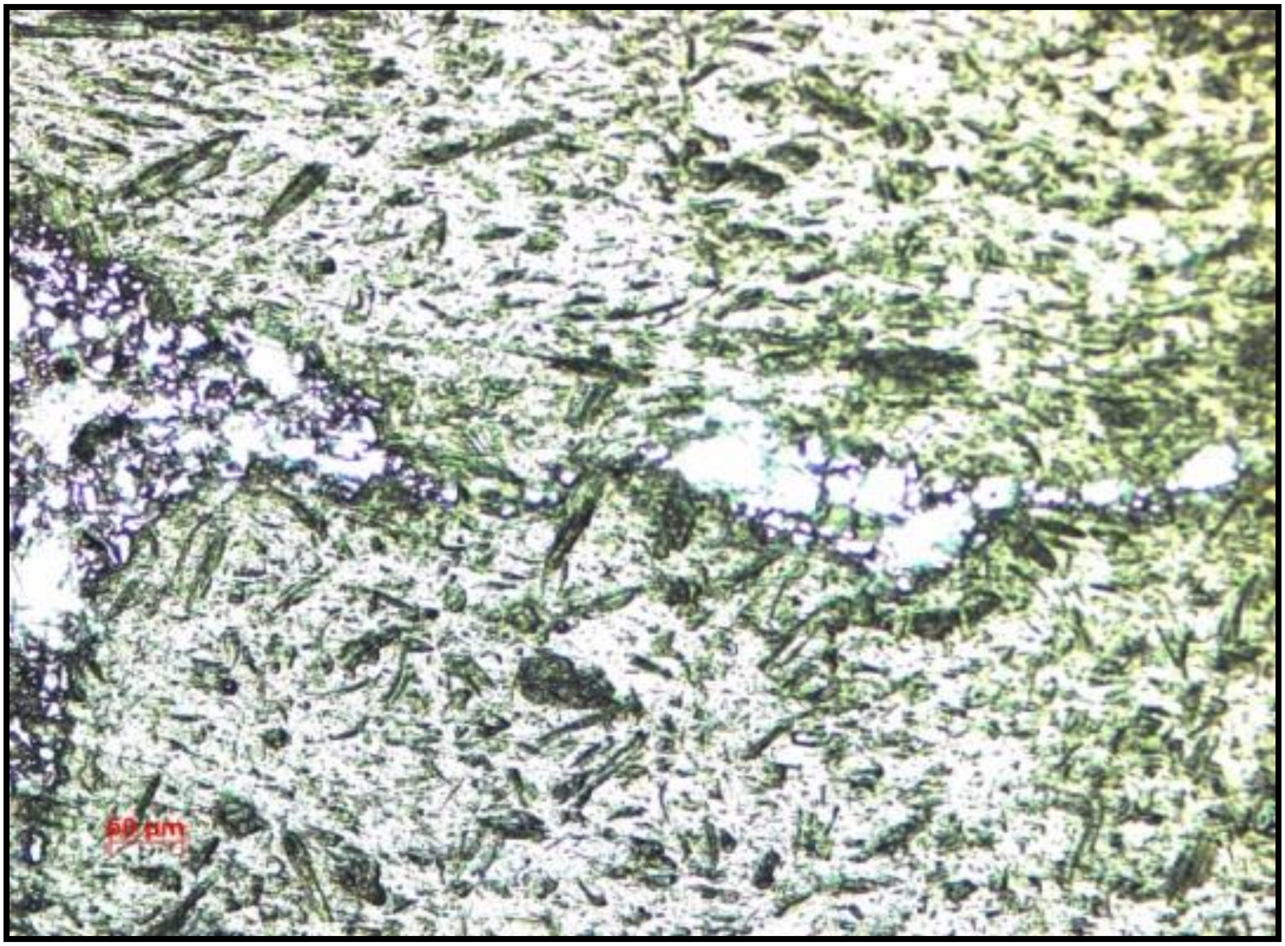

Figure 4.6: microstructure of fine magnetite

From the above microstructure photograph of the fine magnetite, it can be seen that the particles are fibrous in shape and can easily agglomerate. The medium is extremely difficult to wash and dry for dust control purposes. The fine magnetite bed channels badly, as the gas passes through interconnected vertical and inclined cracks extending from the distributor to the bed surface. The pressure drop across the bed is, on the whole, lower than the theoretical value (bed weight per unit cross – sectional area) and can be as little as half. Due to the above challenges associated with the operation of the fine magnetite bed, it was concluded that the fine magnetite with the particle size distribution of (+15 - 150μm) cannot be used for dry coal separation using an air fluidized bed.

4.1.4 Compound mixture of silica and magnetite

The density of most of the coals processed in South Africa varies from (1.30 – 2.70). However, average bed densities of 1.34 and 2.70 were obtained using the silica and magnetite beds respectively when operating at (1.2 – 1.45) U_{mf}. Hence the need to mix silica and magnetite in different proportions so as to get the medium with the capacity to process the wide density range of coals. Before mixing the two different media, their minimum fluidizing velocities for the different particle size distributions were initially calculated using the Ergun equation (2.17) and later on interpolated from the pressure velocity graph as shown in Figure 4.7 below. 45kgs of (+53 - 212µm) magnetite were mixed with 80kgs of (+53 - 300µm) silica to give a compound mixture, which was fluidized at 1.4U_{mf} to give an average bed density of approximately 1.64.The theory behind the determination of the mixing proportions of silica and magnetite is given in section 4.5.

4.1.5 Minimum fluidizing velocities of the medium particles

Minimum fluidizing velocity, U_{mf} is one of the most important parameters in the characterization of the medium particles as it determines the quality of fluidization that can be obtained using medium particles of different sizes and densities. The minimum fluidizing velocity can be calculated using the Ergun equation (2.17) that is for laminar flow or can be determined experimentally through the use of pressure drop versus velocity graphs.

Figure 4.7 shows the pressure velocity diagram for the compound mixture of the silica – magnetite medium and it can be seen that at relatively low gas flow rates in a fixed bed the pressure drop is approximately proportional to the gas velocity until a maximum pressure drop of ΔP_{max} is attained. This is slightly higher than the static pressure of the bed and any further increase in the gas velocity unlocks the fixed bed. The bed voidage increases from ε_{static} to ε_{mf} resulting in a decrease in pressure drop to the static pressure of the bed *(Kunii, Levenspiel etal., 1991)*. Increase in the gas velocity beyond minimum fluidization results in the expansion of the bed and gas bubbles are observed resulting in non homogeneity. However, the pressure drop remains relatively constant because the dense gas – solid phase is well aerated and can deform easily without appreciable resistance. A decrease in the gas velocity results in the fluidized particles settling down to form a loose fixed bed of voidage. When the gas flow is eventually turned off, a gentle tapping or vibration of the bed reduce its voidage to its stable initial value *(Kunii, Levenspiel etal., 1991).*The U_{mf} can be taken as the intersection of the pressure drop versus gas velocity line for the fixed bed of voidage ε_{mf}, with the horizontal line corresponding to the constant pressure drop section as illustrated in Figure 4.7.

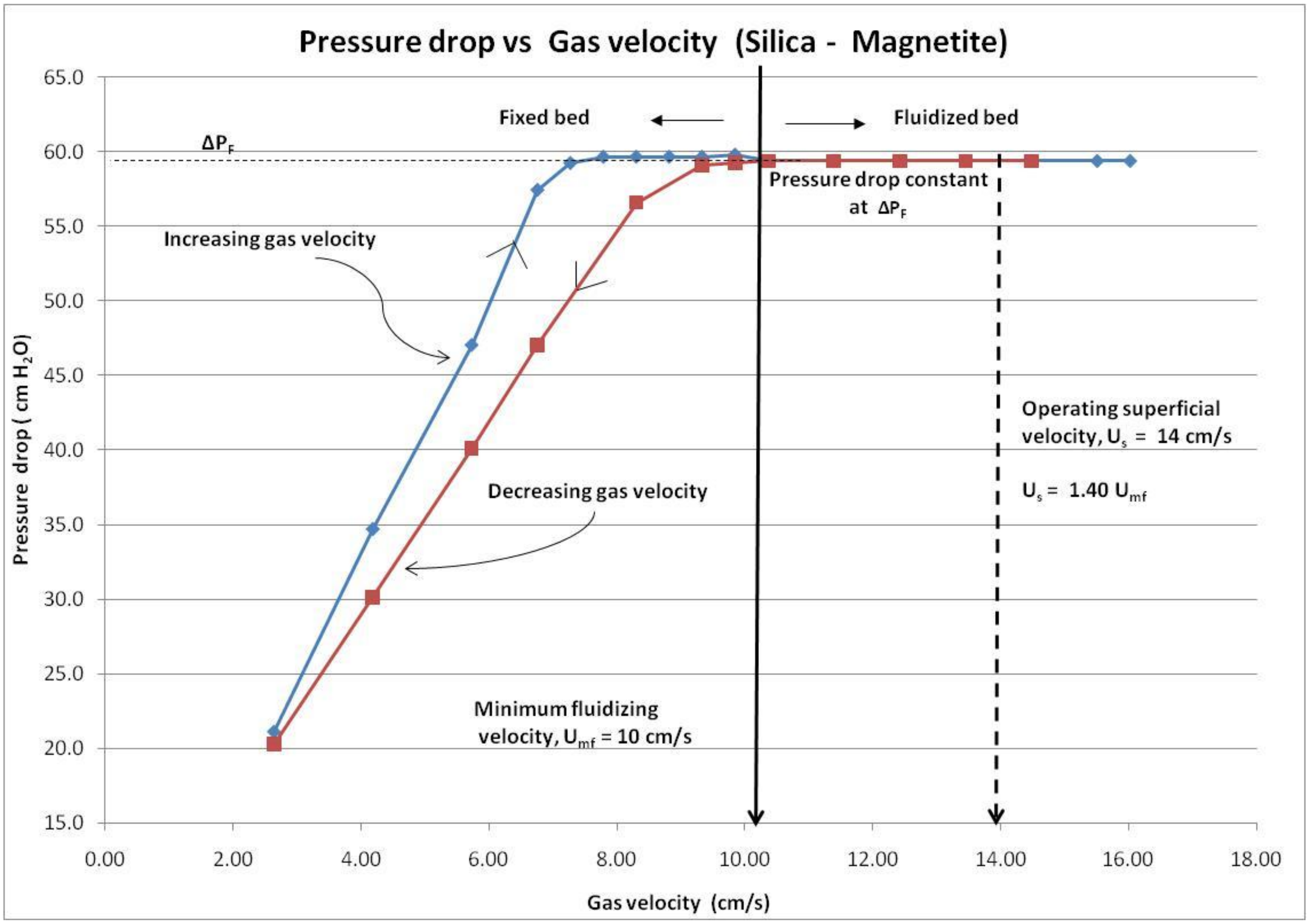

Figure 4.7: Pressure drop versus Gas velocity for silica –magnetite compound medium

Using the above technique, the minimum fluidizing velocity for the compound mixture of silica and magnetite was found to be 10cm/s and an operating superficial velocity of 14cm/s was used for the detailed tests. A similar approach as the one above was used to also determine the minimum fluidizing velocities of the different medium particles that were used during the preliminary characterization tests. The minimum velocities of separate beds of silica and magnetite were estimated at 9cm/s and 11.4cm/s respectively. This data is critical in the determination of the optimum particle size distributions of silica and magnetite that should be mixed in order to obtain the compound medium.

4.2 Characterization of the coal particles

Since this project involves investigating the effect of the particle size and shape on the performance of an air fluidized bed in dry coal beneficiation, coal particles of different sizes, densities and shapes were used for the detailed separation tests. The particles were characterized as discussed in the subsections below:

4.2.1 Particle size

The effect of the particle size was investigated using the particle size ranges outlined in section 3.4.1 of Chapter 3.

4.2.2 Particle density

The particle density ranges discussed in section 3.4.2 were used for the detailed laboratory tests.

4.2.3 Particle shape

It is difficult to define particle shape quantitatively so during the separation tests only qualitative descriptions were used to identify the different particle shapes. The effect of the following shapes was investigated during the tests.

Figure 4.8(a): Blockish Particles

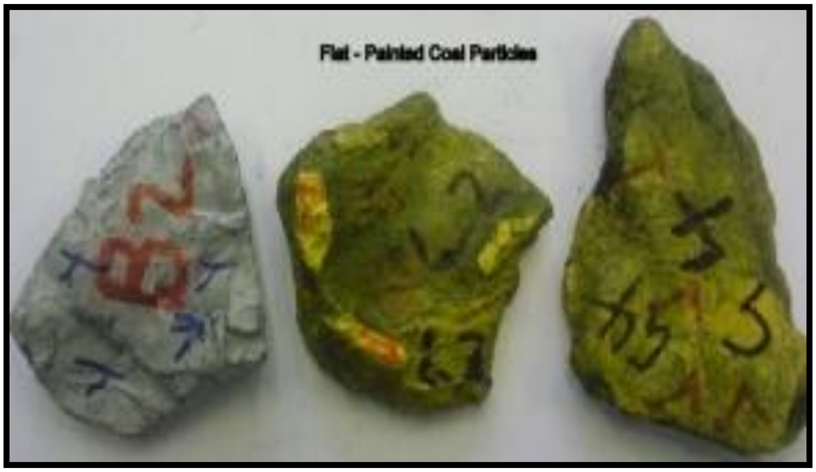

Figure 4.8(b): Flat Particles

Figure 4.8(c): Sharp pointed prism particles

Meanwhile, Heywood's approach was used to characterize some of the coal particles that were used for the rise velocity tests (see Appendix B).

4.3 Characterization of the Silica bed

Preliminary tests were carried out using a silica bed with a fixed bed height of 35cm and silica with a particle size distribution of (+53 - 450µm) was used as the medium. The minimum fluidizing velocity of the bed was determined from the pressure drop versus gas velocity diagram as discussed above and it was found to be 9cm/s. The minimum fluidizing velocity, pressure drop profiles obtained at various gas velocities and bubble behavior observations are some of the tools that were used to determine the optimum operating gas flow rate. For the silica bed characterization tests, an optimum superficial velocity of 11.4cm/s was used.

All the pressure measurements were carried out following the sampling plan (Figure 3.3) and procedures outlined in section 3.5 of Chapter 3. Pressure drop profile plots i.e. (Pressure drop vs. Bed level) were made for each respective sampling point in the bed and the results are discussed below.

Pressure drop profile graphs for the silica bed

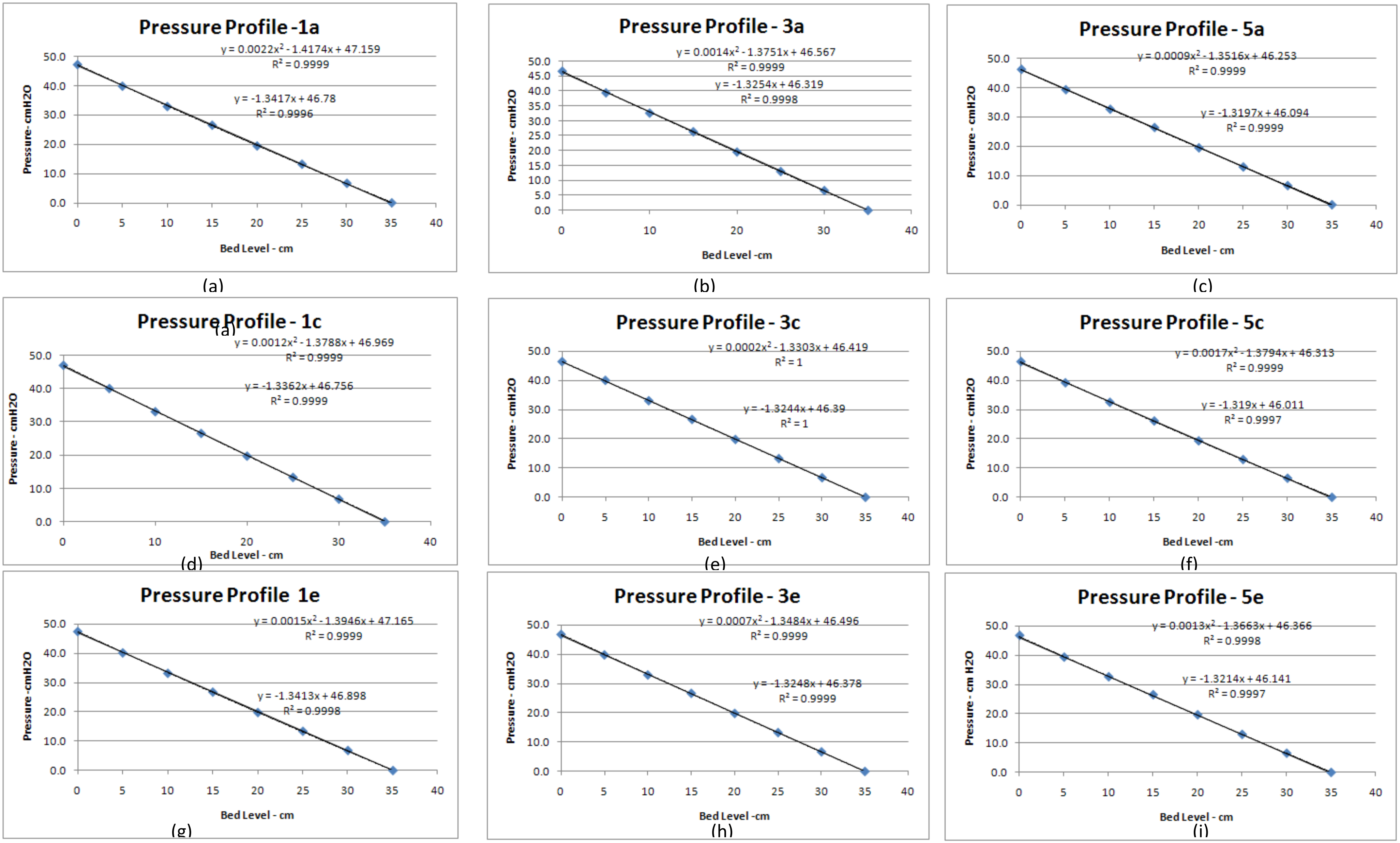

Figure 4.9 (a) – (i): Pressure profile graphs for the silica bed

The pressure drop (cm H_2O) data was plotted against the bed level (cm) and the graphs are shown above. Linear and quadratic fits were used to analyze the behavior of the bed and they both showed strong correlations with an average $R^2 \approx 1$ being obtained. However of the two fits, the quadratic fit is the only one which can be easily evaluated to show how the bed density varies at the different bed levels. On the other hand, the linear fit can also be analyzed and give the average bed density per each sampling point profile. Using equations (3.6), (3.7) and (3.8), the bed densities at the various bed levels can be calculated

$$P = -\rho_{bed}\, g\, (h_{top} - h) \tag{3.6}$$

$$P = -\rho_{bed}\, g\, h_{top} + \rho_{bed}\, g\, h$$

Where $-\rho_{bed}\, g\, h = P_o$ (pressure drop across the bed)

$$\rho_{bed}\, g = gradient = \frac{dP}{dh}$$

To calculate the gradient of a quadratic function, take differentials both sides,

$$dP = -\rho_{bed}\, g\, dh \tag{3.7}$$

$$\rho_{bed} = \frac{-(Gradient \times 10000)}{9.81} \tag{3.8}$$

The calculated bed density data was then plotted against the bed level to give the bed density distribution profiles across the bed. See Figure 4.10 below.

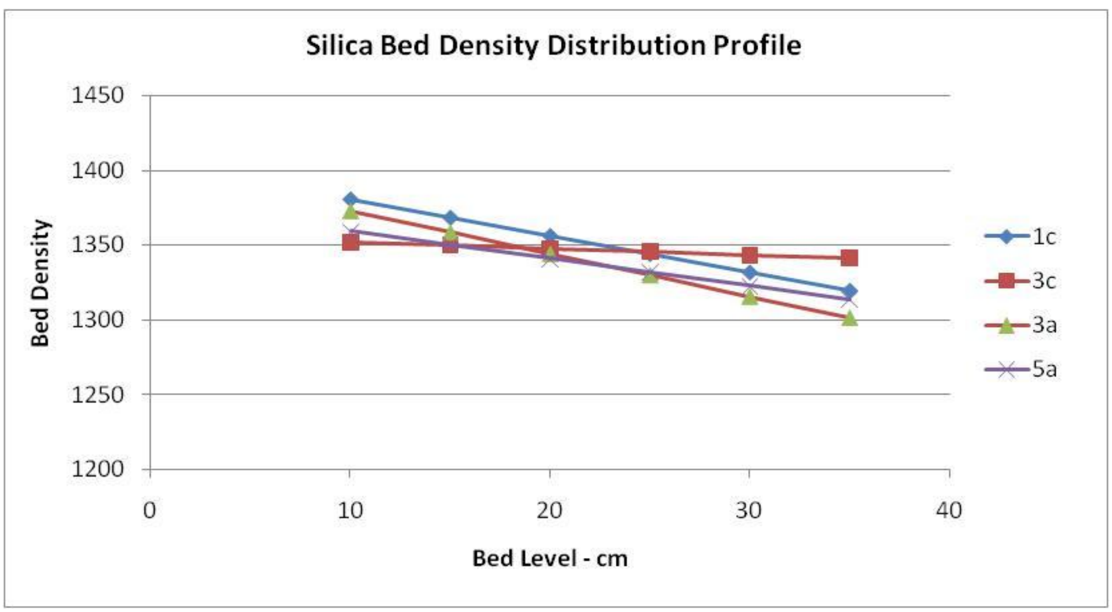

Figure 4.10: Silica bed density distribution profile

From Figure 4.10, it can be seen that the silica bed density is relatively uniform throughout the bed with an average bed density of 1.35 being obtained. A small standard deviation of less than 5 was recorded at the centre of the bed (point 3c). On the other hand, relatively high standard deviations were recorded for profiles 3a and 1c. This could be either as a result of the wall effect since the sampling points are close to the bed walls or this could also be due to the segregation of the medium particles as discussed above. The observed trend stresses the need to determine an optimum particle size distribution of the medium before any detailed tests are carried out.

The density of most of the South African coals varies from (1.30 – 2.70), hence an average silica bed density of 1.35 will be too low for coal processing, hence the need to consider other separation medium with a higher relative density e.g. magnetite.

4.4 Characterization of the Magnetite bed

As part of determining the optimum medium to use for the detailed separation tests, preliminary tests using magnetite with a particle size distribution of (+53 - 450μm) and fixed bed height of 35cm were carried out. The minimum fluidizing velocity of the bed was determined from the pressure drop versus gas velocity diagram as discussed above and it was found to be 11.2cm/s. An optimum operating gas flow rate of 14.5cm/s was used for the magnetite bed characterization tests.

Using a similar approach to the one outlined above for the silica bed, pressure measurements were recorded at the various bed levels following the sampling plan as illustrated in Figure 4.9. The pressure drop data was then plotted against the bed level to give the plots shown below.

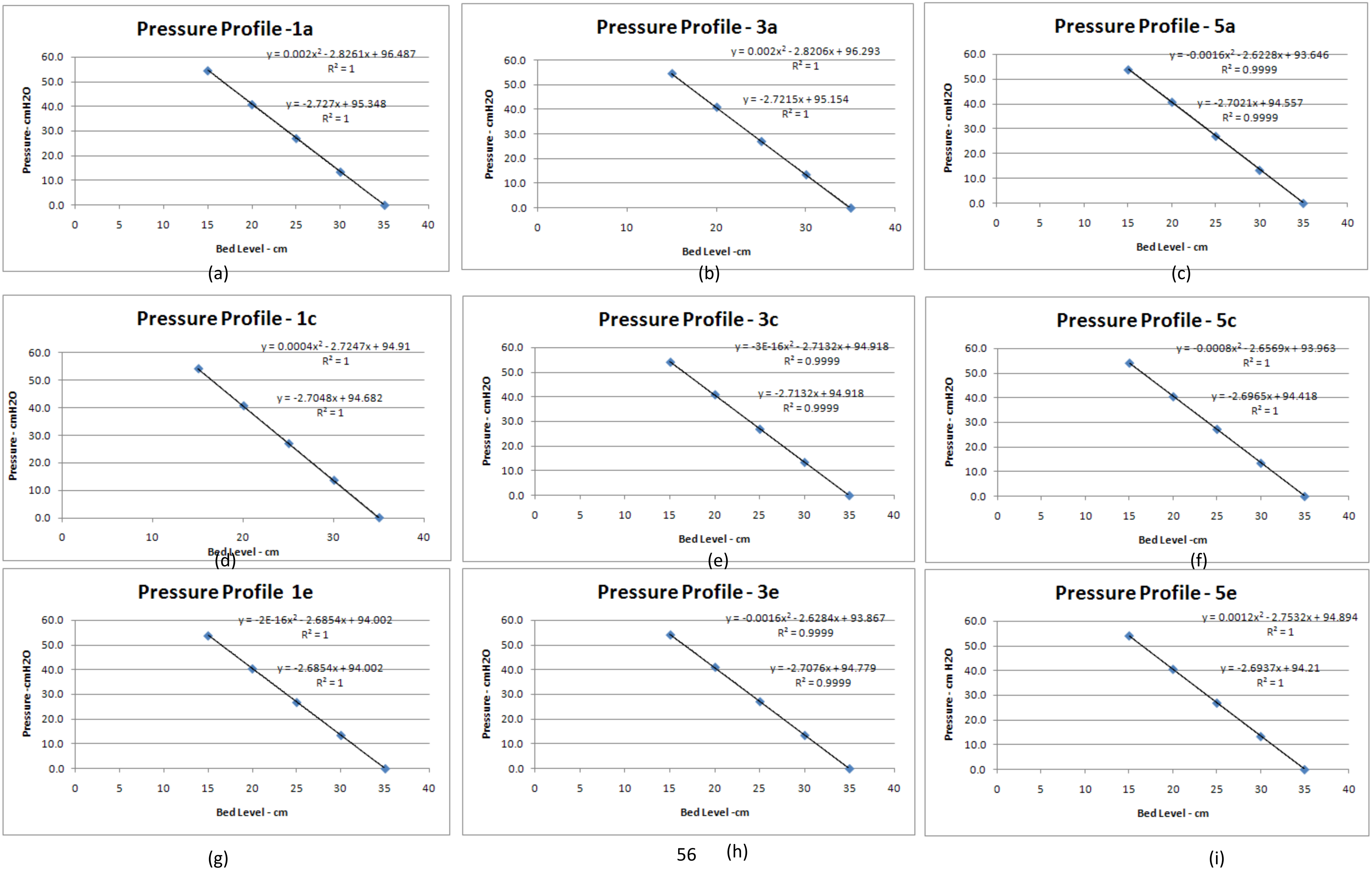

Figure 4.11 (a) – (i): Pressure drop profile graphs for the magnetite bed

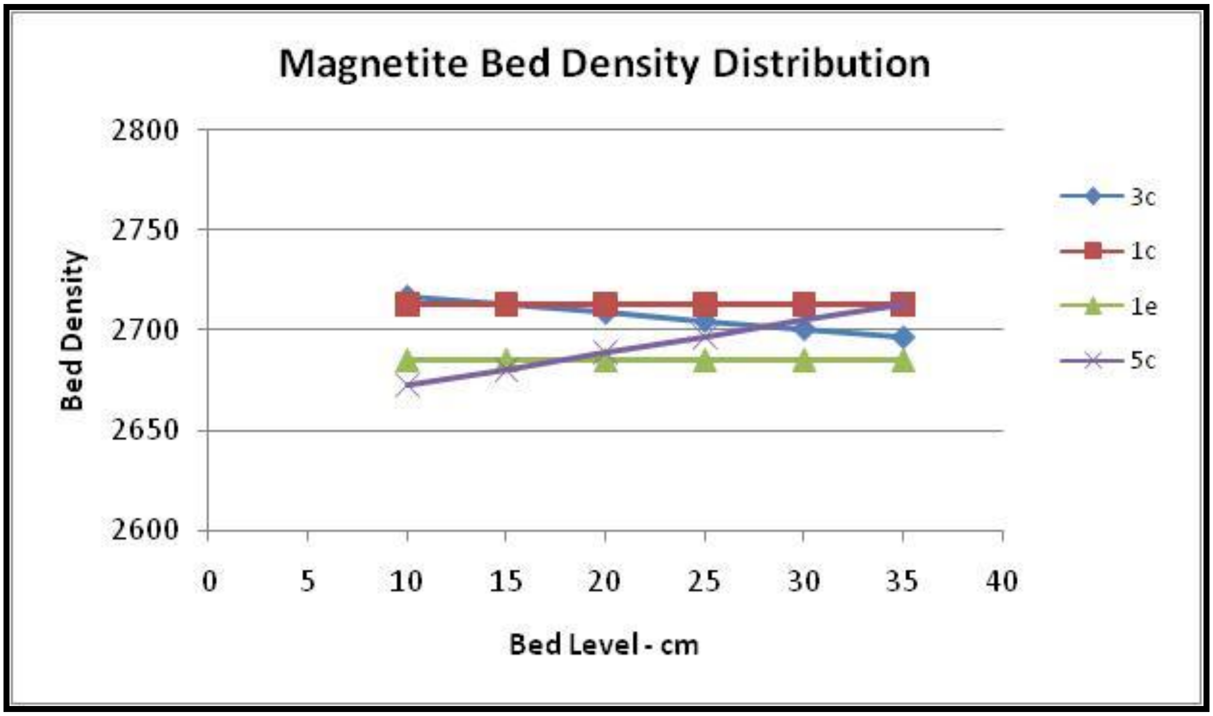

Figure 4.12: Magnetite bed density distribution profile

The bed density distributions of the magnetite bed were determined from the above pressure drop profile plots with equations (3.6), (3.7) and (3.8) used to calculate the bed density as outlined in the discussion for the silica bed. A relatively uniform and stable average bed density of 2.70 was obtained throughout the bed with standard deviations as low as zero being recorded in some instances (see Appendix C). However the bed density is too high to be used as the operating cut density for processing South African coals, hence the need to blend the magnetite with some other medium with a relatively low relative density e.g. silica.

4.5 Characterization of the Silica - Magnetite bed

Different proportions of silica and magnetite were mixed to form a compound mixture of silica and magnetite, which was used for the detailed tests. However, the main challenge on the use of a compound medium is the selection of the optimum parameters that will ensure good quality fluidization without any segregation of the medium particles. The minimum fluidizing velocities of the different particle sizes of both magnetite and silica are very critical at this stage as well as the relative densities of the two different media. The empirical data gathered from the preliminary tests discussed above was used as the basis for selecting the optimum compound mixture parameters. As a result 45kgs of (+53 - 212µm) magnetite were then mixed with 80kgs of (+53 - 300µm) silica to give a compound mixture, which was fluidized at $1.4U_{mf}$ to give an average bed density of approximately 1.64. The theory behind the determination of the optimum mixing proportions of silica and magnetite is discussed below.

From Figure 4.7, it can be seen that the fluidized bed used in dry coal separation is operated in the superficial velocity range where the pressure drop across the bed is constant. A constant pressure drop means the bed voidage and volume is also relatively constant. Using equation 2.2 given in Chapter 2, the bed voidage for both the silica and magnetite beds can be calculated as follows:

From, $\rho_{bed} = (1-\epsilon)\rho_s$ (2.2)

$$\epsilon = 1 - \frac{\rho_{bed}}{\rho_s}$$

The silica bed voidage, ϵ_s is then given by

$$\epsilon_s = 1 - \frac{1.35}{2.60}, \qquad \epsilon_s = 0.48$$

For the magnetite bed voidage, ϵ_m

$$\epsilon_m = 1 - \frac{2.70}{4.864}, \qquad \epsilon_m = 0.45$$

Based on the theory discussed above and assuming that the changes in the bed voidage are negligible then,

$$V_{bed} \approx V_s + V_m \tag{4.1}$$

where V_{bed} - volume of the bed, m^3

V_s - volume of fluidized silica, m^3

V_m - volume of fluidized magnetite, m^3

Since, $Mass\ (M) = volume\ (V) \times density(\rho)$

Then,

$$\frac{M_s + M_m}{\rho_{bed\,(sm)}} = \frac{M_s}{\rho_{bs}} + \frac{M_m}{\rho_{bm}} \tag{4.2}$$

$$\frac{M_s}{\rho_{bed\,(sm)}} + \frac{M_m}{\rho_{bed\,(sm)}} = \frac{M_s}{\rho_{bs}} + \frac{M_m}{\rho_{bm}} \tag{4.3}$$

where M_s - mass of the silica in the compound mixture, kg

M_m - mass of the magnetite in the compound mixture, kg

ρ_{bs} - silica bed density

ρ_{bm} - magnetite bed density

$\rho_{bed\,(sm)}$ - silica – magnetite bed density

For instance, if a silica - magnetite bed density, $\rho_{bed\,(sm)}$ of 1.64 is required and the initial mass of the silica, M_s= 80kg, then the mass of the magnetite required for the compound mixture can be approximated using the equations above. From the previous characterization tests discussed above, the values of ρ_{bs} and ρ_{bm} are 1.35 and 2.70 respectively.

Substituting the given values into equation, then

$$\frac{80}{1.64} + \frac{M_m}{1.64} = \frac{80}{1.35} + \frac{M_m}{2.70} \tag{4.4}$$

Solving the above expression, $M_m \approx 45kg$

Characterization tests of the silica – magnetite bed included pressure drop measurements at the different bed heights. The pressure drop data was then plotted against the bed level as shown in the pressure drop profile plots in Appendix C. Linear and quadratic fits were used in the analysis and study of the bed's behavior. A similar approach to the one that was used for the determining the bed density distribution in the silica and magnetite beds was also applied to the silica – magnetite bed (see Appendix C).

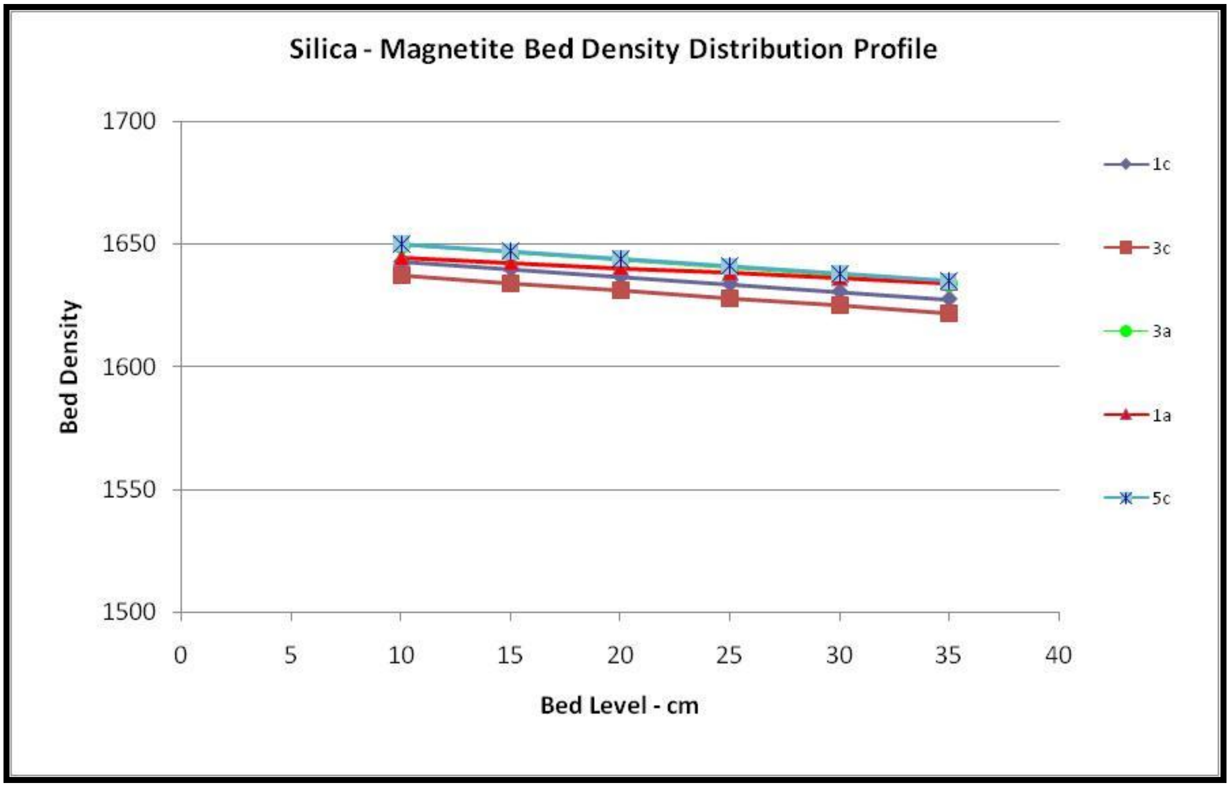

Figure 4.13: Magnetite bed density distribution profile

From the above silica – magnetite density distribution profile, it can be clearly seen that a relatively uniform and stable average bed density of 1.64 was obtained throughout the bed with a STDEV < 0.01 (Appendix C). The bed density can be adjusted by changing the mixing the proportions of silica and magnetite in the bed as discussed above.

4.6 Measuring the performance of the 3D fluidized bed – Partition curves

The performance of the 3D fluidized bed was initially assessed using 20mm disc and cube shaped density tracers. The density range of the tracers used for the tests varied from (1.30 – 2.10) and at least ten particles were picked from each density range. Several tests were carried out using the density tracers at different running times ranging from 15s to 30 minutes (steady state).The collected data was used to plot partition curves discussed below.

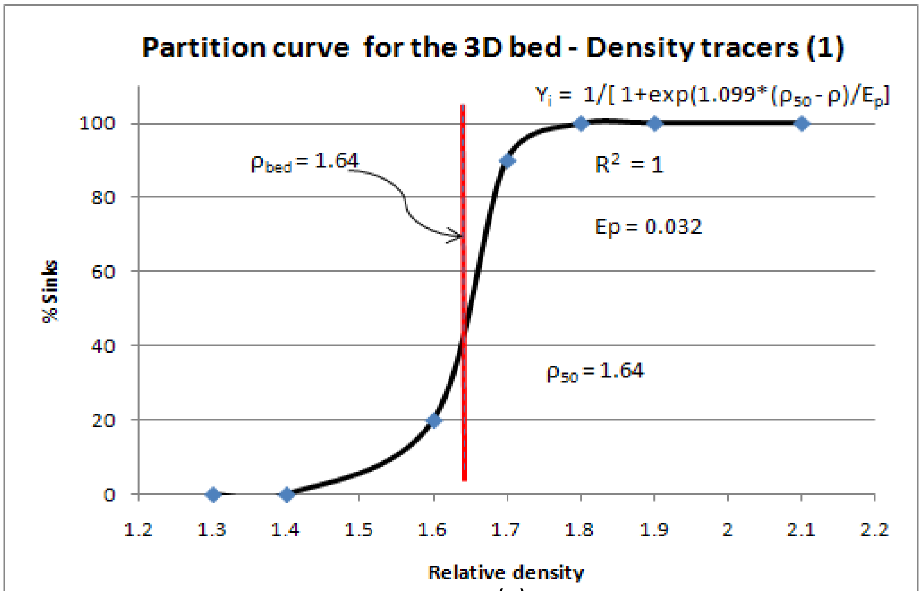

(a)

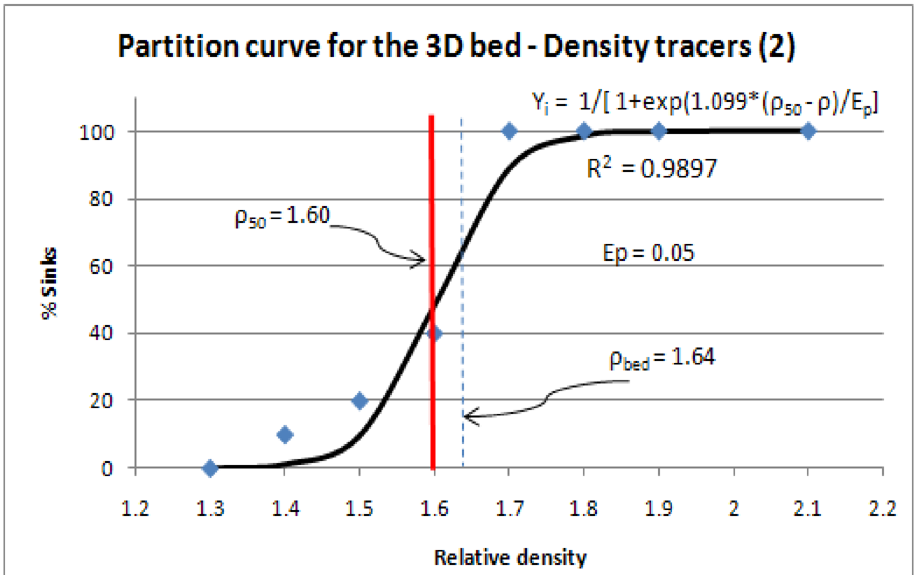

(b)

Figure 4.14 (a) – (b): Partition curves for the 3D fluidized bed using density tracers

The Klima and Luckie model which is one of the widely used partition functions was used to fit the partition curves for the 3 D bed *(Napier Munn etal., 1991)*. The partition function fitted the partition data very well with an $R^2 \approx 1$ being obtained in some instances. Since, the model incorporates two parameters which are most familiar to practitioners (Ep & ρ_{50}), it was also used to estimate the Ep and ρ_{50} values for the 3D fluidized bed. The Klima and Luckie model states that,

$$Y_i = \frac{1}{1 + \exp\left[\frac{1.099\,(\rho_{50} - \rho)}{Ep}\right]} \qquad (4.5)$$

where Y_i - partition coefficient

ρ_{50} - cut density

ρ - particle density

Ep - Separation inefficiency (Ecart Probable Moyen)

1.099 – empirical constant

Figures 4.14 (a) – (b) above illustrate the partition curves that were obtained after 5 minutes and 15s respectively. The 3 D bed proved to be an efficient piece of equipment with Ep values ranging from as low as (0.032 – 0.05) being obtained under steady state conditions characterized by minimum fluctuation of the effective cut density. From the partition curves shown above, it can be clearly seen that the separation process takes place quickly as evidenced by the relatively low average Ep value of 0.05 that was recorded just after 15s. Results of the detailed separation tests that were carried out using coal particles are discussed in the following chapter.

Chapter 5

Rise /Settling velocity Tests

Rise and settling velocity tests were carried out following the different techniques that have already been discussed in Chapter 3. A fixed bed height of 32cm and an average bed density of 1.64 were used for these tests. Given the resources and facilities that were at our disposal in the laboratory, the proposed settling tests technique was more practical than the rise velocity technique hence more quantitative data was generated from the settling tests.

A feed with a wide particle size range (+9.5 – 53mm) and density range (1.30 – 2.60) was used for the settling tests. Different running times ranging from 5s – 600s were used for the dynamic settling tests. After every run, the particles were tracked and sorted out according to their respective positions in the bed. This data was then used to calculate the relative settling velocities of the particles as well as measuring the performance of the separation process for the different particle size ranges after specific time intervals. This was achieved through plotting partition curves for the various particle size ranges as discussed in the following section.

5.1 Settling Tests – Partition curves

A brief outline of the procedures that were followed in order to generate the dynamic and steady state settling partition data is given below. The 3D fluidized bed was turned on and the air flow rate was continuously adjusted until a stable fluidization state was achieved. A feed sample of the material to be separated was then introduced from the top. After running for different time intervals e.g. (5s, 10s, 15s, 30s, 60s and 600s), the air was stopped and all the particles recovered above the 20cm bed height were classified as floats whilst those recovered below the 20cm mark were regarded as sinks. The collected data was treated and summarized in a table like the one shown below where floats and sinks were marked using letters ‘F’ and ‘S’ respectively (see Table 5.1). The following formulae were used to calculate the various parameters such as the float analysis (wt.%), sinks analysis (wt.%), partition coefficient etc *(Wills etal., 2006)*.

$$Floats\ analysis\ (wt.\%) = \frac{mass\ of\ floats\ recovered\ within\ a\ specific\ density\ fraction \times 100\%}{Total\ mass\ of\ the\ float\ particles} \tag{5.1}$$

$$Sinks\ analysis\ (wt.\%) = \frac{mass\ of\ sinks\ recovered\ within\ a\ specific\ density\ fraction \times 100\%}{Total\ mass\ of\ the\ sink\ particles} \tag{5.2}$$

$$Floats\ \%\ of\ feed = \frac{mass\ of\ floats\ recovered\ within\ a\ specific\ density\ fraction \times 100\%}{Total\ mass\ of\ the\ feed\ particles} \tag{5.3}$$

$$Sinks\ \%\ of\ feed = \frac{mass\ of\ sinks\ recovered\ within\ a\ specific\ density\ fraction \times 100\%}{Total\ mass\ of\ the\ feed\ particles} \tag{5.4}$$

$$Reconstituted\ feed\ \% = Floats\ \%\ of\ feed + Sinks\ \%\ of\ feed \tag{5.5}$$

$$Norminal\ specific\ gravity\ (sp.Gr) = Average\ sp.Gr\ per\ density\ fraction \tag{5.6}$$

$$Partition\ coefficient = \frac{Sinks\ \%\ of\ feed}{Reconstituted\ feed\ \%} \times 100\% \tag{5.7}$$

The partition coefficient is the % of feed material of a certain nominal specific gravity which reports to sinks. The yield of the separation process was determined using the following formula:

$$Yield = \frac{Total\ mass\ of\ the\ floats}{Total\ mass\ of\ the\ feed} \times 100\% \tag{5.8}$$

Table 5.1 below shows the partition data for the (+37 -53mm) particles obtained after 15s and 30s of separation respectively. The rest of the partition data tables are included in Appendix D.

Table 5.1: Partition data for the (+37 -53mm) particles

						+37 -53mm																					
						15										30											
Density	Particles	Sp.gr of	Mass -	Volume-	Height / cm	Float/Sink	Mass		Floats	Sinks	Floats %	Sinks %	Reconstituted	Nominal	Partition	Height /cm	Float/Sink	Mass		Floats	Sinks	Floats %	Sinks %	Reconstituted		Nominal	Partition
Range	Used	Particle	Particle	Particle		F/S	Floats	Sinks	wt.%	wt.%	of feed	of feed	Feed %	sp. Gr	Coefficient		F/S	Floats	Sinks	wt.%	wt.%	of feed	of feed	Feed %	/density fraction	sp. Gr	Coefficient
	C2	1.30	78.66	60.51	32.00	F	78.66		5.96	0.00	2.70	0.00	2.70			32.00	F	78.66		6.95	0.00	2.70	0.00	2.70			
	A4	1.31	57.17	43.64	32.00	F	57.17		4.33	0.00	1.97	0.00	1.97			32.00	F	57.17		5.05	0.00	1.97	0.00	1.97			
	H4	1.32	29.56	22.39	32.00	F	29.56		2.24	0.00	1.02	0.00	1.02	1.33	0.00	32.00	F	29.56		2.61	0.00	1.02	0.00	1.02	12.25	1.33	0.00
1.30 - 1.40	C8	1.34	88.19	65.81	32.00	F	88.19		6.68	0.00	3.03	0.00	3.03			32.00	F	88.19		7.80	0.00	3.03	0.00	3.03			
	D8	1.36	53.58	39.40	32.00	F	53.58		4.06	0.00	1.84	0.00	1.84			32.00	F	53.58		4.74	0.00	1.84	0.00	1.84			
	E6	1.36	49.18	36.16	32.00	F	49.18		3.73	0.00	1.69	0.00	1.69			32.00	F	49.18		4.35	0.00	1.69	0.00	1.69			
	I9	1.40	44.74	31.96	32.00	F	44.74		3.39	0.00	1.54	0.00	1.54			31.00	F	44.74		3.96	0.00	1.54	0.00	1.54			
	J1	1.40	61.40	43.86	32.00	F	61.40		4.65	0.00	2.11	0.00	2.11			32.00	F	61.40		5.43	0.00	2.11	0.00	2.11			
	A5	1.41	106.11	75.26	32.00	F	106.11		8.04	0.00	3.65	0.00	3.65	1.42	0.00	32.00	F	106.11		9.38	0.00	3.65	0.00	3.65	14.46	1.42	0.00
	C1	1.41	59.38	42.11	32.00	F	59.38		4.50	0.00	2.04	0.00	2.04			32.00	F	59.38		5.25	0.00	2.04	0.00	2.04			
1.40 - 1.50	H2	1.43	78.82	55.12	32.00	F	78.82		5.97	0.00	2.71	0.00	2.71			32.00	F	78.82		6.97	0.00	2.71	0.00	2.71			
	A8	1.44	69.95	48.58	32.00	F	69.95		5.30	0.00	2.41	0.00	2.41			32.00	F	69.95		6.18	0.00	2.41	0.00	2.41			
	M2	1.50	50.47	33.65	31.00	F	50.47		3.83	0.00	1.74	0.00	1.74			31.00	F	50.47		4.46	0.00	1.74	0.00	1.74			
	F8	1.51	69.94	46.32	32.00	F	69.94		5.30	0.00	2.41	0.00	2.41			32.00	F	69.94		6.18	0.00	2.41	0.00	2.41			
	B9	1.51	49.22	32.60	32.00	F	49.22		3.73	0.00	1.69	0.00	1.69	1.52	0.00	28.00	F	49.22		4.35	0.00	1.69	0.00	1.69	10.11	1.52	0.00
	B4	1.52	60.36	39.71	31.00	F	60.36		4.58	0.00	2.08	0.00	2.08			29.00	F	60.36		5.34	0.00	2.08	0.00	2.08			
1.50 - 1.60	H5	1.53	43.83	28.65	32.00	F	43.83		3.32	0.00	1.51	0.00	1.51			32.00	F	43.83		3.88	0.00	1.51	0.00	1.51			
	E7	1.54	20.28	13.17	30.00	F	20.28		1.54	0.00	0.70	0.00	0.70			30.00	F	20.28		1.79	0.00	0.70	0.00	0.70			
	H9	1.60	68.78	42.99	25.00	F	68.78		5.21	0.00	2.37	0.00	2.37			18.00	M		68.78	0.00	3.87	0.00	2.37	2.37			
	B5	1.61	60.13	37.35	25.00	F	60.13		4.56	0.00	2.07	0.00	2.07			16.00	M		60.13	0.00	3.38	0.00	2.07	2.07			
	E4	1.61	59.26	36.81	29.00	F	59.26		4.49	0.00	2.04	0.00	2.04	1.62	34.47	9.00	S		59.26	0.00	3.34	0.00	2.04	2.04	13.03	1.62	84.11
	C7	1.62	60.23	37.18	33.01	F	60.23		4.57	0.00	2.07	0.00	2.07			21.00	F	60.23		5.33	0.00	2.07	0.00	2.07			
1.60 - 1.70	K1	1.63	56.50	34.66	12.00	S		56.50	0.00	3.56	0.00	1.94	1.94			15.00	M		56.50	0.00	3.18	0.00	1.94	1.94			
	D9	1.66	74.14	44.66	15.00	M		74.14	0.00	4.67	0.00	2.55	2.55			9.00	S		74.14	0.00	4.17	0.00	2.55	2.55			
	B6	1.70	56.92	33.48	18.00	M		56.92	0.00	3.58	0.00	1.96	1.96			9.00	S		56.92	0.00	3.20	0.00	1.96	1.96			
	C6	1.71	58.48	34.20	8.00	S		58.48	0.00	3.68	0.00	2.01	2.01			5.00	S		58.48	0.00	3.29	0.00	2.01	2.01			
	D1	1.74	68.85	39.57	8.00	S		68.85	0.00	4.33	0.00	2.37	2.37	1.74	100	4.00	S		68.85	0.00	3.87	0.00	2.37	2.37	16.27	1.74	100
	G2	1.74	110.96	63.77	7.00	S		110.96	0.00	6.98	0.00	3.82	3.82			4.00	S		110.96	0.00	6.24	0.00	3.82	3.82			
1.70 - 1.80	B1	1.74	92.86	53.37	10.00	S		92.86	0.00	5.84	0.00	3.19	3.19			0.00	S		92.86	0.00	5.23	0.00	3.19	3.19			
	D6	1.78	84.97	47.74	7.00	S		84.97	0.00	5.35	0.00	2.92	2.92			0.00	S		84.97	0.00	4.78	0.00	2.92	2.92			
	A2	1.80	134.82	74.90	6.00	S		134.82	0.00	8.49	0.00	4.64	4.64			0.00	S		134.82	0.00	7.59	0.00	4.64	4.64			
	F3	1.80	61.61	34.23	5.00	S		61.61	0.00	3.88	0.00	2.12	2.12			0.00	S		61.61	0.00	3.47	0.00	2.12	2.12			
1.80 - 2.00	I2	1.89	62.05	32.83	4.00	S		62.05	0.00	3.91	0.00	2.13	2.13	1.88	100	0.00	S		62.05	0.00	3.49	0.00	2.13	2.13	17.51	1.88	100
	K6	1.90	132.58	69.78	9.00	S		132.58	0.00	8.34	0.00	4.56	4.56			0.00	S		132.58	0.00	7.46	0.00	4.56	4.56			
	K7	1.91	54.33	28.45	0.00	S		54.33	0.00	3.42	0.00	1.87	1.87			0.00	S		54.33	0.00	3.06	0.00	1.87	1.87			
	C5	1.95	63.70	32.67	0.00	S		63.70	0.00	4.01	0.00	2.19	2.19			0.00	S		63.70	0.00	3.58	0.00	2.19	2.19			
	F5	2.34	83.62	35.74	0.00	S		83.62	0.00	5.26	0.00	2.88	2.88			0.00	S		83.62	0.00	4.71	0.00	2.88	2.88			
	F1	2.38	40.30	16.93	0.00	S		40.30	0.00	2.54	0.00	1.39	1.39			0.00	S		40.30	0.00	2.27	0.00	1.39	1.39			
	G3	2.41	57.00	23.65	0.00	S		57.00	0.00	3.59	0.00	1.96	1.96	2.44	100	0.00	S		57.00	0.00	3.21	0.00	1.96	1.96	16.37	2.44	100
	K3	2.47	55.55	22.49	0.00	S		55.55	0.00	3.50	0.00	1.91	1.91			0.00	S		55.55	0.00	3.13	0.00	1.91	1.91			
2.30 -2.50	G9	2.48	123.59	49.83	0.00	S		123.59	0.00	7.78	0.00	4.25	4.25			0.00	S		123.59	0.00	6.96	0.00	4.25	4.25			
	G5	2.53	115.91	45.81	0.00	S		115.91	0.00	7.30	0.00	3.99	3.99			0.00	S		115.91	0.00	6.52	0.00	3.99	3.99			
			2907.98				1319.24	1588.74	100.00	100.00	45.37	54.63	100.00					1131.07	1776.91	100.00	100.00	38.90	61.10	100.00			

The average partition coefficient (% Sinks) per each density range was plotted against the respective nominal average relative density to give the partition curves shown below. The Klima and Luckie (1989) model, was used to analyze the partition curves. The Ep and ρ_{50} values for the separation of the various particle size rages mentioned above were easily estimated using the partition function *(Venkoba Rao etal., 2003).*

5.1.1 Dynamic and steady state partition curves for the (+37 – 53mm) particles

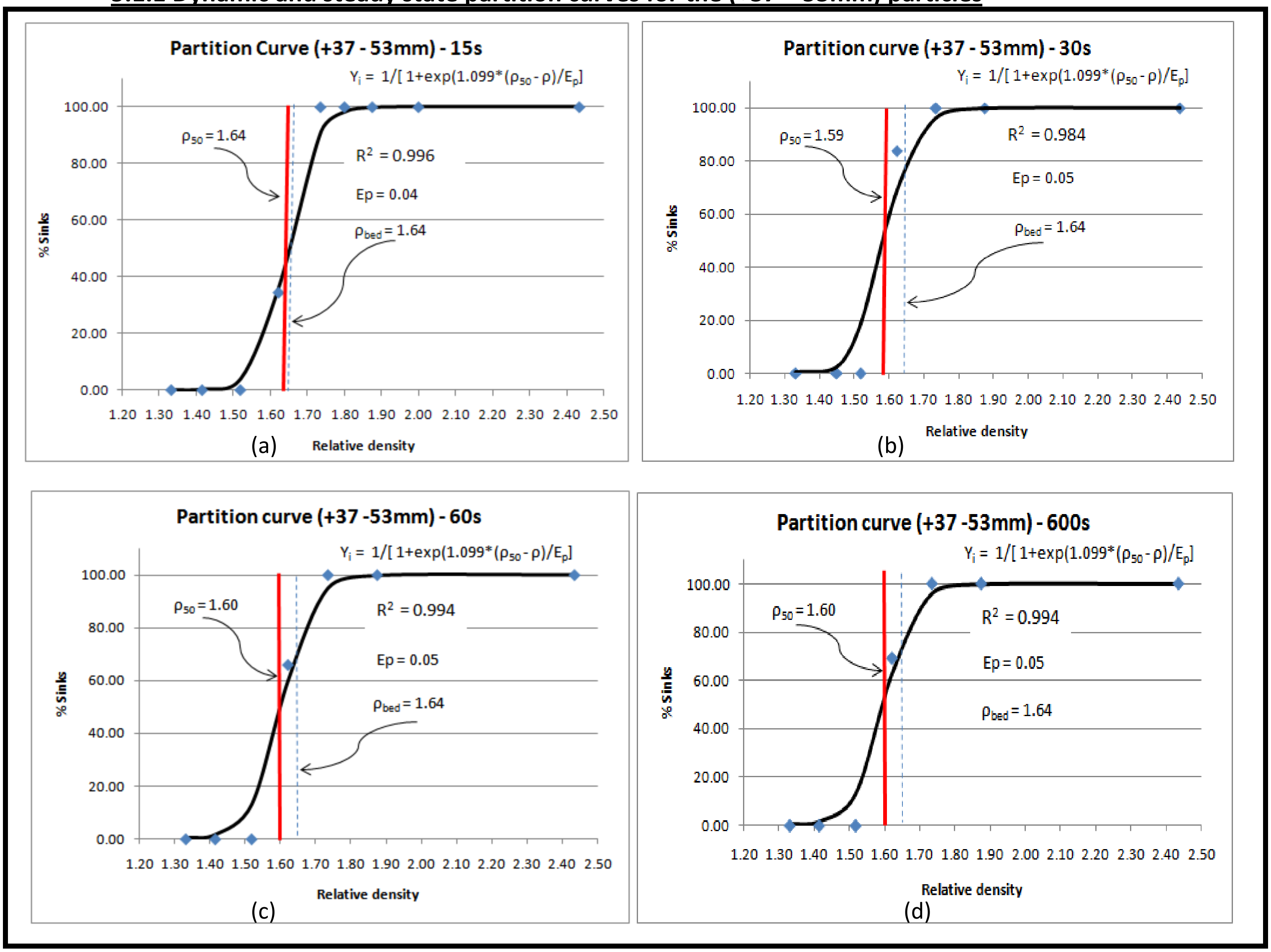

Figure 5.1 (a) – (d): Partition curves for (+37 -53mm) particles after different time intervals

Figures 5.1 (a) – (d) illustrate the partition curves for the (+37 – 53mm) particles obtained after the different separation times of 15s, 30s, 60s and 600s. The Klima and Luckie partition function fitted the partition data very well with an $R^2 \approx 1$ being obtained in all the cases. From the above partition curves it can be clearly seen that the (+37 -53mm) particles separated faster than all the other particle size ranges as evidenced by the Ep and ρ_{50} values which became relatively stable in about 15s. Figure 5.2 below illustrates how the Ep and ρ_{50} varied with time.

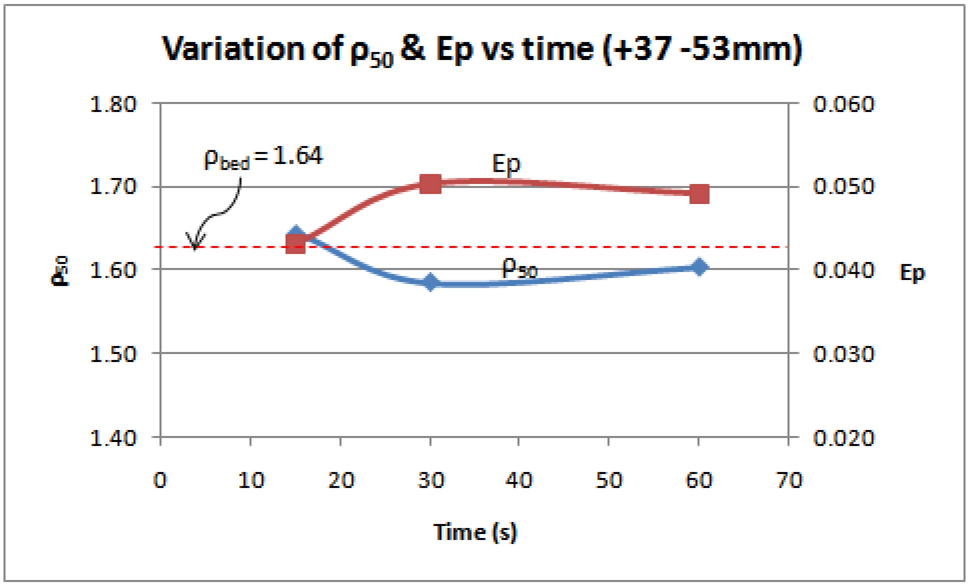

Figure 5.2: Variation of Ep and the ρ_{50} with time (+37 -53mm)

Ep values ranging from 0.04 – 0.05 were recorded for the (+37 – 53mm) particles with minimum fluctuation or shift of the ρ_{50}. A constant cut density of 1.60, which is slightly below the bed density of 1.64, was achieved within 30s. From the above plot, it can be observed that a decrease in the cut density can result in high Ep values being recorded. The slight shift of the cut density is probably due to the misplacement of the near cut density particles during the separation process. However, the above overall Ep and ρ_{50} trends indicate that the 3D fluidized bed can be efficiently used to separate the (+37 -53mm) particles. The yield trend for the (+37 - 53mm) particles is illustrated in Figure 5.3 below.

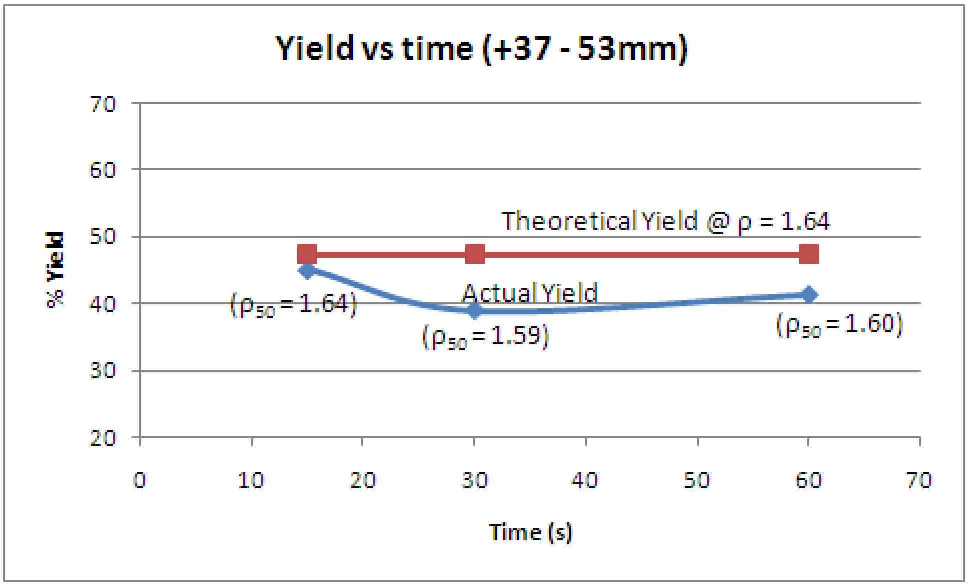

Figure 5.3: Yield vs. time graph (+37 -53mm)

The yield is as defined by equation (5.8) above. The theoretical yield was determined as the % mass fraction of the feed particles whose density is less than the bed density of 1.64. On the other hand, the actual yield was calculated as the % ratio of the total mass of the floats as to total mass of the feed particles. From Figure 5.3 above, it can be seen that a relatively constant actual yield of 40.1% was obtained after 30s and 60s respectively. This further confirms that the separation process was already complete in less than 30s. The small difference in the theoretical yield and the actual yield can be attributed to the misplacement of some of the float particles during the separation process. The misplacement can be minimized by manipulating both the medium and bed operating parameters. The slight fluctuation of the yield after 30s could be as a result of the separation of the near cut density particles which could either report to the floats or sinks regardless of the particle density. The circulating motion of the medium solids in the bed has got a significant effect on the separation performance of the near cut density particles since the settling or rise velocity of the particles is usually close to zero and can be easily dragged in the direction of the circulating forces.

5.1.2 Dynamic and steady state partition curves for (+22 – 31.5mm) particles

Partition curves for the (+22 -31.5mm) particles after 15s, 30s, 60s and 600s of separation are all illustrated in Appendix E1. The Klima and Luckie partition model fitted the partition data for the (+22 – 31.5) particles very well with an $R^2 \approx 1$ being recorded throughout. The separation of the (+22 -31.5) mm particles proved to be very efficient with stable Ep values as low as 0.05 recorded after 15s of separation. The trends of both the cut density and Ep values are illustrated below.

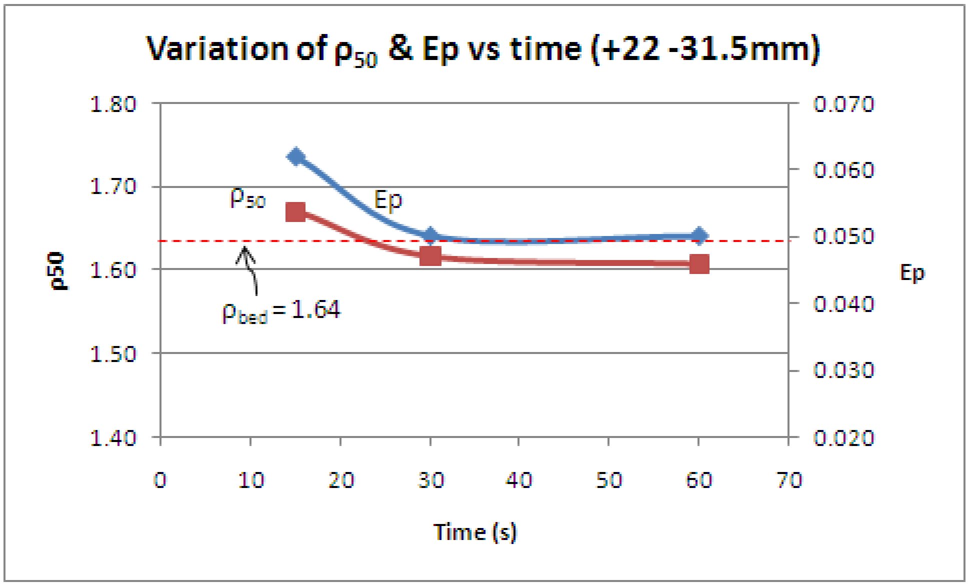

Figure 5.4: Variation of Ep and the ρ50 with time (+22 -31.5mm)

From Figure 5.4 above, it can be observed that the higher the cut density then the higher the Ep value i.e. for ($\rho_{50} > \rho_{bed}$). Both the Ep and ρ_{50} decreased with an increase in the separation time and became relatively constant after 30s. The minimum variation of the Ep and ρ_{50} after 30s indicates that the separation of the (+22 – 31.5mm) particles was already complete within less than 30s. At steady state, the ρ_{50} was found to be slightly below the initial bed density of 1.64. This can be attributed to the circulation motion of the medium particles as discussed in section 5.1.1.

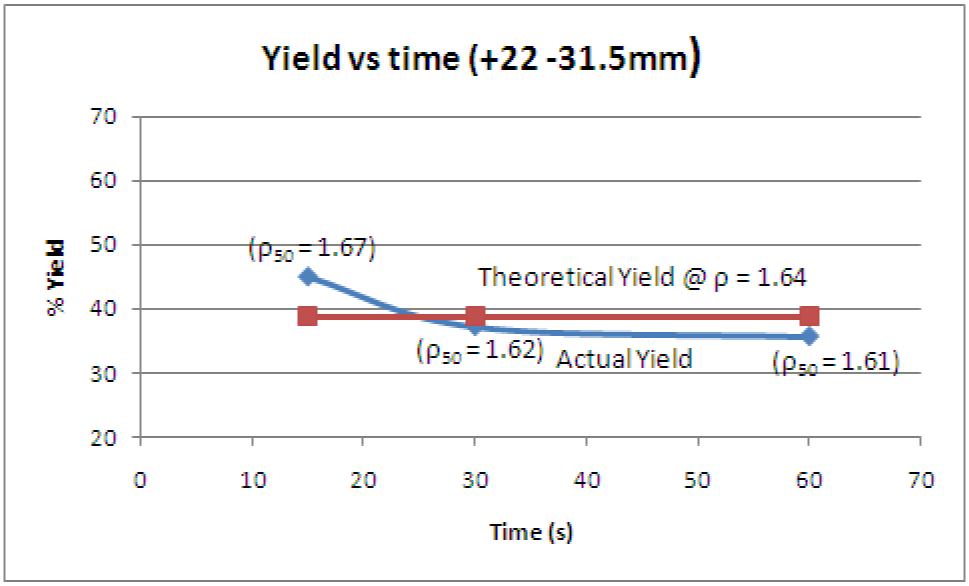

Figure 5.5: Yield vs. time graph (+22 -31.5mm)

Figure 5.5 further illustrates that the separation of the (+22 – 31.5mm) particles using the 3D fluidized bed is a very efficient process as evidenced by the relatively low Ep values and misplacement (<2%). After 15s, the actual yield was greater than the theoretical yield which shows that the separation process was still in progress, the particles were still settling. However, after 30s the actual yield became relatively constant indicating that the separation process was already complete. Based on the trends observed in Figure 5.4 and Figure 5.5, an optimum residence time of approximately 25s can be used for the separation of the (+22 - 31.5mm) particles.

5.1.3 Dynamic and steady state partition curves for (+16 – 22mm Blockish) particles

Dynamic settling tests were also carried out using (+16 -22mm) particles of three different shapes namely the blockish (Blk), sharp pointed prism (SR) and flat particles. The results of the tests are discussed based on the graphs in Appendix E2, Appendix E3 and Appendix E4 respectively.

The R^2 of the all the partition curves for the (+16 -22mm Blk) particles shown in Appendix E2 indicate that the Klima and Luckie partition model can fit the (+16 -22mm Blk) particles partition data well, but not as good as for the (+37 -53mm) and (+22 – 31.5) particles. The cut density densities recorded after 15s, 30s, 60s and 600s were all above the initial bed cut density of 1.64 (see Figure 8 below). The separation inefficiency increased as the cut density also increased but it then dropped with an increase in the separation time until the cut density became relatively constant after 30s.

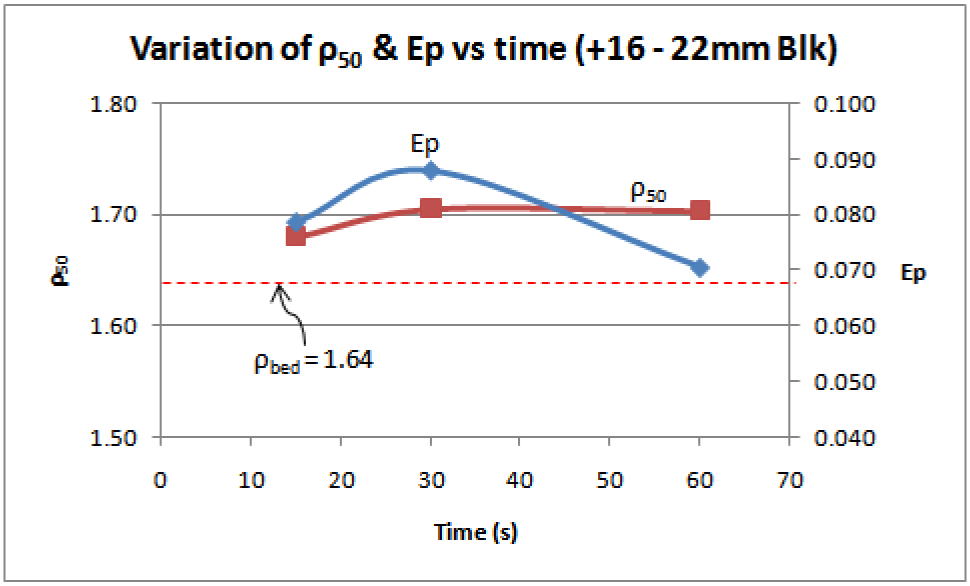

Figure 5.6: Variation of Ep and the ρ50 with time (+16 -22mm Blk)

Under steady state conditions, i.e. after 600s, an average Ep value of 0.056 was obtained at a cut density of 1.69. Although a relatively constant ρ_{50} was achieved after about 30s, the fluctuating Ep values in Figure 5.6 show that the separation was not yet complete. However, the low Ep values of (0.056 – 0.088) that were recorded after the different separation times indicate that the 3 D fluidized bed can efficiently separate the (+16 -22mm) blockish particles under optimum conditions.

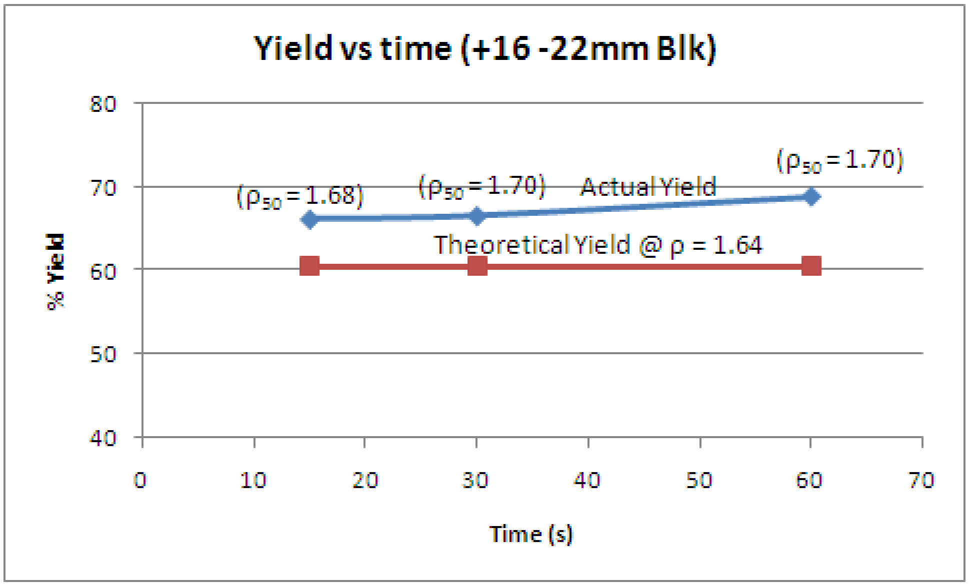

Figure 5.7: Yield vs. time graph (+16 -22mm Blk)

The above graph illustrates how the yield of the (+16 -22mm Blk) particles varied with time during the tests. The variation of the yield was mainly due to the fluctuation of the ρ_{50} after different separation time intervals. From Figure 5.7, it can be clearly seen that the actual yield is higher than the theoretical yield. This can be attributed to the misplacement of the near cut density sink particles, which is probably as a result of the circulation motion of the medium particles associated with the operation of the 3D Fluidized bed as explained in section 5.1.1. During the initial stages of the separation process, the actual yield fluctuated above 60%, but as the process progressed a steady state (t =600s) yield of 64.59% was achieved.

5.1.4 Dynamic and steady state partition curves for (+16 – 22mm SR) particles

The partition curves for the (+16 -22mm) sharp pointed prism particles obtained after 15s, 30s, 60s and 600s are as illustrated in Appendix E3. Analysis of the partition curves was based on the Klima and Luckie partition model. Although the model fitted the partition data quite well, the R^2 values recorded after the different time intervals outlined above were lower than the values recorded for the (+37 -53mm), (+22 -31.5mm) and (+16 -22mm Blk) particles. The partition data points for the (+16 -22mm SR) particles were scattered and the partition curves were flatter than those for all the particle size ranges and shapes discussed above. This could probably be as a result of the relatively high separation inefficiency, Ep values associated with the separation of the (+16 – 22mm SR) particles.

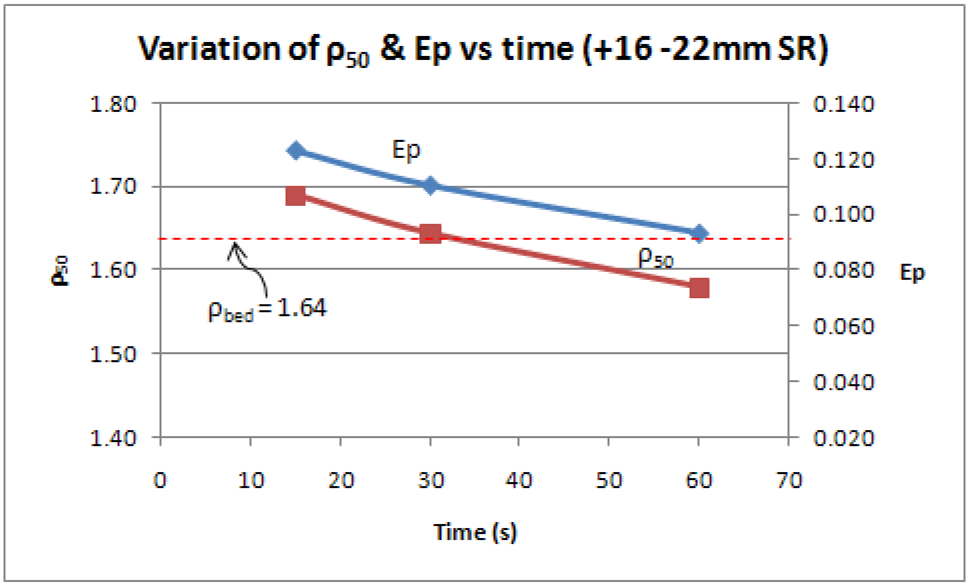

Figure 5.8: Variation of Ep and the ρ50 with time (+16 -22mm SR)

Figure 5.8 shows how the Ep and ρ_{50} of the (+16 -22mm SR) particles varied with separation time. Initially the cut density is above the operating bed density of 1.64, this could be as a result of the upward velocity component of the circulation motion of the medium particles, which opposes the settling of the sinks during the separation process thereby resulting in some of the jetsam particles recovered as floats. However, as the separation time increased, both the Ep and ρ_{50} continued to decrease. The shift in the cut density to below the initial bed density of 1.64 indicate that some near cut density flotsam particles were misplaced into the sinks stream. Depending on the orientation or angle of reposition of the sharp pointed particles during the separation process, some medium particles can settle on the surface of the particles. This can increase the apparent weight of the near cut density particles resulting in some of the flotsam particles reporting to the sinks. Although a relatively high steady state Ep value of 0.093 was recorded for the separation of the (+16 -22mm SR) particles, the 3D bed can be further optimized to efficiently separate the above particles by manipulating the operating parameters such as the separating cut density, residence time, mixing patterns etc .

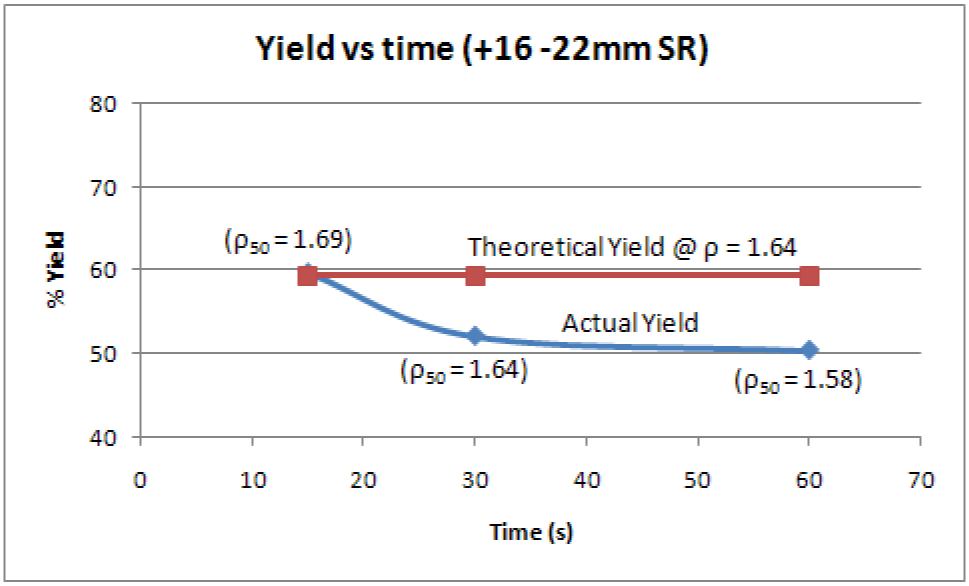

Figure 5.9: Yield vs. time graph (+16 -22mm SR)

Figure 5.9 above illustrates how the yield of the (+16 -22mm SR) particles changed with the separation time. The actual yield of the (+16 -22mm SR) particles initially dropped from 60% to slightly above 50% after 30s of separation and then became relatively constant. The decrease in the yield can be attributed to the shift in the cut density, which is a result of the misplacement of the near cut density particles as discussed in section 5.1.1.The constant yield recorded after 30s and 60s respectively, indicate that the residence time of the (+16 -22mm SR) particles can be optimally controlled to achieve an efficient separation using the 3D fluidized bed.

5.1.5 Dynamic and steady state partition curves for (+16 – 22mm FB) particles

The partition curves for the (+16 -22mm) flat particles obtained after the different settling times of (15s, 30s, 60s and 600s) are illustrated in Appendix E4. The Klima and Luckie model fitted the partition data well and the accuracy of the model improved with the separation time as evidenced by the increase of R^2 with time (see Appendix E4).The partition curves obtained during the first 30s are flatter than those obtained after 60s and 600s. This can be attributed to the relatively high Ep values recorded after 15s and 30s respectively. However the Ep values then dropped with an increase in the separation time, which further point that the separation process was only complete after at least 30s of separation.

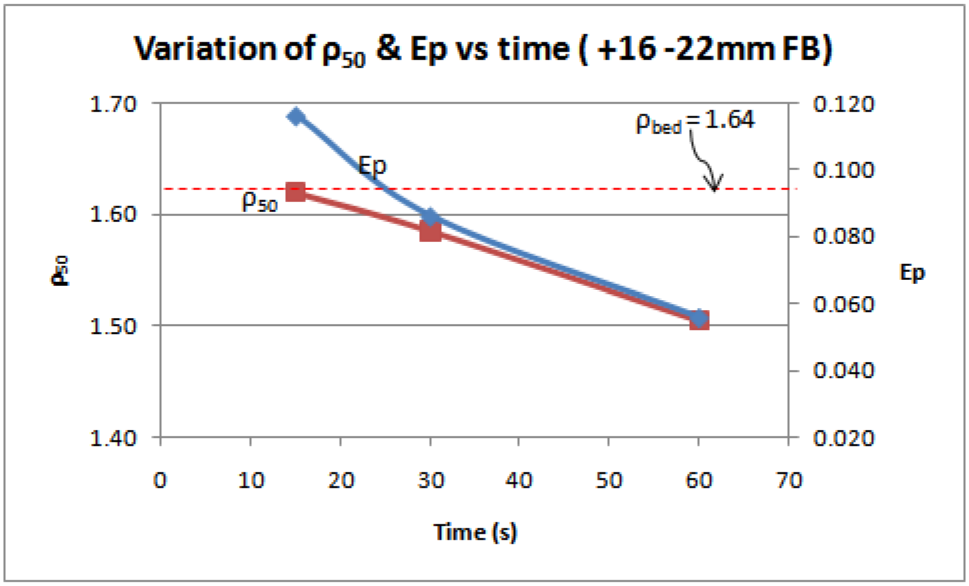

Figure 5.10: Variation of Ep and the ρ50 with time (+16 -22mm FB)

From Figure 5.10, it can be clearly seen that both the Ep and cut density of the (+16 -22mm FB) particles decreased with an increase in the separation time. Separation inefficiency, Ep values as low as 0.056 were recorded under steady state conditions, but the fluctuation of the cut density of the (+16 – 22mm FB) particles makes it difficult to efficiently separate the particles. Flat particles have got wide surface area and some medium particles tend to settle and accumulate on the surface of the particles increasing the apparent weight of the particles as the separation process proceeds. This can lead to the misplacement of the near cut density flotsam particles, which will end up reporting to the sinks thereby forcing the cut density of the particles to drop to as low as 1.50 after 60s.

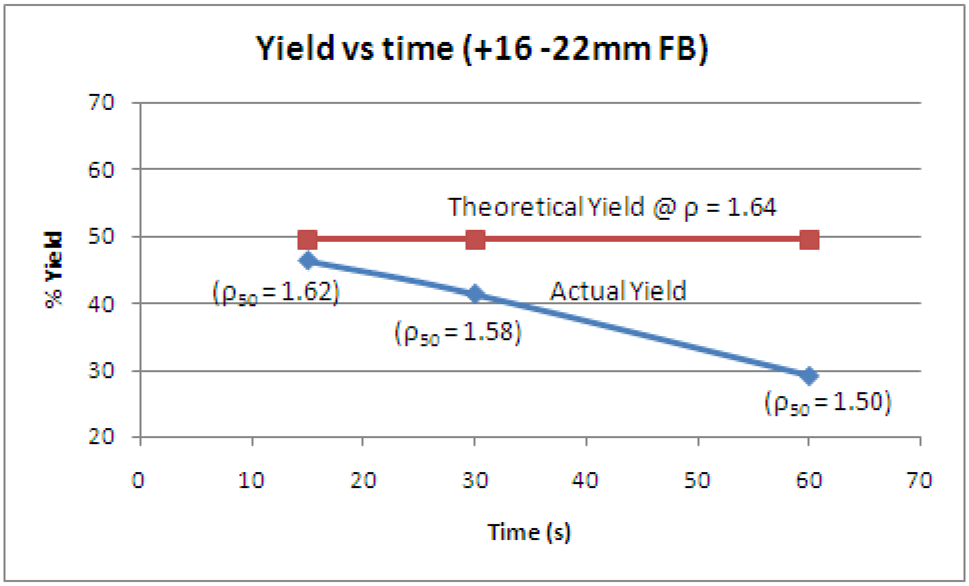

Figure 5.11: Yield vs. time graph (+16 -22mm FB)

Figure 5.11 above illustrates the variation of yield with separation time. The actual yield continued to decrease and deviate further from the theoretical yield as the cut density dropped from 1.62 to 1.50. This shows that the longer the separation time for the (+16 -22mm) flat particles, the higher the misplacement resulting from the scenario discussed above. The trend observed in Figure 5.11 further stresses on the need why it is important to study the effect of particle shape on the separation performance of a 3 D fluidized bed. Although, the fluctuation of the Ep and ρ_{50} point to the fact that it is difficult to efficiently separate the (+16 -22mm FB) particles using the 3 D fluidized bed, the performance of the bed can be improved by manipulating operating parameters such as the superficial gas velocity, residence time, feed rate and feed composition etc. All the above mentioned parameters have got a significant effect on the bed density distribution and mixing patterns in the fluidized bed.

5.1.6 Dynamic and steady state partition curves for (+9.5 – 16mm) particle size range

The dynamic and steady state partition curves for the (+9.5 – 16mm) particles recorded after 15s, 30s, 60s and 600s are illustrated in Appendix E6. The Klima and Luckie model fitted the partition data for the (+9.5 -16mm) particles very well except for the data obtained after 15s of separation where a low R^2 value of 0.9245 was recorded. The partition curves obtained after 15s and 30s were flatter than those obtained after 30s and 60s respectively. The flatness of the partition curves is directly linked to the separation inefficiency of the particles, the higher the Ep value then the flatter the partition curve.

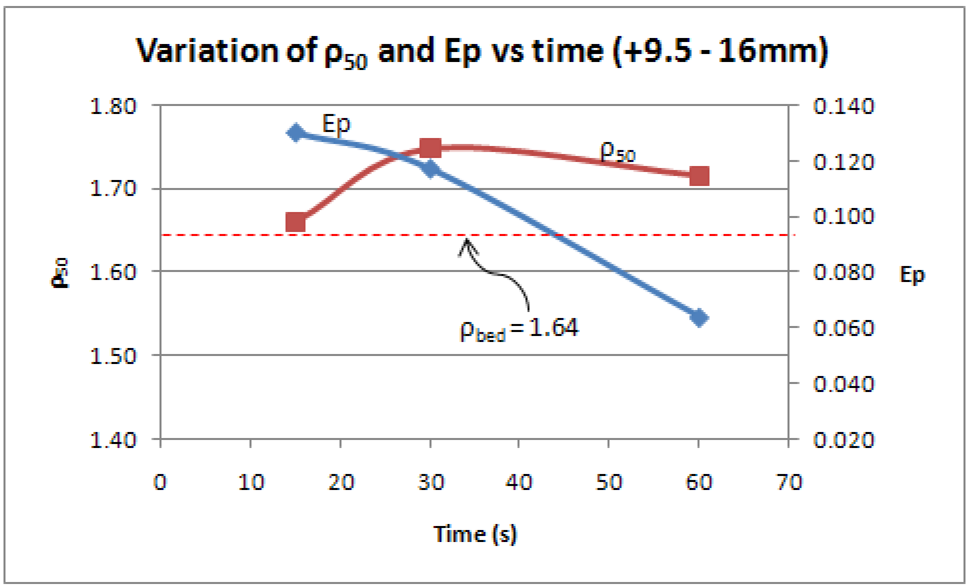

Figure 5.12: Variation of Ep and the ρ_{50} with time (+9.5 -16mm)

From Figure 5.12, it can be seen that the Ep values decreased with time whilst the ρ_{50} fluctuated with time. High average Ep values of 0.13 and 0.117 were recorded after 15s and 30s respectively. The trend of the Ep values after 30s suggest that the separation process was still incomplete. Although some relatively low Ep values were recorded after 30s, the continuous fluctuation of the ρ_{50} with time makes it difficult to obtain an efficient separation of the (+9.5 – 16mm) particles. The fluctuation of the ρ_{50} could be as a result of the circulation motion of the medium particles in the bed, which seem to have a more pronounced effect on the separation of the +9.5 – 16mm particles as compared to all the other size ranges discussed above.

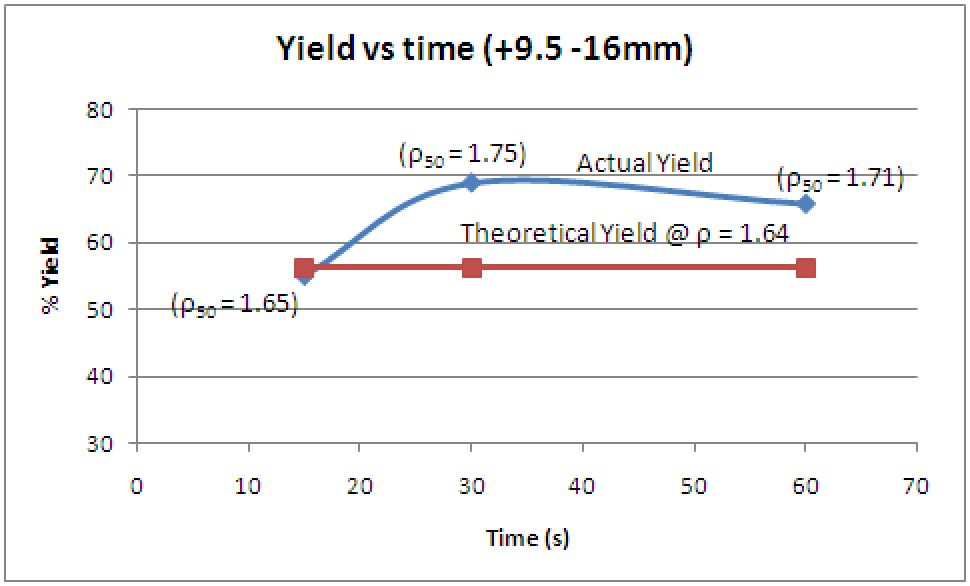

Figure 5.13: Yield vs. time graph (+9.5 -16mm)

From Figure 5.13, it can be clearly seen that the actual yield is greater than the theoretical yield. The shift in the cut density also shows that some of the sink/jetsam particles were recovered in the floats stream resulting in the actual yield greater than the theoretical yield being recorded as illustrated in Figure 5.13 below. This could be as a result of the settling velocities of the near cut density sink particles being lower than the upward velocity component of the circulation motion and as such, the resultant motion of the particles was upwards. The short circuiting of the sinks into the floats can adversely affect the quality of separation, hence the need to adjust the operating parameters of the 3D in order to ensure that optimum conditions are generated for the separation of the (+9.5 – 16mm) particles.

5.1.7 Effect of particle size on the separation performance of the 3 D fluidized bed

The separation performance of the 3 D fluidized bed was mainly measured based on the variation of the Ep and ρ_{50} for the different particle size ranges with time. Figure 5.14 and Figure 5.15 below illustrate how the Ep and ρ_{50} for the different particle size ranges varied with time. The steady state values achieved after 600s are summarized in Appendix E7.

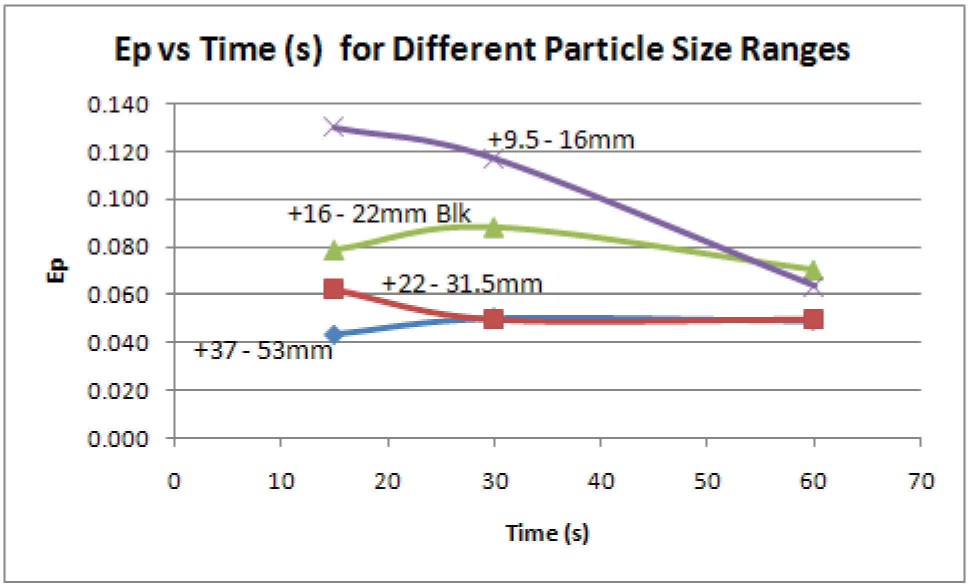

Figure 5.14: Ep vs. Time (s) graph for the different particle size ranges

From Figure 5.14, it can be observed that the particle size has got a significant effect on the separation performance of the 3 D fluidized bed. Generally, the bigger particles tend to separate faster and more efficiently than the smaller particles. The observed trend in Figure 5.14 indicate that within 20s, the (+37 -53mm) particles had completely separated, followed by the (+22 -31.5mm) particles which took approximately 25s. Low steady state Ep values of 0.05 were recorded for both (+37 – 53mm) and (+22 – 31.5mm) particles. This means that the air fluidized bed can be used to efficiently separate the above mentioned particles size ranges. However, based on the literature from China, the separation performance of the (+37 – 53mm) can be further improved by using a bed height deeper than 40cm. The research findings from China state that a fluidized bed with a bed height of ≤ 400mm does not provide enough space for effective beneficiation of > 50mm coal. Therefore, the bed height required for the beneficiation of the >50mm coal should be controlled at about 1200mm to form a stable fluidized bed with small bubbles and a uniform bed density, which can be used to efficiently beneficiate the >50mm coal with Ep values as low as 0.02 being achieved *(Chen, Yang etal., 2003)*.

Although, the Ep values of the (9.5 – 16mm) particles improved with time, the values recorded during the first 50s were always higher than those of all the other particle size ranges outlined above. This shows that a relatively longer separation time is required for the efficient separation of the (+9.5 – 16mm) particles as compared to the (+16 – 22mm), (+22 – 31.5mm) and (+37 – 53mm) particles. On the other hand, the separation of the (+16 -22mm Blk) particles was associated with an average Ep value of about 0.07, which is lower than the average Ep for the (+9.5 – 16mm) particles, but higher than the average Ep of the (+22 – 31.5mm) and (+37 – 53mm) particles. The performance of the 3 D fluidized bed was also assessed based on the cut density shift as illustrated in Figure 5.15 below.

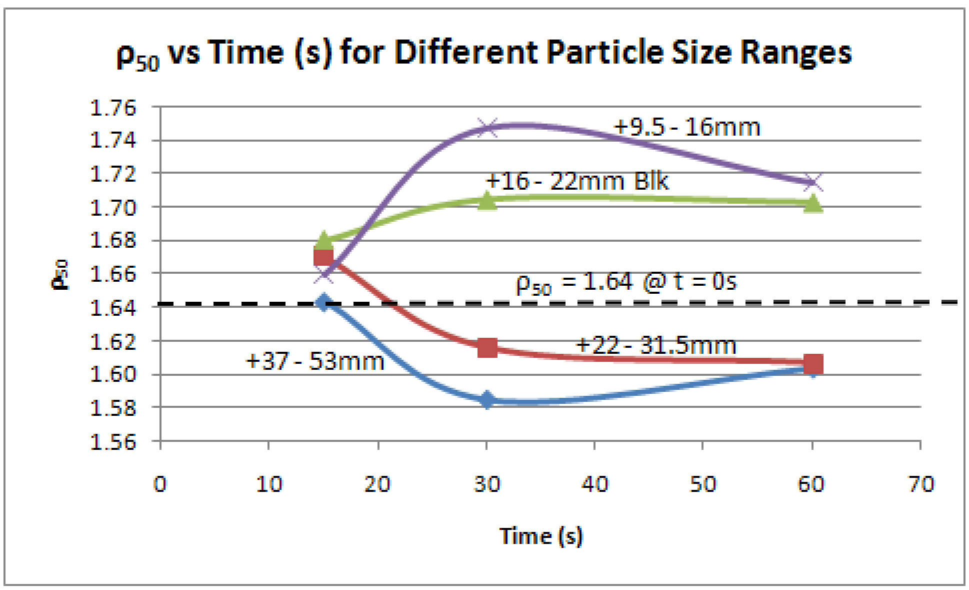

Figure 5.15: ρ50 vs. Time(s) graph for the different particle size ranges

Figure 5.15 above illustrates that the cut densities of the (+9.5 – 16mm) and (+16 -22mm Blk) particles shifted to above the initial cut density of 1.64 whilst the cut densities of the (+22 – 31.5mm) and (+37 – 53mm) particles shifted to slightly below 1.64. Figure 5.16 below would be used to discuss the observed trend which is probably as a result of the circulation of the medium particles associated with the operation of the 3 D fluidized bed.

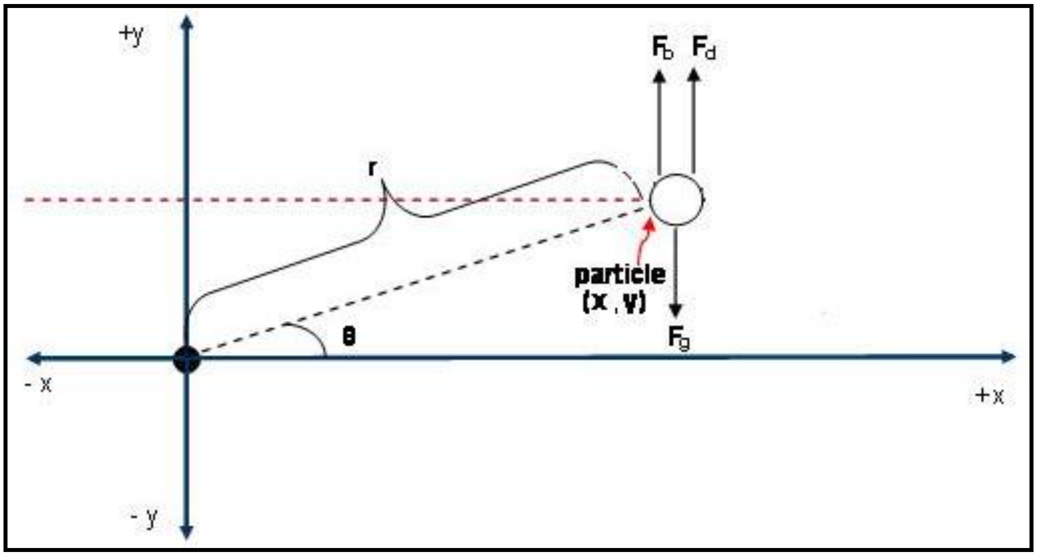

Figure 5.16: Some of the forces acting on the particles in the 3 D fluidized bed

Figure 5.16 illustrates some of the forces that can act on the particles in the 3 D fluidized bed, where :F_d is the drag force, F_b –buoyancy force, F_g - gravitational force and r – distance of the particle from the centre of the circulation motion.

The shift in the cut densities for the (+9.5 – 16mm) and (+16 -22mm Blk) particles indicate that the near cut density jetsam particles have probably got settling velocities smaller than the upward vertical component of the circulating velocity and as a result the particles were pushed upwards and ended up reporting to the float stream. In other words, (F_d + Fb > Fg).The continuous fluctuation of the the cut density of the (+9.5 – 16mm) particles shown in Figure 5.15 indicates that it is quite difficult to efficiently separate the particles unless optimum operating conditions are used.

Although relatively constant cut densities were achieved for the separation of the (+22 – 31.5mm) and (+37 – 53mm) particles, the fact that after 30s, the cut densities were below the initial bed density of 1.64 indicate that some near cut density flotsam particles were misplaced during the separation process. The (+22 – 31.5mm) and (+37 – 53mm) particles have got wider surface areas as compared to the (+9.5 – 16mm) and (+16 -22mm Blk) particles, such that as the separation process proceeds, the medium particles tend to accumulate on the surfaces of the particles resulting in the increased apparent weight of the near cut density flotsam particles, which will end up recovered as sinks since (F_d + Fb < Fg).

The Ep and ρ_{50} trends shown in Figure 5.14 and Figure 5.15 indicate that different optimum separating conditions would be required for the efficient separation of the different particle size ranges discussed above. Meanwhile, the (+22 – 31.5mm) and (+37 – 53mm) particles can be efficiently separated under almost similar optimum conditions, whilst on the other hand the (+16 – 22mm Blk) and (+9.5 -16mm) particles can be optimally separated in the same bath.

5.1.8 Effect of particle shape on the separation of the (+16 -22mm) particles

The effect of the particle shape on the performance of the 3 D fluidized bed was investigated using the (+16 -22mm) particles of different shapes namely the blockish (Blk), flat (FB) and sharp pointed prism (SR) particles.

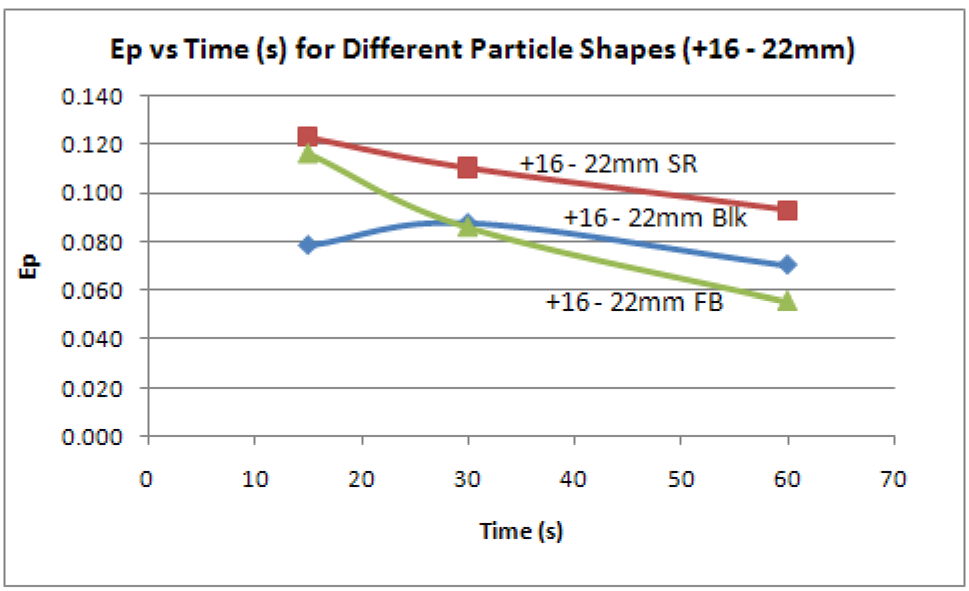

Figure 5.17: Ep vs. Time (s) graphs for the (+16 -22mm) of different shapes

Figure 5.17 illustrates how the Ep values of the (+16 -22mm) particles of three different shapes varied with time. The blockish particles separated better than flat and the sharp pointed particles as evidenced by the relatively low and constant Ep values obtained after about 30s of separation. Although relatively constant Ep values were achieved for separation of (+16 – 22mm SR), high average Ep values of approximately 0.10 were recorded. On the other hand, the Ep values of the (+16 – 22mm FB) particles improved with time, but the continuous shift of the cut density makes it difficult to efficiently separate the flat particles. The flatter partition curves obtained during the early stages of the separation of all the (+16 - 22mm) particles were as a result of the high Ep values.

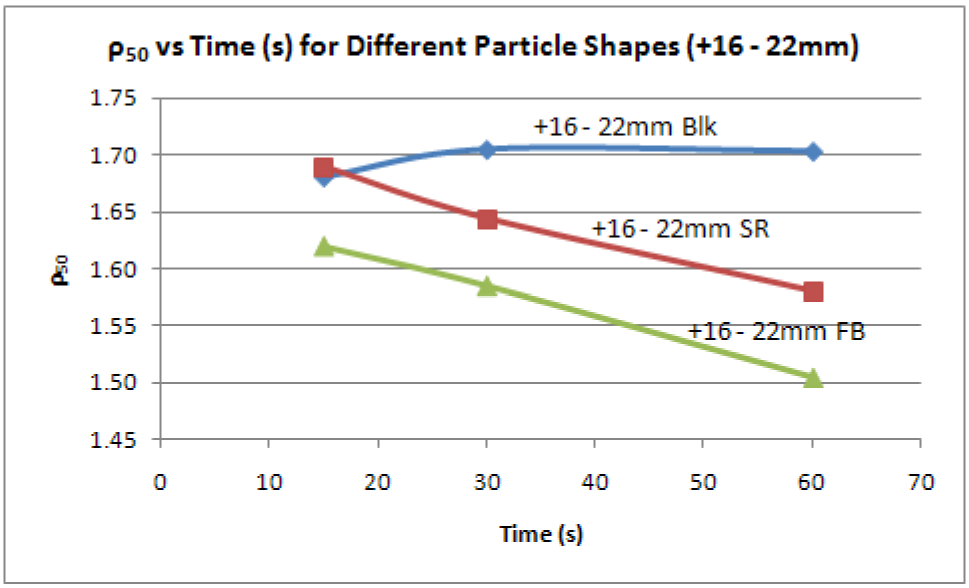

Figure 5.18: ρ_{50} vs. Time (s) for the (+16 -22mm) of different shapes

Figure 5.18 above illustrates how the ρ_{50} of the (+16 – 22mm Blk), (+16 – 22mm SR) and (+16 – 22mm FB) particles varied with time. The difference in the observed trends of the cut densities of the (+16 -22mm) particles of different particle shapes highlight that particle shape is one of the parameters which has got a significant effect on the separation performance of the 3 D fluidized bed and as such, different optimum operating conditions should be used for the efficient separation of different particle shapes. The dynamic cut densities of the blockish particles fluctuated above the initial cut bed density of 1.64, with an average cut density of 1.70 being attained under steady state conditions. This means that some of the particles that could have been recovered as sinks short circuited into the floats stream probably due to the fact that their settling velocity was smaller than the upward velocity component of the circulation motion of the medium particles. On the other hand, the cut density of the flat particles fluctuated from 1.62 after 15s to 1.50 after 60s whilst the cut density of the sharp pointed prism shifted from 1.69 after 15s to 1.55 after 60s (see Figure 5.18).

Although relatively low Ep values were obtained with flat particles than those obtained for the separation of the sharp pointed particles, the continuous cut density shift made it difficult to efficiently separate the flat particles. Both the flat and the sharp pointed particles have got wide surfaces areas in contact with the pseudo fluid and hence as the separation process proceeds, some medium particles tend to settle on the surfaces of the particles. This alters the apparent weight of the particles resulting in the misplacement of the near cut density material as the particles with density slightly less than that of the medium end reporting to the sinks stream. The shift in the cut density due to the above condition also depends on the angle of orientation and reposition of the particles.

5.2 Rise velocity Tests

Rise velocity tests were carried out using particles of different sizes, densities and shapes. However, given the technique that was used to measure the rise velocity of the particles, only limited data was obtained and it's all summarized in Figure 5.19 below and Appendix B. The rise velocity of the particle mainly depends on the density of the particle as well as the balance between the buoyancy forces, gravitational force, bed circulation forces and the drag forces as shown in Figure 5.16. If the buoyancy force is greater than the gravitational and drag forces, then the net force on the particle would be upward. The strength of the buoyancy force is proportional to the volume of the object. In other words, the buoyancy force is equal to the weight of the fluid displaced by the particle.

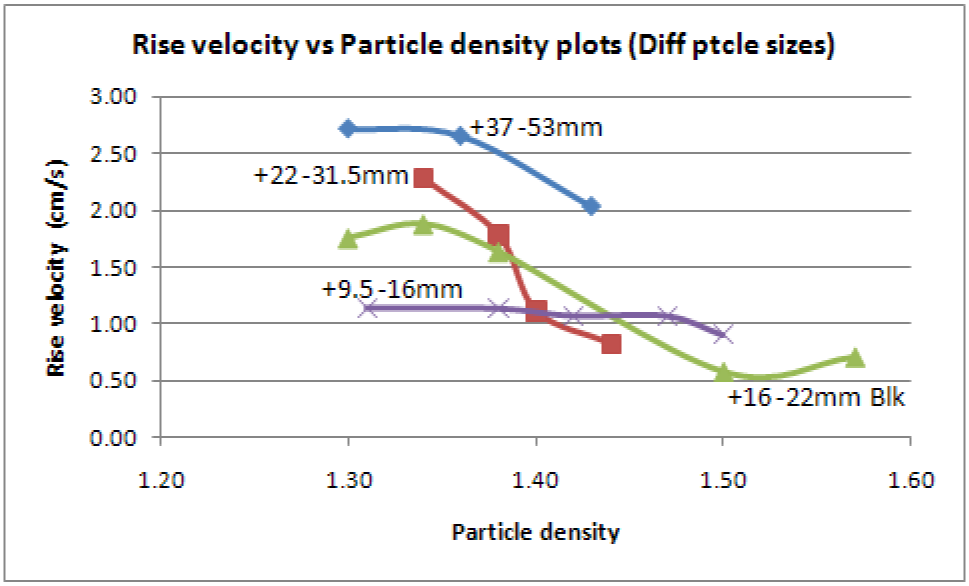

Figure 5.19: Rise velocity graphs for the different particle sizes

From Figure 5.19 above it can be seen that for all the flotsam particles (1.30 – 1.35), the larger the particles the higher the rise velocity. For instance the (+37 -53mm) particles with a density of 1.30 rose faster than all the other particles sizes with the same density. As the particle density increased towards the cut density, the rise velocity of the (+37 -53mm) particles significantly dropped to less than of all the other particle size ranges. This is probably due to the increase in the magnitude of the gravitational forces acting on the particles. On the other hand the rise velocities for the (+9.5 – 16mm) particles were relatively constant for particles in the (1.30 -1.45) density range, the rise velocities only started to drop when the particle density exceeded 1.45. This is because the volume of the particles in the (1.30 -1.45) density range was relatively constant. (+22 -31.5mm) particles of different shapes were used for the rise velocity tests and it was observed that angular tetrahedral flat flotsam particles tend to rise faster than the angular prismoidal particles because the flat particles have got a wide surface area and tend to displace more fluid than the angular prismoidal particles. Hence, their buoyancy force is stronger than that for the prismoidal particles. However, as the particle density gets closer to the bed cut density, the gravitational forces become stronger, hence the rise velocities of the particles drop (see Appendix B - 1).

5.3 Rise/ settling velocity model

The separation performance of the 3D air fluidized bed largely depends on the rise and settling velocities of the feed particles in the bed. As such, a deep understanding of the rise and settling behavior of the particles in the bed is of fundamental importance in the design and optimization of the continuous separation system. Regrettably, this importance is not matched by the availability of analytically based formulae for calculation of the velocity except in the simplest of cases *(Terence Smith etal., 1997)*. Hence as part of this study, several rise /settling tests were carried out in order to gather adequate data which can be successfully applied in the development of a simple empirical model that can be used to predict the rise/settling velocities of the particles of different sizes, shapes and densities in the 3D air fluidized bed.

According to *(Napier Munn etal., 1991),* an intuitive approach to modeling separation baths is to accept a correlation between particle settling velocity (negative or positive, depending on density), separation characteristics and residence time. In any given separator, particles which rise or fall only slowly, by virtue of their fine size or a density close to that of the medium, may not have time to report to the correct product before they leave the separator. This is the separation rate determining step since both the cut-point and the separation inefficiency, Ep are all principally defined by this mechanism, which can result in the offset of the cut-point from the medium density *(Napier Munn etal., 1991)*.

The above point further illustrates why it is important to study and understand the rise/settling behavior of the particles in order to efficiently operate the 3 D air fluidized bed coal separator. The rise or settling velocity of the feed particles is a function of many complex parameters, which include the interaction between particles and fluid and between the particles themselves, particle size, fluid viscosity, density difference between the particle and separating fluid, particle shape etc. Meanwhile, as part of developing a simple rise/settling velocity empirical model with the capability to predict the partitioning behavior of the different particle size ranges, densities and shapes, the Stokes' law was used as the basis and the following assumptions were made.

5.3.1 Assumptions

- The Reynolds number, Re of the fluid is very low. Preliminary approximate calculations of the Re of the separating medium indicate that Re < 150, hence the Stokes law can still be applied as a good approximation in this region.

- The wall effect is negligible in the (40 x 40 x 60) cm 3D air fluidized bed.

- The bed density/ separating fluid density is uniform throughout the three dimensional space, this is supported by the STDEV < 0.01 that was obtained for the silica - magnetite bed (see Appendix C).

- The coal particles instantaneously reach terminal velocity when they are introduced in the 3 D air fluidized bed. In other words, there is no acceleration and the relative rise/settling velocities of each particle is constant.

- The particle – particle interactions are negligible.

- All the feed particles were treated as perfect spheres.

- The fluid is continuous, that is the diameter of the coal particles is far greater than the mean free path of the fluidized bed particles.

- The circulating motion of the fluid medium in the bed has got a negligible effect on the rise/settling velocities of the coal particles.

Based on the above assumptions, only three forces act on the feed particles in the 3 D air fluidized and these include the buoyancy force (F_b), drag force (F_d) and gravitational force (F_g). Figure 5.20 below illustrates the forces acting on the particle.

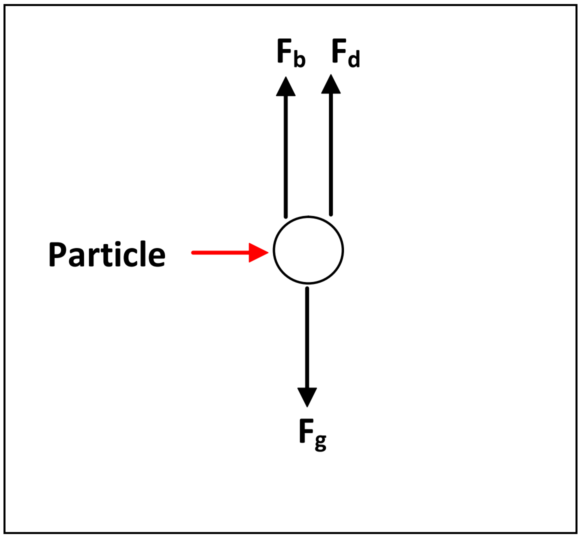

Figure 5.20: Forces acting on the particle in the 3 D air fluidized bed

At equilibrium, that is when the particles reaches terminal velocity (constant relative velocity), then;

$$F_g = F_d + F_b \tag{5.9}$$

but;

$$F_g = mg \tag{5.10}$$

$$Mass\ (m) = volume\ (v_p) \times density\ (\rho_p) \tag{5.11}$$

$$v_p = \frac{\pi d^3}{6} \tag{5.12}$$

$$m = \frac{\pi d^3 \rho_p}{6} \tag{5.13}$$

where m – mass of the particle

d - average diameter of the particle

ρ_p – density of the particle

Substituting equation 5.13 into equation 5.10 then,

$$F_g = \frac{\pi d^3 \rho_p g}{6} \tag{5.14}$$

In general, total drag force acting on a particle is given by:

$$F_d = \frac{\pi d^2 \rho_{bed} V^2 C_D}{4} \tag{5.15}$$

where ρ_{bed} – bed density / separating fluid density

V - constant relative velocity (terminal velocity)

C_D – drag coefficient

For Stokes' law,

$$C_D = \frac{12}{Re} \tag{5.16}$$

but Re is given by;

$$Re = \frac{V d \rho_{bed}}{\mu} \tag{5.17}$$

Substituting equations 5.16 and 5.17 into 5.15

$$F_d = 3\pi d \mu V \tag{5.18}$$

On the other hand, the buoyancy force F_b is given by:

$$F_b = m_f g \tag{5.19}$$

where m_f – mass of the separating medium/ fluid displaced by the particle

$$F_b = v_f \rho_{bed} g \tag{5.20}$$

$$F_b = \frac{\pi d^3 \rho_{bed} g}{6} \tag{5.21}$$

Substituting equations 5.14, 5.18 and 5.21 into eqn 5.9, then:

$$\frac{\pi d^3 \rho_p g}{6} = \frac{\pi d^3 \rho_{bed} g}{6} + 3\pi d \mu V \tag{5.22}$$

Making V subject of the formula

$$V = \frac{d^2 g(\rho_p - \rho_{bed})}{18\mu} \qquad \text{(Stokes' law)} \tag{5.23}$$

Due to the lack of the necessary equipment required to measure the viscosity of the air fluidized bed in the laboratory, the viscosity of the separating medium/fluid could not be determined during the rise/settling tests. As such, the denominator in equation (5.23) was treated as an empirical constant as shown below:

$$18\mu = A \ (empirical\ constant) \tag{5.24}$$

Equation (5.23) was then simplified into the following expression given below;

$$V = \frac{d^2 g(\rho_p - \rho_{bed})}{A} \tag{5.25}$$

A negative sign (-) was used to denote settling velocity whilst the positive sign (+) denoted the rise velocity of the particles, because of the above sign conversion a negative sign was introduced in equation (5.25) and the expression simplified to:

$$V = -\frac{d^2 g(\rho_p - \rho_{bed})}{A} \tag{5.26}$$

Equation (5.26) was optimized using excel solver. The results for the different particles size ranges and shapes are analyzed and discussed in detail below.

5.3.2 Analysis of the Rise/settling velocity plots for the different particle size ranges and shapes

The rise/settling velocity data for the different particle sizes ranges and shapes was plotted against the respective relative densities of the particles. The proposed expression or model labeled as equation (5.26) above was used to fit the data and the results are discussed below.

5.3.2.1 Rise/settling velocity plot for the (+37 -53mm) particles

Figure 5.21 below illustrates the rise /settling velocity plot for the (+37 – 53mm) particles. The proposed empirical model is linear and it fitted the rise/settling data very well as shown by the high R^2 of 0.9935. The model plot is symmetrically linear about the initial bed cut bed density of 1.64. However, most of the data points are slightly below the values predicted by the empirical model. This can be partly attributed to the circulating motion of the medium particles which is associated with the operation of the 3 D air fluidized bed. In as much as the medium particles in the 3 D air fluidized bed behave like a pseudo fluid; some medium particles always tend to settle on the surfaces of the feed particles thereby resulting in increased apparent weight of the particles. This can result in the (+37 -53mm) particles sinking faster than predicted by the proposed rise/settling model. The opposite can also be true, the particles can rise at a slower rate than predicted due to the altered density.

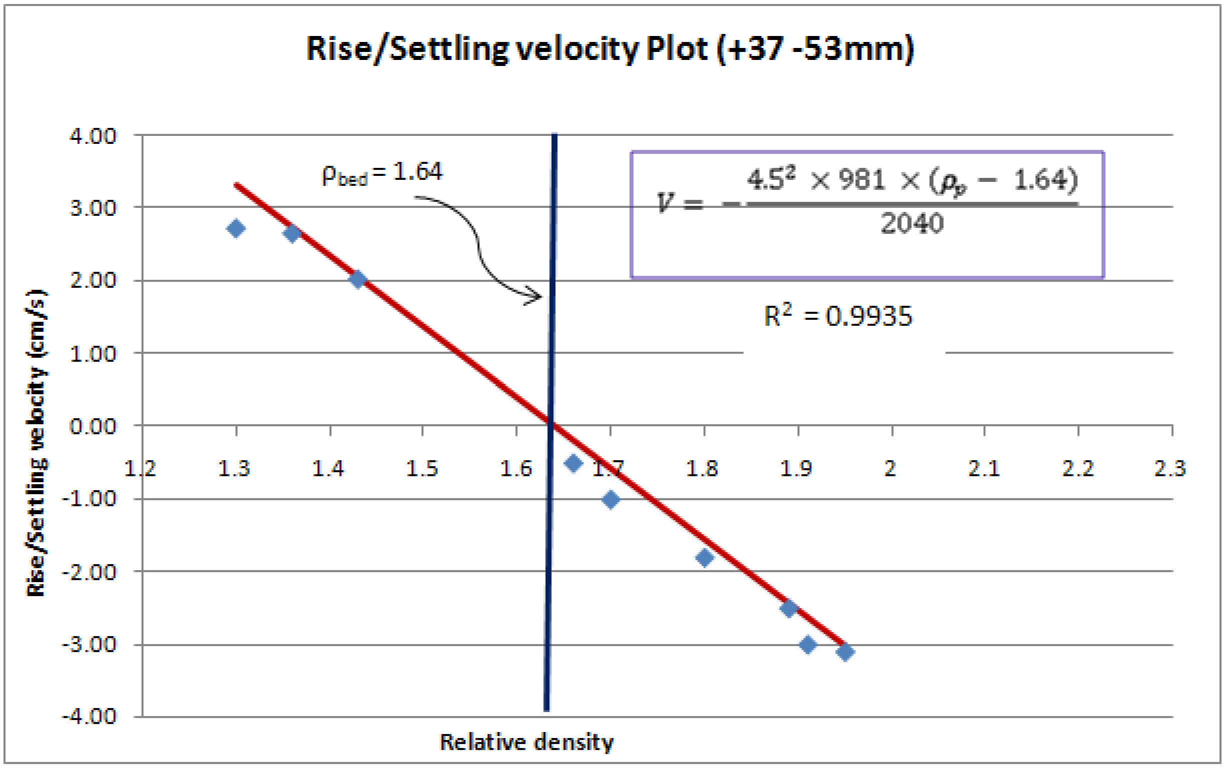

Figure 5.21: Rise /Settling velocity plot for the (+37 -53mm) particles

The observed trend in Figure 5.21 could be as a result of the condition discussed above. The (+37 -53mm) tend to separate faster because just after 10s of separation, all the +1.95 density particles had already settled, only the near cut density particles remained in suspension. An empirical constant of approximately 2040 $gcm^{-1}s^{-1}$ was obtained for the (+37 -53mm) particles. The empirical constant incorporates the machine constant, dynamic viscosity of the fluid, average shape factor of all the (+37 -53mm) particles.

5.3.2.2 Rise/settling velocity plot for the (+22 -31.5mm) particles

The proposed rise/settling model fitted the (+22 -31.5mm) rise and settling data well with an R^2 value of 0.9583 being recorded (see Figure 5.22 below). The fact that most of the settling data points are slightly higher the predicted values is probably as a result of the condition discussed in section 5.3.1.1, where the medium particles can settle on the surface of the particles thereby altering the apparent density of the particles. On the other hand, some of the particles' settling velocities are slightly lower that the predicted velocities. This can be attributed to the circulation motion associated with the operation of the 3 D air fluidized coal separator. If the vertical upward component of the circulating velocity is relatively high then it can retard the settling velocity of the particles.

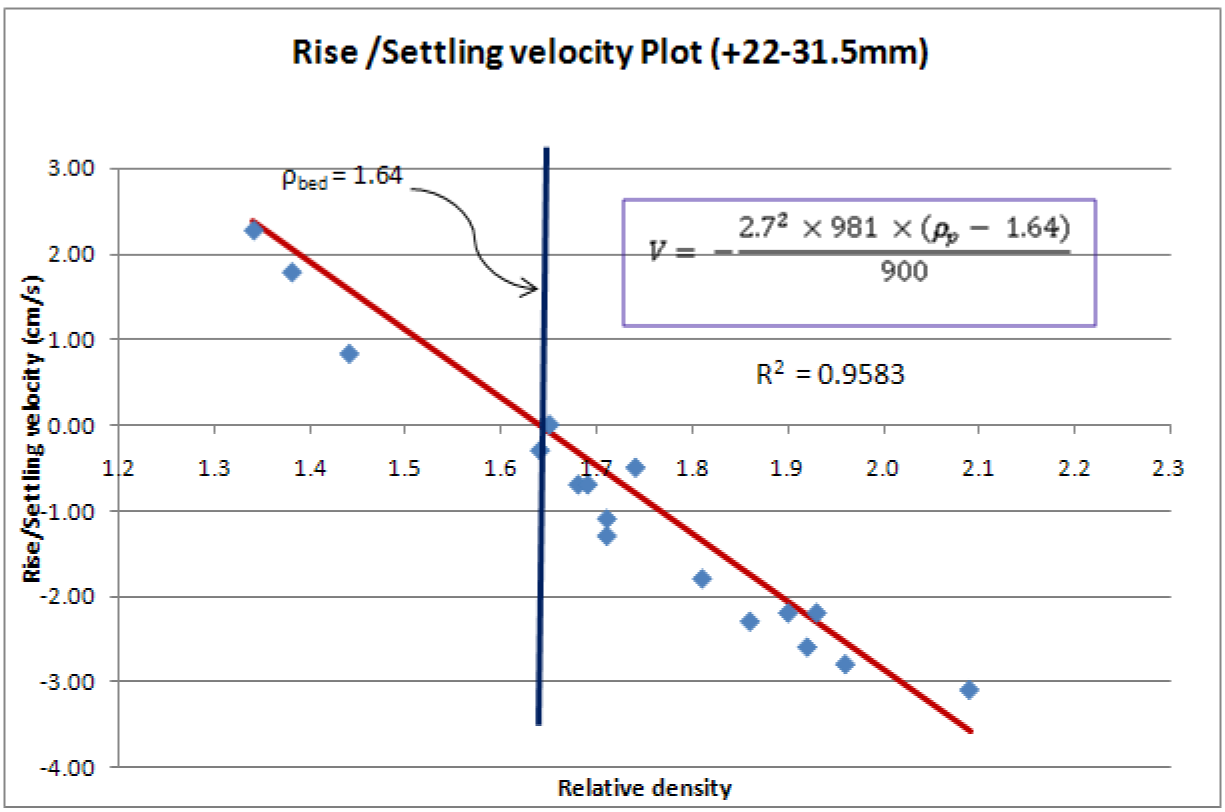

Figure 5.22: Rise /Settling velocity plot for the (+22 -31.5mm) particles

The empirical constant for the (+22 – 31.5mm) was found to be 900 gcm-1s-1 which is almost half less than the empirical constant for the (+37 -53mm) particles.

5.3.2.3 Rise/settling velocity plot for the (+16 -22mm Blk) particles

Figure 5.23 below illustrates the rise/settling velocity plot for the (+16 – 22mm Blk) particles. The proposed empirical model (eqn 5.26) fitted the data quite well with a relatively high R^2 value of 0.9288 being recorded. The rise and settling data points were all uniformly scattered about the linear model plot. The distribution of the settling data points from (1.64 – 1.80) further indicate how difficult it can be to accurately predict the settling velocities of the near cut density particles. This probably as a result of the complex hydrodynamics associated with the operation of the 3 D fluidized bed coal separator.

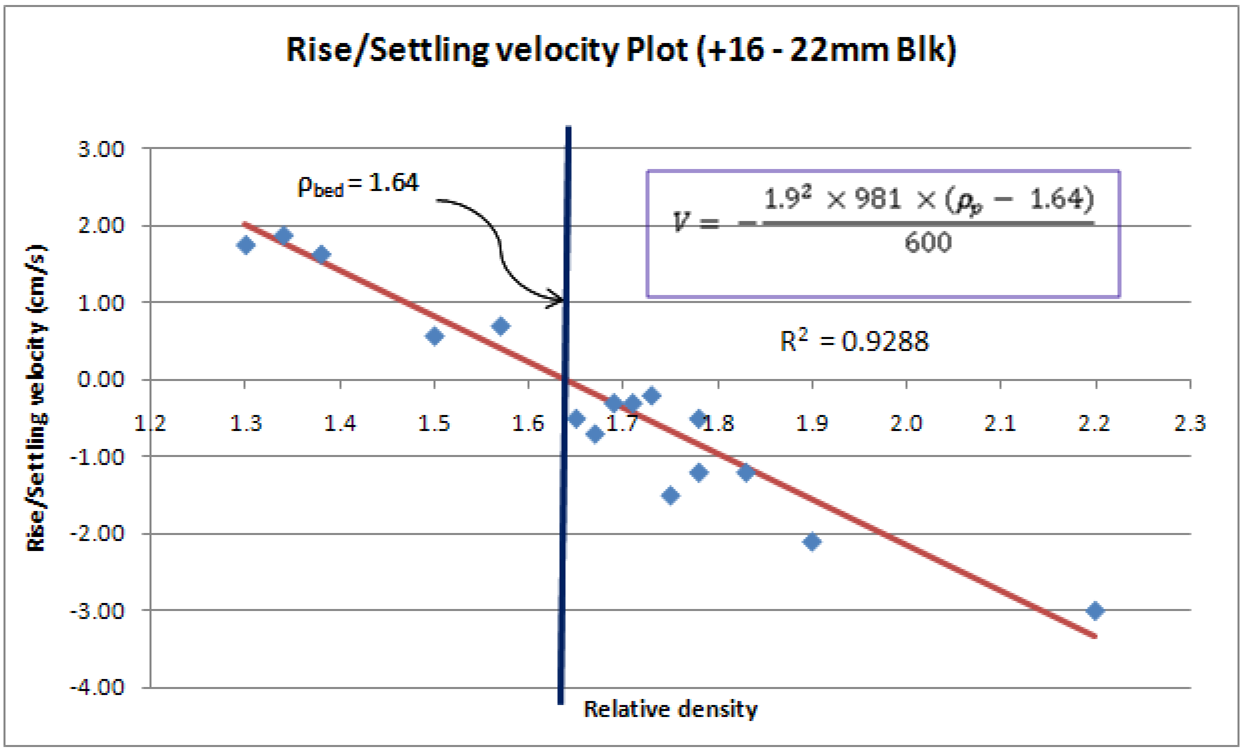

Figure 5.23: Rise /Settling velocity plot for the (+16 -22mm Blk) particles

The fact that the 2.2 density particles were still settling after 10s of separation indicate that it takes a bit longer to efficiently separate the (+16 -22mm Blk) particles as compared to the other particle size ranges discussed above. An empirical constant of 600 $gcm^{-1}s^{-1}$ was obtained for the separation tests of the (+16 -22mm Blk) particles.

5.3.2.4 Rise/settling velocity plot for the (+16 -22mm SR) particles

The proposed rise/settling velocity model fitted the (+16 -22mm SR) rise and settling data very well, with a relatively high R^2 value of 0.9564 recorded. Although the data points are uniformly distributed about the linear model plot, some of the (+16 – 22mm SR) flotsam particles were settling instead of rising as expected. This is attributed to the circulation motion of the medium particles which is associated with the operation with the 3 D bed. The near cut density particles have got rise / settling velocity close to zero hence they their motion is easily affected by the circulating motion generated when the 3 D fluidized bed is in operation.

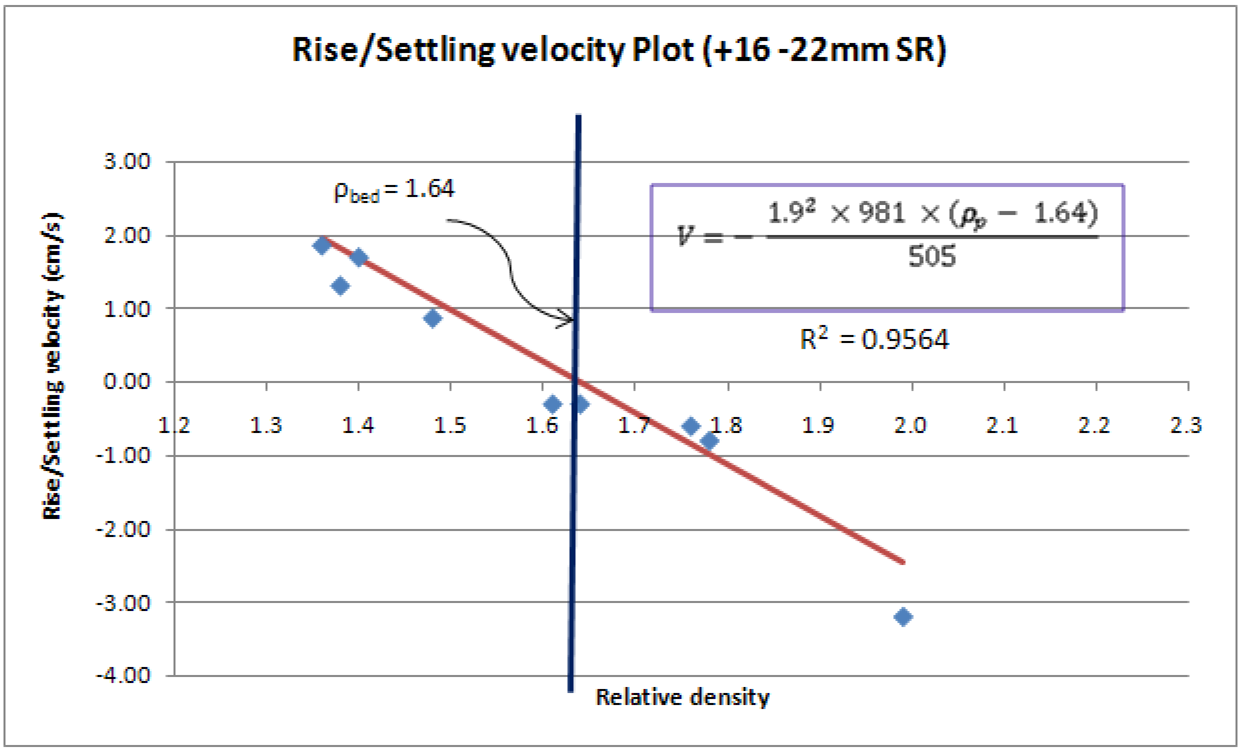

Figure 5.24: Rise /Settling velocity plot for the (+16 -22mm SR) particles

From the numerical analysis of the (+16 -22mm SR) rise and settling data, the empirical constant of the (+16 -22mm SR) particles was found to be 505 $gcm^{-1}s^{-1}$.

5.3.2.5 Rise/settling velocity plot for the (+16 -22mm FB) particles

Although the proposed empirical model fitted the (+16 -22mm FB) well with an R^2 value of 0.9022 being recorded, the data points were scattered (see Figure 5.25 below), which further highlight how difficult it can be to efficiently separate the (+16 – 22mm FB) particles. The observed rise velocity trend of the (1.30 – 1.40) density particles could be as a result of the accumulation of medium particles on the surfaces of the particles. Flat particles have got relatively wider surface areas such that silica and magnetite medium particles can easily settle on the surface of the particles thereby altering their apparent densities.

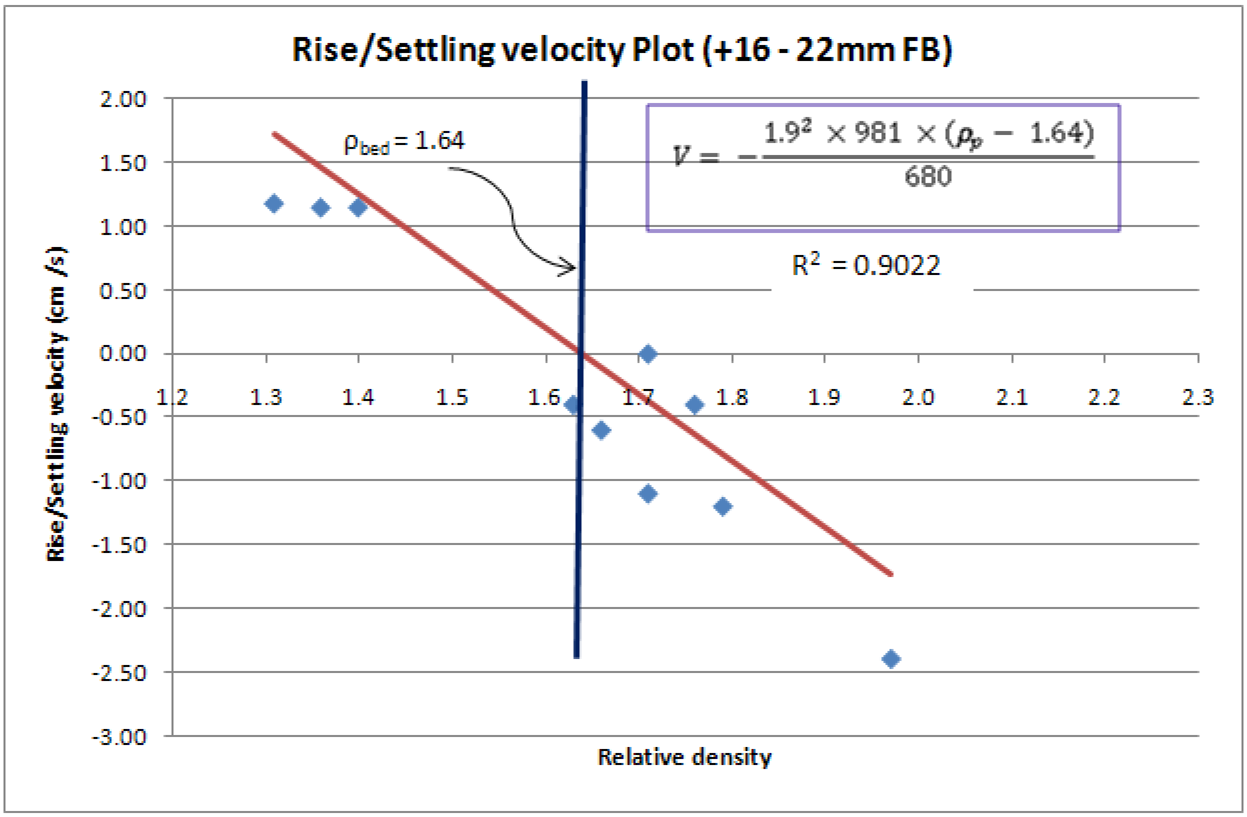

Figure 5.25: Rise /Settling velocity plot for the (+16 -22mm FB) particles

An empirical constant of 680 gcm-1s-1 was obtained for the (+16 – 22mm FB) particles.

5.3.2.6 Rise/settling velocity plot for the (+9.5 -16mm) particles

The model fit for the (+9.5 -16mm) particles was not as good as for the other particle size ranges discussed above. An R^2 value of 0.8679 was obtained and most of the rise/settling data points were below the linear model plot. The observed trend in Figure 5.26 is probably as a result of circulating velocities associated with the operation of the 3 D air fluidized coal separator. More so, the particle- particle interactions or particle – fluid interaction can have some adverse effects on the separation efficiency of the (+ 9.5 -16mm). All the above mentioned factors makes it difficult to accurately predict the rise/settling velocities of the particles in the fluidized bed.

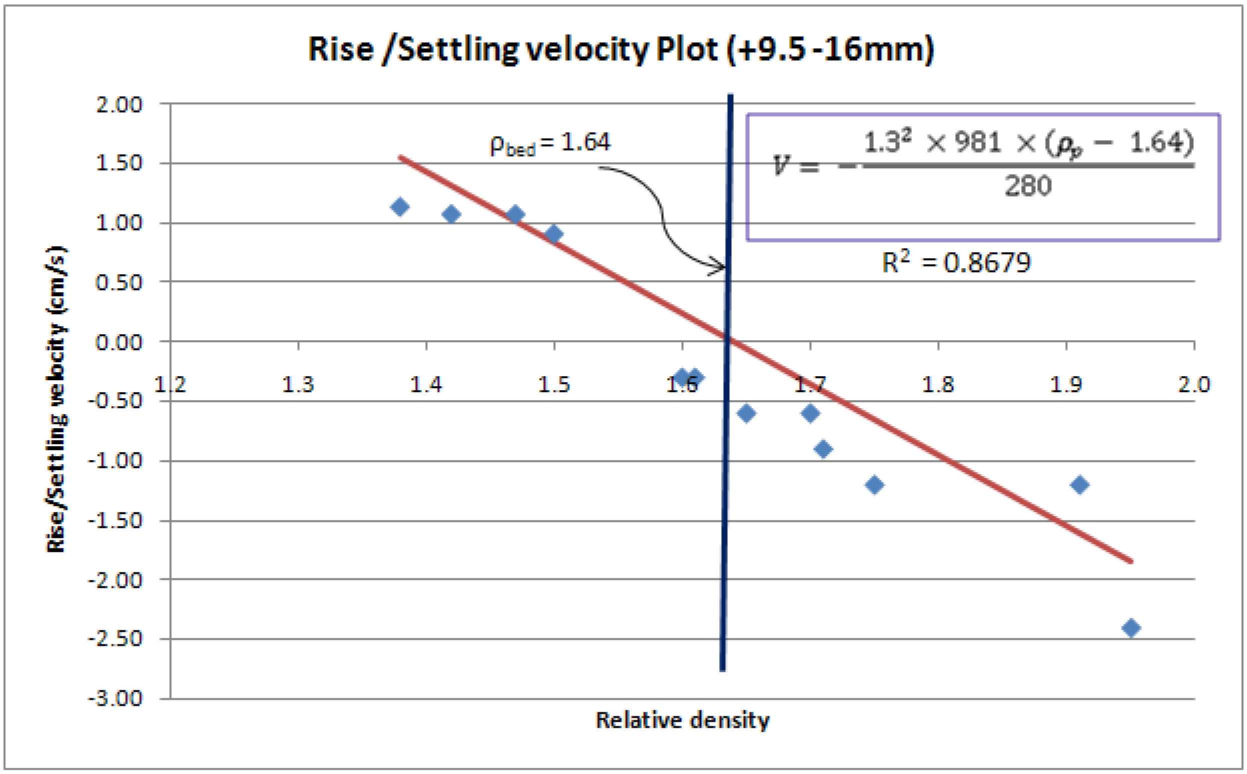

Figure 5.26: Rise /Settling velocity plot for the (+9.5 -16mm) particles

A relatively low empirical constant of 280 gcm-1s-1 was recorded for the (+9.5 -16mm) particles.

5.3.2.7 Rise/settling velocity plots for the different particle size ranges

Figure 5.27 below compares the rise/settling velocity plots for the various particle size ranges which include (+9.5 – 16mm), (+16 – 22mm), (+22 – 31.5mm) and (+37 – 53mm).

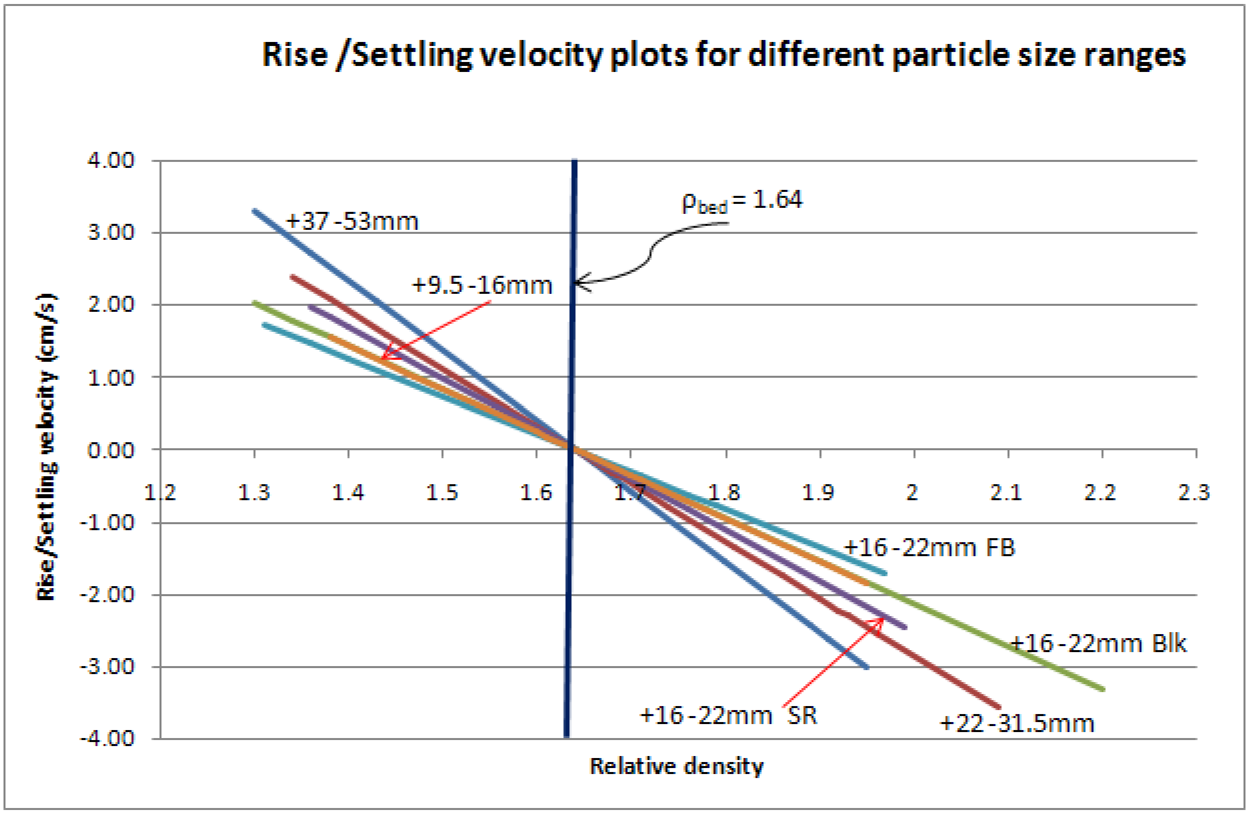

Figure 5.27: Rise /Settling velocity plot for the different particle size ranges

From Figure 5.27 above, it can be seen that that the (+37 – 53mm) particles whose density was lower than the bed density of 1.64 rose faster than all the other particle size ranges followed by the (+22 -31.5mm), (+16 -22mm) and (+9.5 -16mm) particles respectively. On the other hand, the same trend was also observed for the settling particles whose density was greater than the bed density, the (+37 -53mm) particles settled faster than all the other particle size ranges mentioned above. The observed trends indicate that particle size has got a significant effect on the separation performance of the air fluidized bed separator. The bigger particles tend to separate faster than the smaller particles hence in a continuous separation system; different residence times should be used. In dense medium separation, the difference between the particle density and the medium density determine whether a particle will rise or settle. Generally, particles with density less than the medium density will rise to the top of the bed, but their rise velocities mainly depend on the magnitude of the buoyancy force. The higher the buoyancy force than all the other particles acting on the particle in the separating fluid then the faster the particle will rise to the top of the bed. Big particles such as the (+37 -53mm) particles tend to displace more fluid than the smaller particles hence their buoyancy force is relatively high and they tend to rise faster. However the opposite is true for the high density (+37 -53mm) particles, they settle faster than all the other particle size ranges discussed above. This is because the gravitational forces acting on the high density (+37 -53mm) particles are greater than the buoyancy and drag forces acting on the particles and as such, the particles will sink faster as compared to the other smaller particle size ranges.

The rise and settling velocities for all the near cut density particles (+1.55 -1.70) were all close to zero regardless of the particle size. This makes the separation of the near cut density particles a critical step in determining the separation efficiency of the air fluidized bed coal separator as the separation of these particles can be easily other factors such as the particle – fluid interactions or particle – particle interactions.

Analysis of the empirical constants for the different particle size ranges outlined above indicates that the empirical constants decreased with particle size. Empirical constants of 2040 $gcm^{-1}s^{-1}$, 900 $gcm^{-1}s^{-1}$, 600 $gcm^{-1}s^{-1}$, 505 $gcm^{-1}s^{-1}$, 680 $gcm^{-1}s^{-1}$ and 280 $gcm^{-1}s^{-1}$ were recorded for the (37 -53mm), (+22 -31.5mm), (+16 – 22mm Blk), (+16 – 22 SR), (+16 -22 FB) and ((+9.5 -16mm) particles respectively. The drag forces acting on the bigger particles are relatively stronger than those acting on the smaller particles (see equation 5.18). However, the bigger particles whose specific densities are greater than the bed density are always associated with stronger gravitational forces because of their large volumes and high densities. Hence, their resultant motion is always downwards and they always tend to settle faster than the smaller particles.

On the other hand, particle shape proved to be a very important parameter in determining the separation performance of the air fluidized bed as evidenced by the observed trends of the (+16 -22mm) particles of different shapes in Figure 5.27. This is going to be discussed in detail in the following section.

5.3.2.8 Rise/settling velocity plots for the (+16 -22mm) particles of different shapes

Figure 5.28 below illustrates the rise/settling velocity plots for the (+16 -22mm) of different shapes. The high density sharp pointed prism, (+16 -22mm SR) particles settled faster than the blockish (+16 -22mm Blk) and flat, (+16 – 22mm FB) particles. The same trend was also observed for the less dense or rising particles, where the sharp pointed prism particles rose faster than all the other shapes followed by the blockish and flat particles respectively.

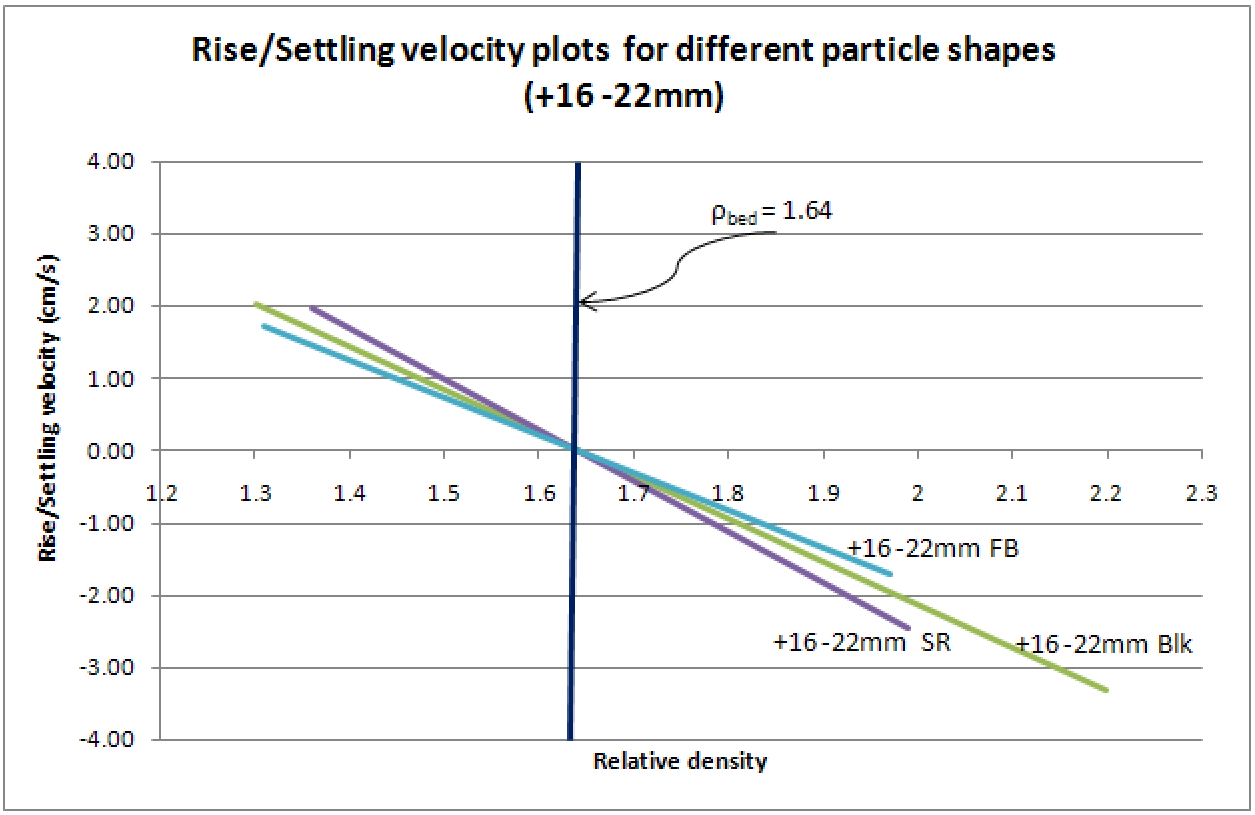

Figure 5.28: Rise /Settling velocity plot for the (+16 -22mm) particles of different shapes

All the (+16 -22mm) particles of different shapes used for the rise/settling tests had almost the same masses, which means that the gravitational forces that were acting on the different particles were almost the same. However, the buoyancy and drag forces acting on the particles varied from one particle to another depending on the particle shape, which has got a significant effect on the surface area of the particle in contact with the fluid. A relatively high empirical constant of 680 $gcm^{-1}s^{-1}$was recorded for the flat particles which probably explain why the particles rose or settled slower than the blockish and sharp pointed prism particles. The empirical constant is a function of the viscosity, which is directly proportional to the drag force, the higher the form viscosity then the higher the drag force (see equation 5.18). Empirical constants of 505 $gcm^{-1}s^{-1}$ and 600 $gcm^{-1}s^{-1}$ were recorded for the (+16 -22mm SR) and (+16 -22mm Blk). This means that there was less resistance to the motion of the (+16 -22mm SR) particles in the air fluidized bed, hence why they settled and rose faster than all the other (+16 -22mm) particles of different shapes. The observed trends in Figure 5.28 indicate that although particle shape is a difficult parameter to control, it has got a significant effect on the separation performance of the air fluidized coal separator; hence it needs to be optimally controlled where possible.

5.4 Validation of the empirical rise/ settling velocity model

Rise/settling tests aimed at validating the proposed empirical model were carried out using a separation time of 15s and a fluidized bed height of 32cm. For the rising tests, the particles were released from the bottom of the bed and the fluidized bed was switched off exactly after 15s. The respective positions /levels of the particles after 15s were recorded; the bottom of the bed was regarded as the start point (0cm) whilst the top of the bed corresponded to the fluidized bed height (32cm).On the other hand, for the settling tests the particles were introduced from the top of the bed and the bed was switched off after 15s of separation. A positive (+) level/height (cm) was used for the rising particles whilst a negative sign (-) was used to denote the level of the settling particles.

The proposed simple empirical model was used to predict the position of the particles in the bed by treating equation (5.26) as illustrated below.

$$V = -\frac{d^2 g(\rho_p - \rho_{bed})}{A} \tag{5.26}$$

Rise/settling velocity is a derivate of the bed height/level (cm), h

Therefore,

$$\frac{dh}{dt} = -\frac{d^2 g(\rho_p - \rho_{bed})}{A} \qquad (5.27)$$

Integrating equation (5.27),

$$\int_{h_1}^{h_2} dh = -\frac{d^2 g(\rho_p - \rho_{bed})}{A} \int_{t_1}^{t_2} dt \qquad (5.28)$$

$$h_2 - h_1 = -\frac{d^2 g(\rho_p - \rho_{bed})}{A} (t_2 - t_1) \qquad (5.29)$$

where h_1 – bed height at the start of the tests ($h_1 = 0$)

t_1 – time at the start of the tests ($t_1 = 0$)

h_2 - position of the particle after 15s of separation (cm)

t_2 - separation time (s)

$$h_2 = -\frac{d^2 g(\rho_p - \rho_{bed})}{A} \; t_2 \qquad (5.30)$$

Equation (5.30) was used to predict the respective positions of the different particles and this was compared with the actual/experimental values. % absolute errors were calculated for the different particle size ranges, shapes and densities. The results are summarized in Appendix F.

Meanwhile, the graphs of the % Error vs. particle density for the (+37 -53mm), (+22 -31.5mm), (+16 -22mm Blk), (+16 -22mm SR), (+16 -22mm FB) and (+9.5 -16mm) particles were plotted and are going to be discussed in the following section.

5.4.1 % Error vs. Particle density graphs for different particle size ranges and shapes

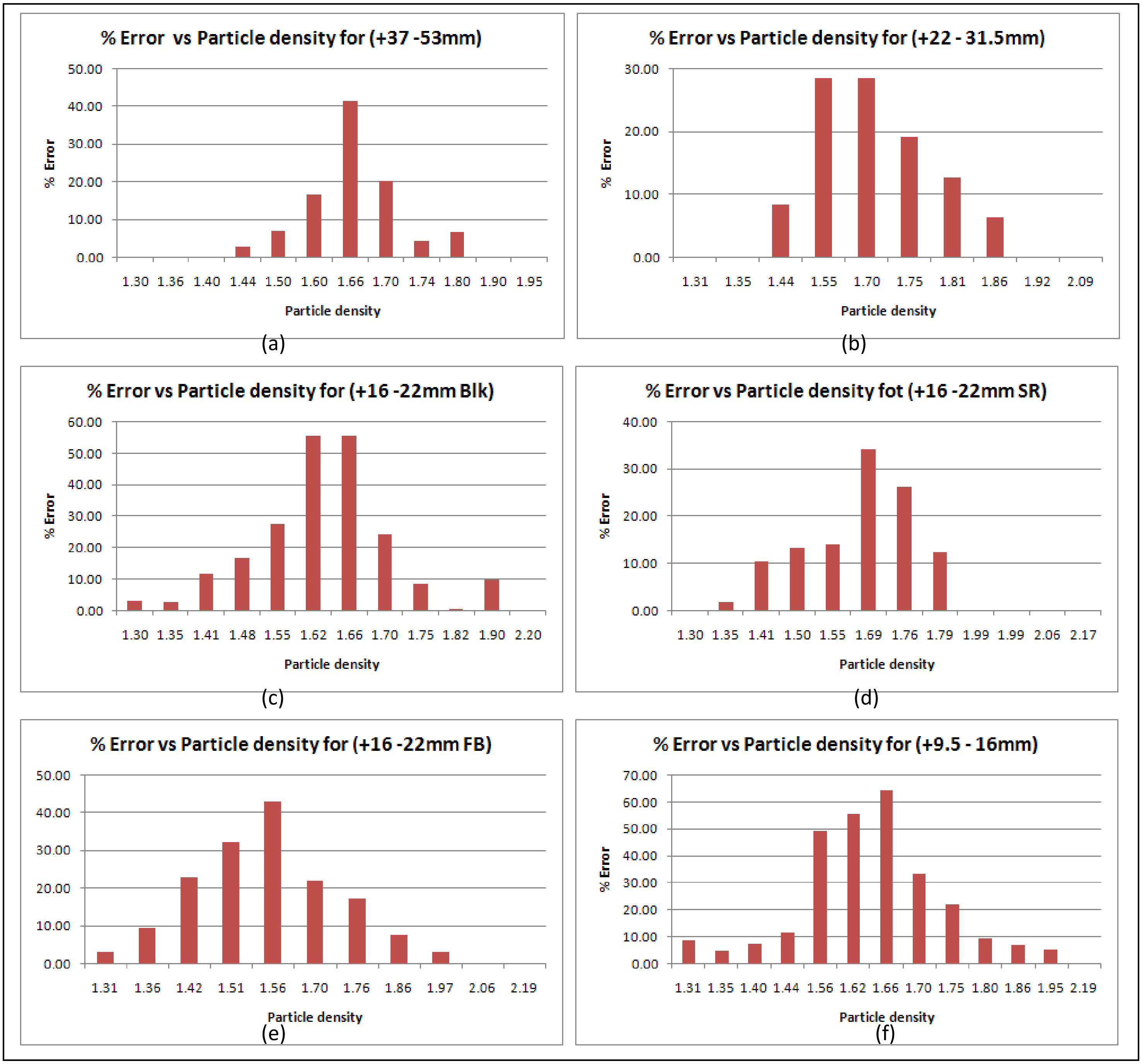

Figure 5.29 (a) – (f): % Error vs. particle density graphs for the different particle size ranges

Average % absolute errors of 8.25%, 10.34%, 17.92%, 9.34%, 14.57% and 21.37% were recorded for the (+37 -53mm), (+22 -31.5mm), (+16 -22mm Blk), (+16 -22mm SR), (+16 -22mm FB) and (+9.5 -16mm) particles respectively. Based on the % errors data given above, it can be concluded that the proposed empirical model predict the rise/settling velocities of all various particle size ranges very well except for the (+9.5 -16mm) where a relatively high % error of 21.37% was recorded. However, it can be clearly seen in Figure 5.29 (a) – (f) that the proposed empirical model cannot accurately predict the rise/settling velocities of the near cut density particles (1.55 – 1.75) as evidenced by the high % errors recorded for all the particle size ranges. The % error seems to increase with decrease in the particle size. The high % error encountered in the prediction of the position of the near cut density particles in the bed is partially attributed to the fact that the particles have got very low rise/settling velocities which are close to zero. As such the separation or position of particles in the bed is mainly depends on the circulating forces in the bed as well as the particle – particle interactions. Otherwise, the proposed model can accurately predict the rise/settling velocities or respective positions of the particles in the bed after a certain separation especially for the particles whose relative densities are far from the cut density.

Chapter 6

Conclusions and Recommendations

The study on the effects of particle size, density and shape on the performance of an air fluidized bed revealed some critical information which is expected to go a long way in the further development of a more efficient continuous separation processing system. The operation of the air fluidized bed coal separator is associated with some complex hydrodynamics, which makes it difficult to fully understand all the principles behind the operation of such systems. However, the performance of the dry separator can be successfully optimized by manipulating some of the operating parameters such as particles size, shape and density of the feed and medium particles etc as highlighted by some of the research findings outlined below.

The first critical step in the development of an efficient air fluidized bed separation system involves designing a 3 D air fluidized bed, which ensures a uniform distribution of air throughout the three dimensional space. Although there is a lack of simple and generalized criteria, which can be applied in the design of multiphase flow systems, the pressure drop across the distributor is one of the most important parameters which should be seriously considered. The pressure drop across the distributor is a function of many complex variables which include pressure drop required across the bed, bed weight, bed height, bed expansion ratio, fluidizing velocity, medium properties, geometry of the distributor and fraction of the distributor plate or cloth area open for gas flow. Some of these critical parameters have already been discussed in detail in Chapter 3.

Selection of the medium with the optimum properties which give rise to a relatively uniform and stable bed density is very crucial to the efficient operation of the air fluidized bed separator. The medium properties such as the particle size, density and shape have got a significant effect on the quality of fluidization. Before any detailed tests could be carried out, some preliminary tests aimed at establishing the optimum medium properties required for the separation of the South African coals were carried out separately using (+53 -450 µm) silica and (+53 -450 µm) magnetite particles. Relatively uniform and stable average bed densities of 1.35 and 2.70 were obtained for the silica and magnetite beds respectively, but the density of most South African coals vary from 1.30 -2.70. Hence, both the silica and magnetite beds cannot be used separately to efficiently separate coals with a wide density range. As such a mixture of silica and magnetite was prepared for the detailed tests. A wide particle size distribution of the medium particles promotes good quality fluidization, but the wider the particle size distribution the more likely is segregation going to take place. Segregation can adversely affect the bed density distribution, so medium particles with similar minimum fluidizing velocities should always be selected. The Ergun equation (2.17) can always be used to estimate the minimum fluidizing velocities of the different medium particles especially if the bed pressure drop, bed voidage, particle density and size are known.

The silica- magnetite medium that was used for detailed tests was prepared by mixing 80kgs of (+53 - 300µm) silica and 45kgs of (+53 -212µm) magnetite. The medium was fluidized at $1.4U_{mf}$ to give a uniform average bed density of 1.64 and STDEV < 0.006 g/cm^3. The bed density can be easily varied by changing the mixing ratios of silica and magnetite, equation (4.2) can be used to determine the optimum mixing proportions required to achieve any specific bed density.

In order to assess the performance of the silica – magnetite bed, 20mm diameter cube and disc density tracers were used to measure the partition curve of bed, which proved to be very efficient with some Ep values as low as 0.032 being recorded. Before any detailed tests could be carried out, particles with densities varying from 1.30 – 2.70 were selected from the following particle size ranges: (+9.5 -16mm, (+16 -22mm), (+22 -31.5) and (+37 -53mm). Particle shape is a parameter which is difficult to quantitatively define, so only qualitative descriptions were used to distinguish the (+16 -22mm) particles of different shapes namely blockish, flat or sharp pointed prism particles.

Analysis of the separation performance of the different particle size ranges was carried out based on the Klima and Luckie partition model (1989) which fitted the partition data very well, with high R^2 values ranging from (0.9210 - 0.9992) being recorded. Generally, the bigger particles, that is the (+37 -53mm) and (+22 -31.5mm) particles separated faster and more efficiently than the smaller particles, (+16 -22mm) and (+9.5 -16mm) particles. The separation performance of the different particles was measured mainly based on the separation inefficiency, Ep and the fluctuation or shift of the bed cut density, ρ_{50}. Average Ep values as low as 0.05 were recorded for the separation of (+37 -53mm) and (+22 -31.5mm) particles under steady state conditions with minimum fluctuation of the cut density. However, a further decrease in the particle size was associated with relatively high Ep values and a continuous shift of the cut density as evidenced by the average Ep values of 0.07 and 0.11 that were recorded for the (+16 -22mm) and (+9.5 – 16mm) particles respectively, after 30s of separation.

The 3 D fluidized bed can efficiently separate the (+16 -22mm), (+22 – 31.5mm) and (+37 - 53mm) particles and the separation efficiency of the particles can be further improved by using deeper beds (bed height > 40cm). Analysis of both the settling and rise velocity test results indicates that different optimum operating conditions such as the residence time, feed rate, cut density etc are required for the efficient separation of the different particle size ranges. While the (+37 -53mm) and (+22 -31.5mm) particles can be efficiently separated using the same bed, separate beds with different optimum operating parameters are required for the efficient separation of the (+16 -22mm) and (+9.5 – 16mm) particles respectively. This further illustrates why prescreening of the coal particles into relatively narrow ranges is important in the optimization of dry coal beneficiation using an air fluidized bed. Particles of different sizes and densities interact with the separating medium/fluid in various ways and the resultant rise/settling velocities of the near cut density particles have got a significant effect on the separation performance of the air fluidized bed coal separator. If the rise or settling velocities of the near cut density particles are lower than the circulating velocities then the resultant direction or motion of the particles would be determined by the direction of the circulating forces. In as much as the air fluidized bed behaves like a pseudo fluid; some medium particles can always accumulate on the surfaces of the particles thereby altering their apparent densities. This has got a negative effect on the separation performance of the near cut density flotsam particles as they end up recovered as sinks.

The amount of medium particles that accumulate on the surfaces of the particles is directly linked to the surface area of the particle in contact with the fluid. The above conclusion further illustrates the importance of particle size, shape and density on the separation performance of particles in the air fluidized bed. Although, particle shape is a parameter which is very difficult to control, the separation results of the (+16 -22mm) of different shapes indicate that particle shape has got a significant effect on the separation performance of the particles in the air fluidized bed. Three different particle shapes that were used during the tests included the flat (+16 -22mm FB), blockish (+16 -22mm Blk) and sharp pointed prism (+16 -22mm SR) particles. The blockish particles separated better than flat and the sharp pointed particles as evidenced by the relatively low and constant Ep values obtained after about 30s of separation. Despite relatively constant Ep values being achieved for the separation of (+16 – 22mm SR) particles; high average Ep values of approximately 0.10 were recorded. On the other hand, the Ep values of the (+16 – 22mm FB) particles improved with time, but the continuous shift of the cut density made it difficult to efficiently separate the flat particles and this can be attributed to the scenario discussed above.

The separation performance of the 3D air fluidized bed largely depends on the rise and settling velocities of the feed particles in the bed and a deep understanding of the rise and settling behavior of the particles in the bed is of fundamental importance in both the design and optimization of the continuous separation system. As part of this study, a simple rise/settling velocity empirical model was developed based on the Stokes' law. The Re of the fluid was estimated using the empirical data and it was found to be relatively low (Re< 150). Moreso, the bed density/ separating fluid density throughout the three dimensional space was measured and found to be relatively uniform (STDEV < 0.006 g/cm^3), hence the Stokes' Law could be applied in the development of the empirical model. Meanwhile, the following assumptions were made: the wall effect in the (40 x 40 x 60) cm 3D air fluidized bed was negligible, the coal particles instantaneously reached terminal velocity when they were introduced in the 3 D air fluidized bed, the particle – particle interactions were negligible etc.

The proposed empirical model fitted the rise/settling data for the different particle size ranges very well and R^2 values as high as 0.9935, 0.9583, 0.9564, 0.9288, 0.9022 and 0.8672 were recorded for the (+37 -53mm), (+22 -31.5mm), (+16 -22mm SR), (+16 -22mm Blk), (+16 -22mm FB and (+9.5 -16mm) particles respectively. Although the proposed simple rise/settling velocity model can be used to predict the rise and settling velocities for particles of different sizes, shapes and densities, the accuracy of the model decreased with particle size as evidenced by the trend of the R^2 values given above. The distribution of the near cut density particles' rise/settling velocities data points for all the different particle size ranges indicate that it is very difficult to accurately and precisely predict the rise/ settling velocities of the particles since the rise and settling velocities were all close to zero. This makes the separation of the near cut density particles a very critical step in determining the separation efficiency of the air fluidized bed coal separator as the separation of these particles is mainly influenced by the particle – fluid interactions or particle – particle interactions.

Different empirical constants of 2040 $gcm^{-1}s^{-1}$, 900 $gcm^{-1}s^{-1}$, 600 $gcm^{-1}s^{-1}$, 505 $gcm^{-1}s^{-1}$, 680 $gcm^{-1}s^{-1}$ and 280 $gcm^{-1}s^{-1}$ were recorded for the (37 -53mm), (+22 -31.5mm), (+16 – 22mm Blk), (+16 – 22 SR), (+16 -22 FB) and ((+9.5 -16mm) particles respectively. Analysis of the empirical constants for the different particle size ranges and shapes outlined above indicate that the constants decreased with particle size and varied for different particle shapes. The particle size, shape and density all affect the three main forces acting on the particle in the air fluidized bed and these include the gravitational, buoyancy and drag forces. As such, the resultant motion of the particles in the air fluidized bed mainly depends on the above mentioned parameters. This further illustrates that the particle parameters have got a very significant effect on the separation performance of the air fluidized bed separator.

Validation of the empirical model was done using rise and settling data that was collected after 15s of separation and average % absolute errors of 8.25%, 10.34%, 17.92%, 9.34%, 14.57% and

21.37% were recorded for the (+37 -53mm), (+22 -31.5mm), (+16 -22mm Blk), (+16 -22mm SR), (+16 -22mm FB) and (+9.5 -16mm) particles respectively. This means that the proposed empirical model can be used to accurately predict the rise or settling velocities or positions for all the other particle size ranges mentioned above except for the (+9.5 -16mm) particles where a relatively high average % error (21.37%) was recorded.

Although the proposed empirical model predicted the respective positions of the different particles well after 15s of separation, the accuracy of this model can be improved by carrying out further detailed rise/settling tests using more accurate and precise equipment such as the gamma camera to track the motion of the particles in the fluidized bed. Quantitative information related to the different projectiles followed by the particles in the fluidized bed as well as the instantaneous relative velocities of the particles can be easily established through the use of the above method. The air fluidized bed viscosity data is very critical to the further development of the proposed empirical model and in future, the viscosity of the bed should always be measured using a viscometer.

The proposed simple rise/settling empirical model and partitioning data obtained during the separation tests establishes a strong basis for developing a partition function/model which incorporates the rise/settling velocity of the particles and two of the most familiar parameters in the coal processing industry (Ep and ρ_{50}). The partitioning performance of the particles in dense separation is a strong function of the rise/settling velocities of the particles. However, in order to improve on the practical applicability of the proposed model, there is probably a need to incorporate some machine constants and particle – fluid parameters such as the circulating velocities etc. This will probably result in a more complex model, but it will aid in the scale up and design of a more efficient continuous separation system. Computational fluid dynamics is one of the tools which can be used to efficiently model such complex systems.

From a general perspective, the air dense fluidized bed using the silica – magnetite mixture as the separating medium proved to be an efficient separation processing system, but in order to minimize segregation problems and maintain a uniform bed density distribution in the bed, there is a need to investigate if there is any other single phase medium which can be used in place of the compound mixture. Typically, the medium should be readily available, density greater than 2800kg/m^3 depending on the desired cut point density and the medium should also have excellent fluidizing properties. In future, the use of a vibrating fluidized bed should also be investigated as this may promote a relatively uniform bed density distribution ideal for dry dense separation.

References

Chen Q. R., Yang Y., Tao X. X., Liang C. C. and Chen Z. Q., 1994, 50t=h Coal Dry Cleaning Demonstration Plant with Air Dense Medium Fluidized Bed, Fluidization '94 Science and Technology Conference Proceedings, Fifth China-Japan Symposium, China, pp. 381–389

Clark N., Turton R. and Anderson R., 1993, Start-up of large, slumped, shallow fluidized beds, Proc. Powder and Bulk Solids Conf, Rosemont, IL, USA

Cranfield R. R. and Geldart D., 1973, Large Particle Fluidization, Chemical Engineering Science, Vol. 29, pp 935 – 947

Davison J.F. and Harrison D., 1971, Fluidization, Academic Press, New York, p. 248

Dong X. and Beeckmans J., 1990, Separation of particulate solids in a pneumatically driven counter-current fluidized cascade. Powder Technology, Vol.62, pp. 261 – 267

Foscolo P., Gibilaro L., 1991, A fully predictive criterion for the transition between particulate and aggregate fluidization, Chemical Engineering Science, Vol. 39, pp 1667

Geldart D., 1986, Gas Fluidization Technology, Wiley, Chichester, UK, pp. 65-78

Hoffmann C., Janssen M. and Prins J., 1992, Particle Segregation in Fluidized Binary Mixtures, Chemical Engineering Science, Vol. 48, pp. 1583-1592

Jin H., Zhang J. and Zhang B., 2007, The effect of vibration on bed voidage behaviors in fluidized beds with large particles, Brazilian Journal of Chemical Engineering, Vol. 24, No.3, pp. 389-397

Kretzschmar S., Pocock J. and Loveday B., *2008*, Industrial Fluidization in South Africa (IFSA 2008), Proceedings of a conference on fluidization in South Africa, Johannesburg

Kunii D. and Levenspiel O., 1991, Fluidization Engineering, Butterworth-Heinemann, Boston, MA, 2nd edition, pp. 95-108

Lockhart N., 1984, Dry beneficiation of Coal, Powder Technology, Vol. 40, pp. 17 – 42

Luckos A and Smit P., 2005, Industrial Fluidization in South Africa (IFSA 2005), Proceedings of a conference on fluidization in South Africa, Johannesburg, pp 345 - 355

Luo Z., Chen Q. and Tao X., 2000, Formation Mechanism of Vibrated Fluidized Bed (VFB), J. China University of Mining & Technology, Vol.29, pp. 230–234

Luo Zhenfu and Chen Qingru, 2001, Dry beneficiation technology of coal with an air dense-medium fluidized bed, International Journal of Minerals Processing, Vol.63, pp. 167 – 175

Luo Zhenfu and Chen Qingru, 2002, Effect of fine coal accumulation on dense phase fluidized bed performance, International Journal of Minerals Processing, Vol.63, pp. 217 – 224

Max Leva, 1959, Fluidization, McGraw – HILL Company INC

Napier – Munn T., 1991, Modelling and simulating dense medium separation processes – a progress report, International Journal of Minerals Processing, Vol.4, pp. 329 – 346

Netshidongololwe T., 2004, DEM modeling of fluidized Behavior, University of Witwatersrand MSc Thesis

Qureshi A. and Creasyd D., 1991, Fluidized Bed Gas Distributors, Chemical Engineering and Processing, Vol. 33, pp 419 - 428

Smith T. N., 1998, A model of settling velocity , Chemical engineering Science, Vol. 53, No.2, pp. 315 – 323

Terence Allen, 1990, Particle size measurement, Powder Technology Series, 4th edition, pp 95 – 123

Wills B., 2006, Minerals Processing Technology, Butterworth-Heinemann, 7th edition, pp 77 - 190

Yaomin Zhao and Lubin Wei, 2000, Rheology of gas-solid fluidized bed, Fuel Processing Technology, Vol.68, pp. 153 – 160

Appendix A

Appendix A - 1: Calibration of the pressure sensor

A 100cm H_2O manometer was used to calibrate the Action Instruments pressure sensor before any tests were carried out. The manometer readings were then plotted against the pressure sensor readings and the calibration curve was found to be linear as illustrated in the chart below.

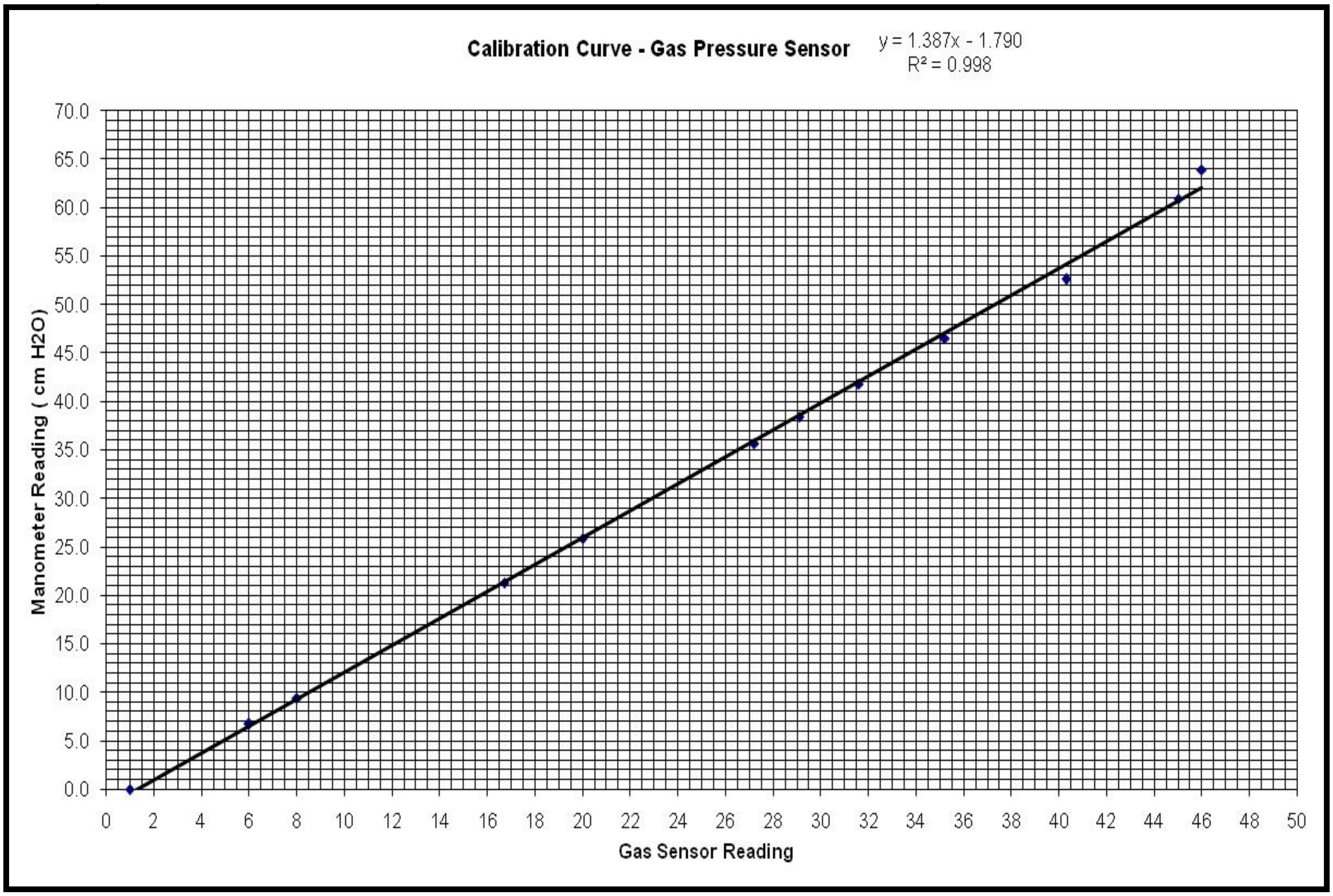

The following linear relationship was used to convert the pressure sensor readings to cm H_20.

$$y = 1.387x - 1.790$$

where x is the pressure sensor reading and y is the manometer reading (cm H_2O) respectively.

1 cm H_2O = 98.0665 Pa *(Resident's Handbook Basel, 1996)*

Appendix A - 2: Calibration of the GEC - ELLIOT gas rotameter

The manufacturer's calibration curve for the GEC – Elliot gas rotameter was missing, so the rotameter was calibrated by connecting it in series with another rotameter whose calibration curve was available. The calibration data was tabulated as shown in the table below.

Table A2: Calibration data for the GEC – Elliot gas rotameter

Rotameter Reading	Gas Flow Rate (m^3/min)			Gas Flow Rate @ s.t.p	Rotameter 1a Mass Flow Rate	Rotameter 2 Mass Flow Rate	Rotameter 3 Mass Flow Rate	Actual Gas Flow rate
cm	Test 1	Test 2	Avg	L/s	kg/s	kg/s	kg/s	L/s
2.25	0.13	0.15	0.14	2.3	2.80E-03	2.56E-03	5.60E-03	4.65
4.00	0.21	0.19	0.20	3.3	4.00E-03	3.66E-03	8.00E-03	6.64
5.25	0.22	0.21	0.22	3.6	4.30E-03	3.93E-03	8.61E-03	7.14
7.25	0.24	0.26	0.25	4.2	5.01E-03	4.57E-03	1.00E-02	8.30
8.00	0.26	0.28	0.27	4.5	5.41E-03	4.94E-03	1.08E-02	8.96
10.25	0.33	0.33	0.33	5.5	6.61E-03	6.03E-03	1.32E-02	10.95
12.00	0.37	0.37	0.37	6.2	7.41E-03	6.76E-03	1.48E-02	12.28
15.00	0.44	0.43	0.44	7.3	8.71E-03	7.95E-03	1.74E-02	14.44
16.00	0.46	0.48	0.47	7.8	9.41E-03	8.59E-03	1.88E-02	15.60
18.70	0.53	0.55	0.54	9.0	1.08E-02	9.87E-03	2.16E-02	17.92
20.00	0.56	0.56	0.56	9.3	1.12E-02	1.02E-02	2.24E-02	18.59
21.00	0.58	0.60	0.59	9.8	1.18E-02	1.08E-02	2.36E-02	19.58
23.00	0.65	0.65	0.65	10.8	1.30E-02	1.19E-02	2.60E-02	21.57
24.00	0.67	0.67	0.67	11.2	1.34E-02	1.22E-02	2.68E-02	22.24
25.00	0.70	0.70	0.70	11.7	1.40E-02	1.28E-02	2.80E-02	23.23
26.00	0.72	0.74	0.73	12.2	1.46E-02	1.33E-02	2.92E-02	24.23
27.25	0.76	0.75	0.76	12.6	1.51E-02	1.38E-02	3.02E-02	25.06
28.00	0.78	0.79	0.79	13.1	1.57E-02	1.43E-02	3.14E-02	26.05

The rotameter that was used to calibrate the GEC – Elliot rotameter was initially calibrated at 1atm and 20^{o}C. However, the atmospheric conditions in the Mineral Processing laboratory at the University of the Witwatersrand are 0.83kPa and 20^{o}C, so all the gas flow rate readings were corrected to the standard conditions in the laboratory using the equations given below.

According to *(Head etal. 1954),* the mass flow rate through a rotameter is given by

$$w = q\rho = KD_f \sqrt{\frac{W_f(\rho_f - \rho)\rho}{\rho_f}} \qquad (1)$$

Where, w – mass flow rate

q – volume flow rate

ρ – fluid density

ρ_f - float density

W_f – float weight

K – flow parameter

The ratio of flow rates of two different fluids A and B at the same rotameter reading is given by

$$\frac{w_A}{w_B} = \frac{K_A}{K_B}\sqrt{\frac{(\rho_f - \rho_A)\rho_A}{(\rho_f - \rho_B)\rho_B}} \qquad (2)$$

Since,

$(\rho_f \gg \rho_A), (\rho_f - \rho_A) \approx \rho_f$

$(\rho_f \gg \rho_B), (\rho_f - \rho_B) \approx \rho_f$

Then,

$$\frac{w_A}{w_B} = \sqrt{\frac{\rho_A}{\rho_B}} \qquad (3)$$

Equation (1) given above was used to calculate the mass flow rate of the air at 1atm and 20^oC, the density of the air, ρ_{air} =1.20135 kg/m^3 under the above conditions. The calculated mass flow rates of the air at 1atm and 20^oC are summarized under the Rotameter 1a column in Table A2 above. Since, the atmospheric conditions in the Minerals Processing Laboratory at the University of the Witwatersrand were different from the conditions under which the other rotameter was calibrated. All the mass flow rates under the Rotameter 1a column were corrected to 0.83atm and 20^oC using equation (3). The density of the air at 0.83atm and 20^oC, ρ_{air} =1.00kg/m^3 was interpolated from the air density – temperature and pressure tables *(www.engineeringtoolbox.com)*. The corrected mass flow rates were recorded under the Rotameter 2 column shown in Table A2 above.

Due to the fact that relatively high gas flow rates were required for the detailed separation tests using the 3 D fluidized bed, an inlet gas pressure of 320kPa was used so as to increase the operating range of the gas rotameter. Meanwhile, all the necessary pressure corrections were carried out using equation (3). The density of the air at 20^oC and a gauge pressure of 320kPa was interpolated from the air density – temperature and pressure tables and it was found to be, ρ_{air} =4.800kg/m^3. All the corrected mass flow rate data was tabulated under the Rotameter 3 column in Table A2. The actual air volume flow rate was then calculated using the ideal gas equation given below:

$$PV = \frac{wRT}{M_r}$$

$$V = \frac{wRT}{PM_r}$$

Where, V- volume flow rate, w – mass flow rate of the air (320kPa and 20^oC) , R- universal gas constant , T – temperature of the air, P – absolute pressure (atmospheric pressure in this case) and Mr – molecular mass of air. Shown below is the calibration curve for the GEC – Elliot rotameter.

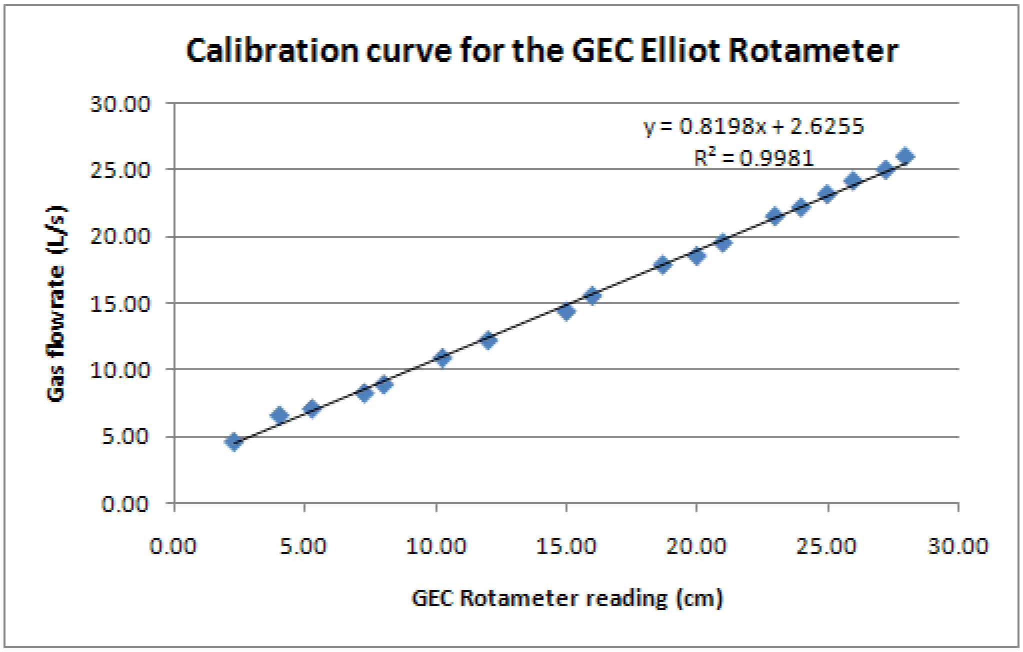

The calibration curve was found to be linear and the following equation was used to calculate the gas flow rate:

$$y = 0.8198x - 2.6255$$

where x is the rotameter reading

Appendix B

The Heywood's approach was used to describe the shapes of all the particles that were used for the rise velocity tests. All the Heywood's dimensions in Appendix B – 1 were all determined based on the equations 2.14 and 2.15 (a) – (c) outlined in section 2.5.2.1. Appendix B – 1 below provides a summary of the Heywood shape classification of all the particles that were used for the rise velocity tests. On the other hand, Appendix B -2 illustrates the rise velocity graphs for the different particle size ranges and shapes.

Appendix B - 1: Heywood’s shape classification

						Heywood's dimensions								
Shape description	Density Range	Particles Used	Sp.gr of Particle	Mass - Particle	Volume-Particle	B	L	T	m	n	d_a	p_r	α_a	Rise velocity (cm/s)
+37 - 53mm														
Angular - Prismoidal	1.30 - 1.40	C2	1.30	78.66	60.51	4.0	5.5	2.2	1.4	1.8	4.9	0.73	0.85	2.73
Angular - Prismoidal (rectangular)		D8	1.36	53.58	39.40	3.6	5.8	2.0	1.6	1.8	4.2	0.67	0.67	2.66
Angular - Prismoidal	1.40 - 1.50	H2	1.43	78.82	55.12	3.8	5.3	2.1	1.4	1.8	4.7	0.70	0.87	2.03
+22 -31.5mm														
Angular - Tetrahedral (flat)	1.30 - 1.40	D4	1.34	13.09	9.77	2.6	3.0	1.2	1.2	2.2	2.7	0.40	0.71	2.27
Angular - Prismoidal (sharp pointed)		B5	1.38	21.08	15.28	3.0	3.8	1.5	1.3	2.0	3.1	0.50	0.65	1.78
Angular - Prismoidal (Sharp pointed)	1.40 - 1.50	C6	1.40	16.1	11.50	2.6	3.3	1.5	1.3	1.7	2.8	0.50	0.72	1.11
Rounded (blockish)		C4	1.44	21.71	15.08	2.8	3.7	2.0	1.3	1.4	3.1	0.67	0.71	0.83
+16 -22mm Blk														
Angular - (Prismoidal & Tetrahedral)	1.30 - 1.40	J5	1.30	3.73	2.87	1.4	2.1	1.4	1.5	1.0	1.8	0.47	0.83	1.76
Angular - Prismoidal (blockish)		H9	1.34	7.87	5.87	1.7	2.7	1.6	1.6	1.1	2.2	0.53	0.86	1.88
Angular - Tetrahedral (blockish)		L1	1.38	6.60	4.78	1.8	2.7	1.3	1.5	1.4	2.1	0.43	0.71	1.64
Angular - Tetrahedral (blockish)	1.50 -1.57	L2	1.50	6.16	4.11	1.6	2.7	1.2	1.7	1.3	2.0	0.40	0.72	0.57
Angular - Tetrahedral (blockish)		I7	1.57	7.68	4.89	2.0	2.7	1.2	1.4	1.7	2.1	0.40	0.65	0.70
+16 -22mm SR														
Prismoidal and sharp pointed	1.30 - 1.40	X22	1.30	2.70	2.08	1.5	2.6	0.8	1.7	1.9	1.6	0.27	0.50	1.09
Angular - Tetrahedral (sharp pointed)		H2	1.36	7.05	5.18	1.3	3.5	1.2	2.7	1.1	2.1	0.40	0.80	1.86
Angular - Prismoidal (sharp pointed)		F9	1.38	6.02	4.36	1.6	2.6	1.8	1.6	0.9	2.0	0.60	0.78	1.31
Angular Prismoidal (sharp pointed)	1.40 -1.50	H3	1.40	8.58	6.13	1.8	2.8	1.7	1.6	1.1	2.3	0.57	0.80	1.70
Angular - Tetrahedral (sharp pointed)		F4	1.48	6.14	4.15	2.0	3.0	1.5	1.5	1.3	2.0	0.50	0.52	0.87
+16 -22mm FB														
Flat and cuboid	1.30 - 1.40	C5	1.31	4.72	3.60	1.6	2.1	1.0	1.3	1.6	1.9	0.33	0.85	1.18
Angular - Tetrahedral (flat)		D6	1.36	5.72	4.21	2.4	2.8	1.2	1.2	2.0	2.0	0.40	0.47	1.15
Angular - Tetrahedral (flat)	1.40 - 1.50	C7	1.40	3.93	2.81	1.3	2.4	1.2	1.8	1.1	1.8	0.40	0.77	1.15
+9.5 - 16mm														
Angular (Prismoidal & Tetrahedral)	1.30 - 1.40	**10**	1.31	2.27	1.73	0.9	2.4	1.1	2.7	0.8	1.5	0.37	0.81	1.14
Angular (Prismoidal & Tetrahedral)		**9**	1.38	3.11	2.25	1.0	2.4	1.2	2.4	0.8	1.6	0.40	0.87	1.13
Blockish and prismoidal	1.40 - 1.50	**20**	1.42	2.29	1.61	0.9	2.2	0.9	2.4	1.0	1.5	0.30	0.84	1.07
Flat and sharp pointed		**30**	1.47	1.98	1.35	0.8	2.2	0.8	2.8	1.0	1.4	0.27	0.84	1.07
Flat and prismoidal	1.50 - 1.60	**33**	1.50	1.23	0.82	0.6	2.0	0.6	3.3	1.0	1.2	0.20	0.88	0.90

Appendix C

Appendix C illustrates the bed density distribution profiles for the silica, magnetite and silica – magnetite beds. STDEV represents the standard deviation.

Appendix C- 1: Bed density distribution profile for the Silica bed

3D Bed Density Distribution Profile - Silica bed

Bed Level	Sampling Point 1			Sampling Point 3			Sampling Point 5				
cm	a	c	e	a	c	e	a	c	e	Avg	STDEV
10	1400	1381	1391	1373	1352	1360	1359	1371	1366	1373	16
15	1378	1369	1376	1359	1350	1353	1350	1354	1353	1360	11
20	1355	1357	1360	1345	1348	1346	1341	1337	1340	1348	8
25	1333	1344	1345	1330	1346	1339	1332	1319	1327	1335	9
30	1310	1332	1330	1316	1344	1332	1323	1302	1313	1322	13
35	1288	1320	1315	1302	1342	1325	1314	1285	1300	1310	18
Average	1344	1350	1353	1338	1347	1342	1336	1328	1333	1341	
STDEV	42	23	29	27	4	13	17	32	25		

Appendix C - 2: Bed density distribution profile for the Magnetite bed

3D Bed Density Distribution Profile - Magnetite bed

Bed Level	Sampling Point 1			Sampling Point 3			Sampling Point 5				
cm	1a	1c	1e	3a	3c	3e	3a	3c	3e	Avg	STDEV
10	2786	2717	2685	2781	2713	2660	2655	2673	2729	2711	46
15	2766	2713	2685	2761	2713	2676	2671	2681	2717	2709	33
20	2746	2709	2685	2741	2713	2692	2687	2689	2705	2707	21
25	2726	2705	2685	2721	2713	2708	2703	2697	2693	2706	12
30	2706	2701	2685	2701	2713	2724	2719	2705	2681	2704	13
35	2686	2697	2685	2681	2713	2740	2735	2713	2669	2702	23
Avg	2736	2707	2685	2731	2713	2700	2695	2693	2699	2707	25
STDEV	34	7	0	37	0	30	30	15	22		

Appendix C - 3: Bed density distribution profile for the Silica – Magnetite bed

3D Bed Density Distribution Profile (Silica - Magnetite bed)

Bed Level	Sampling Point 1			Sampling Point 3			Sampling Point 5				
cm	1a	1c	1e	3a	3c	3e	5a	5c	5e	Avg	STDEV
10	1658	1648	1659	1647	1675	1647	1659	1659	1648	1655	9
15	1654	1646	1653	1647	1667	1647	1654	1654	1647	1652	7
20	1650	1644	1647	1647	1659	1646	1649	1649	1646	1648	4
25	1646	1642	1641	1647	1650	1646	1643	1643	1645	1645	3
30	1642	1640	1635	1647	1642	1646	1638	1638	1644	1641	4
35	1638	1638	1628	1646	1634	1646	1633	1633	1643	1638	6
Avg	1648	1643	1644	1647	1655	1646	1646	1646	1645	1647	3
STDEV	7	3	10	0	14	0	9	9	2	6	6

Appendix C - 4: Pressure drop profile graphs for the Silica – Magnetite bed

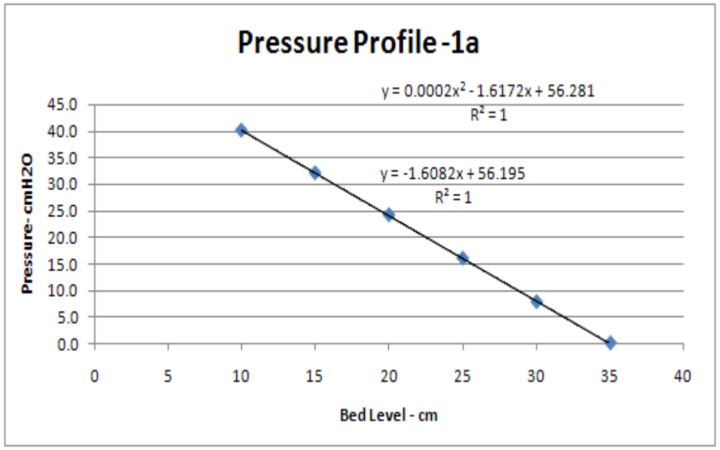

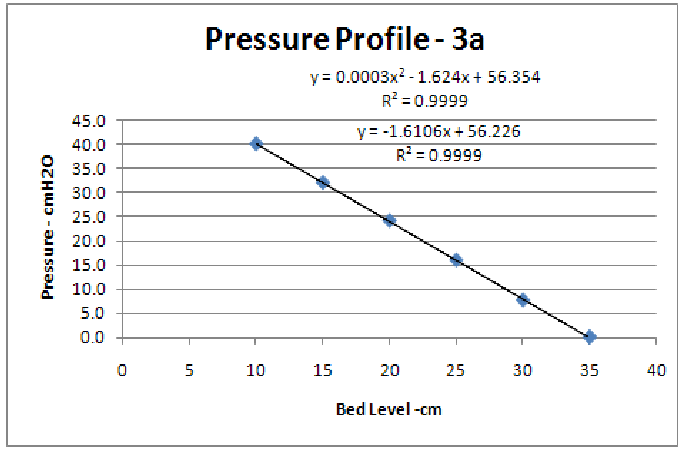

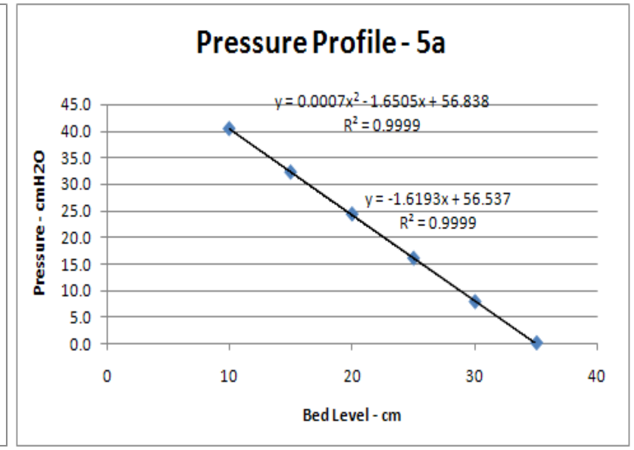

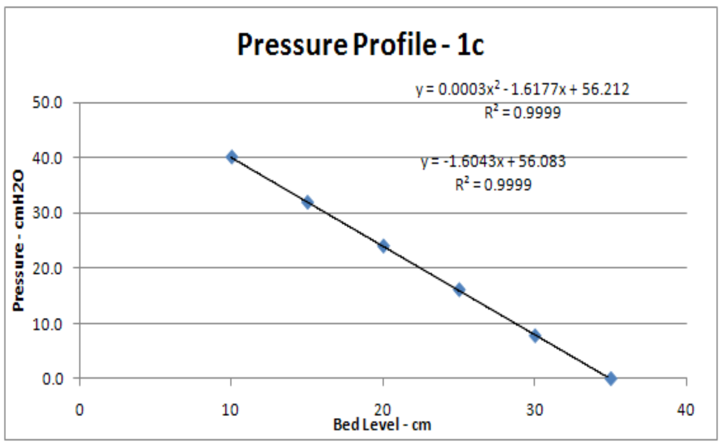

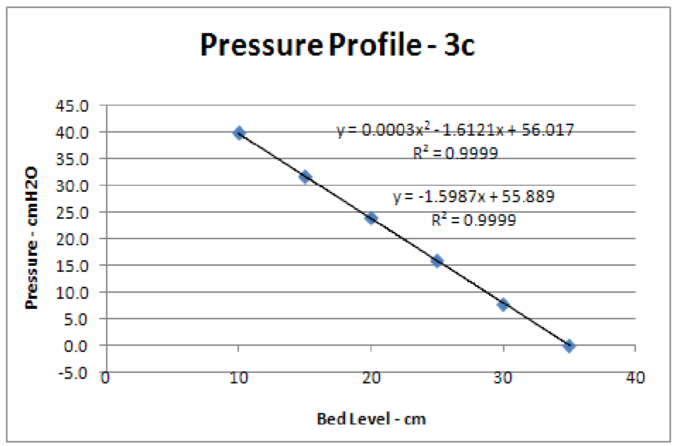

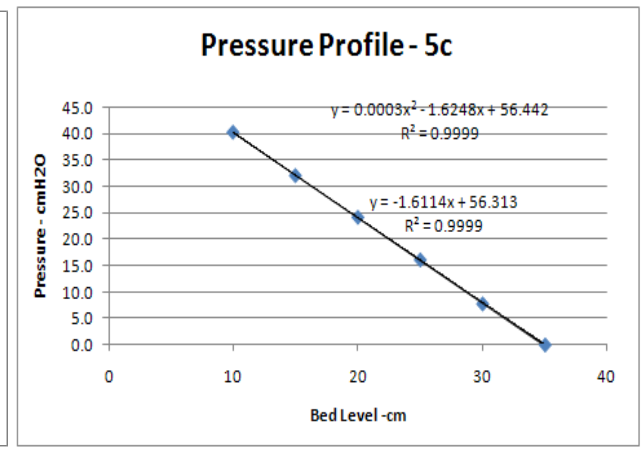

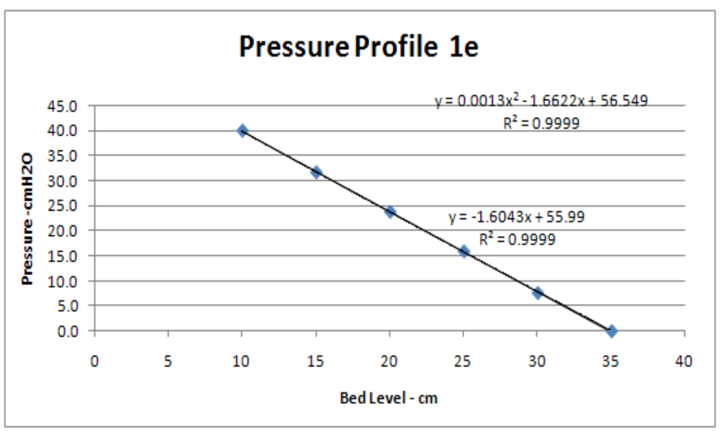

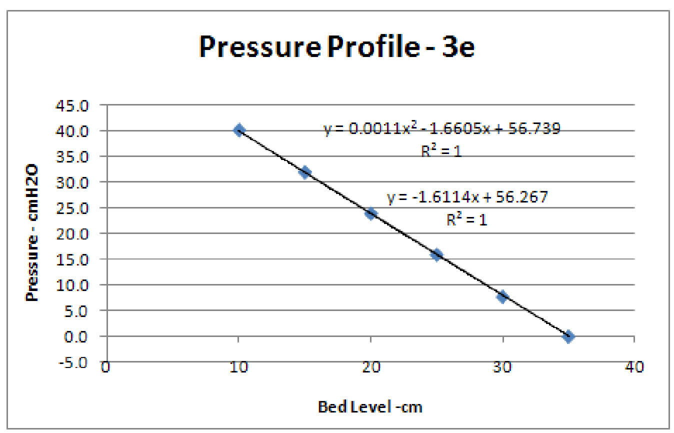

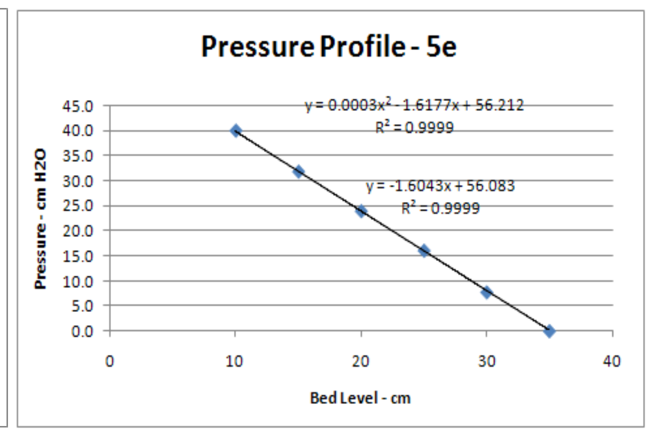

Appendix D

Appendix D illustrates the partition data of the (+22 -31.5mm), (+16 -22mm Blk), (+16 – 22mm SR), (+16 – 22mm FB) and (+9.5 – 16mm) particles that was obtained after 15s and 30s of separation respectively.

Appendix D - 1: Partition data for the (+22 -31.5mm) particles obtained after 15s & 30s

+22 - 31.5 mm

15

Density Range	Particles Used	Sp.gr of Particle	Mass - Particle	Volume- Particle	Height / cm	Float/Sink F/S	Mass Floats	Mass Sinks	Floats wt.%	Sinks wt.%	Floats % of feed	Sinks % of feed	Reconstituted Feed %	Nominal sp. Gr	Partition Coefficient
	G7	1.31	6.27	4.79	31.00	F	6.27		1.36	0.00	0.61	0.00	0.61		
	E2	1.32	15.12	11.45	32.00	F	15.12		3.27	0.00	1.47	0.00	1.47		
1.30 - 1.40	B8	1.33	13.11	9.86	32.00	F	13.11		2.83	0.00	1.28	0.00	1.28		
	D4	1.34	13.09	9.77	32.00	F	13.09		2.83	0.00	1.28	0.00	1.28	1.34	0.00
	D7	1.35	10.90	8.07	32.00	F	10.90		2.36	0.00	1.06	0.00	1.06		
	C2	1.37	12.13	8.85	32.00	F	12.13		2.62	0.00	1.18	0.00	1.18		
	B5	1.38	21.08	15.28	32.00	F	21.08		4.56	0.00	2.05	0.00	2.05		
	C6	1.40	16.1	11.50	32.00	F	16.1		3.48	0.00	1.57	0.00	1.57		
	D3	1.42	17.46	12.30	32.00	F	17.46		3.77	0.00	1.70	0.00	1.70		
1.40 - 1.50	C4	1.44	21.71	15.08	32.00	F	21.71		4.69	0.00	2.11	0.00	2.11		
	G6	1.45	13.16	9.08	29.00	F	13.16		2.85	0.00	1.28	0.00	1.28	1.45	0.00
	C9	1.46	17.43	11.94	32.00	F	17.43		3.77	0.00	1.70	0.00	1.70		
	C7	1.48	16.66	11.26	28.00	F	16.66		3.60	0.00	1.62	0.00	1.62		
	D8	1.48	12.95	8.75	31.00	F	12.95		2.80	0.00	1.26	0.00	1.26		
	A9	1.50	13.11	8.74	24.00	F	13.11		2.83	0.00	1.28	0.00	1.28		
	A3	1.51	8.32	5.51	24.00	F	8.32		1.80	0.00	0.81	0.00	0.81		
1.50 - 1.60	E3	1.53	24.66	16.12	32.00	F	24.66		5.33	0.00	2.40	0.00	2.40		
	E7	1.54	12.56	8.16	31.00	F	12.56		2.72	0.00	1.22	0.00	1.22		
	G2	1.55	29.53	19.05	27.00	F	29.53		6.38	0.00	2.88	0.00	2.88	1.54	0.00
	D9	1.56	13.59	8.71	30.00	F	13.59		2.94	0.00	1.32	0.00	1.32		
	K1	1.57	25.88	16.48	27.00	F	25.88		5.60	0.00	2.52	0.00	2.52		
	F6	1.59	15.00	9.43	29.00	F	15.00		3.24	0.00	1.46	0.00	1.46		
	B7	1.60	5.23	3.27	22.00	F	5.23		1.13	0.00	0.51	0.00	0.51		
1.60 - 1.70	D4	1.64	11.11	6.77	28.00	F	11.11		2.40	0.00	1.08	0.00	1.08		
	J8	1.65	32.27	19.56	28.00	F	32.27		6.98	0.00	3.14	0.00	3.14		
	F9	1.66	31.60	19.04	24.00	F	31.60		6.83	0.00	3.08	0.00	3.08	1.66	40.96
	C2	1.67	16.26	9.74	29.00	F	16.26		3.52	0.00	1.58	0.00	1.58		
	J7	1.68	35.30	21.01	19.00	M		35.30	0.00	6.26	0.00	3.44	3.44		
	I7	1.69	31.62	18.71	18.00	M		31.62	0.00	5.61	0.00	3.08	3.08		
	C5	1.70	19.52	11.48	18.00	M		19.52	0.00	3.46	0.00	1.90	1.90		
	H4	1.71	16.24	9.50	24.00	F	16.24		3.51	0.00	1.58	0.00	1.58		
1.70 - 1.80	H8	1.71	32.71	19.13	14.00	M		32.71	0.00	5.80	0.00	3.19	3.19		
	J6	1.72	23.49	13.66	9.00	S		23.49	0.00	4.16	0.00	2.29	2.29	1.73	90.03
	C3	1.74	18.57	10.67	8.00	S		18.57	0.00	3.29	0.00	1.81	1.81		
	G1	1.75	26.03	14.87	10.00	S		26.03	0.00	4.61	0.00	2.54	2.54		
	H9	1.77	26.30	14.86	8.00	S		26.30	0.00	4.66	0.00	2.56	2.56		
	G6	1.81	34.61	19.12	6.00	S		34.61	0.00	6.14	0.00	3.37	3.37		
	E8	1.83	34.85	19.04	3.00	S		34.85	0.00	6.18	0.00	3.39	3.39		
1.80 - 2.00	I4	1.86	50.61	27.21	4.00	S		50.61	0.00	8.97	0.00	4.93	4.93		
	H7	1.90	11.48	6.04	3.00	S		11.48	0.00	2.04	0.00	1.12	1.12	1.89	100.00
	L1	1.92	26.21	13.65	2.00	S		26.21	0.00	4.65	0.00	2.55	2.55		
	L2	1.93	26.42	13.69	2.00	S		26.42	0.00	4.68	0.00	2.57	2.57		
	I5	1.96	22.34	11.40	1.00	S		22.34	0.00	3.96	0.00	2.18	2.18		
	G7	2.09	31.15	14.90	0.00	S		31.15	0.00	5.52	0.00	3.03	3.03		
	F2	2.18	24.91	11.43	0.00	S		24.91	0.00	4.42	0.00	2.43	2.43		
2.30 -2.50	E7	2.22	40.41	18.20	0.00	S		40.41	0.00	7.16	0.00	3.94	3.94	2.30	100.00
	G3	2.71	47.55	17.55	0.00	S		47.55	0.00	8.43	0.00	4.63	4.63		
			1026.61				462.53	564.08	100.00	100.00	45.05	54.95	100.00		

30

Density Range	Particles Used		Float/Sink F/S	Mass Floats	Mass Sinks	Floats wt.%	Sinks wt.%	Floats % of feed	Sinks % of feed	Reconstituted Feed %		Nominal sp. Gr	Partition Coefficient
	G7	32.00	F	6.27		1.64	0.00	0.61	0.00	0.61			
	E2	32.00	F	15.12		3.95	0.00	1.47	0.00	1.47			
1.30 - 1.40	B8	32.00	F	13.11		3.43	0.00	1.28	0.00	1.28			
	D4	32.00	F	13.09		3.42	0.00	1.28	0.00	1.28	8.93	1.34	0.00
	D7	32.00	F	10.90		2.85	0.00	1.06	0.00	1.06			
	C2	32.00	F	12.13		3.17	0.00	1.18	0.00	1.18			
	B5	32.00	F	21.08		5.51	0.00	2.05	0.00	2.05			
	C6	32.00	F	16.10		4.21	0.00	1.57	0.00	1.57			
	D3	32.00	F	17.46		4.57	0.00	1.70	0.00	1.70			
1.40 - 1.50	C4	31.00	F	21.71		5.68	0.00	2.11	0.00	2.11			
	G6	32.00	F	13.16		3.44	0.00	1.28	0.00	1.28	11.25	1.45	0.00
	C9	32.00	F	17.43		4.56	0.00	1.70	0.00	1.70			
	C7	30.00	F	16.66		4.36	0.00	1.62	0.00	1.62			
	D8	32.00	F	12.95		3.39	0.00	1.26	0.00	1.26			
	A9	32.00	F	13.11		3.43	0.00	1.28	0.00	1.28			
	A3	23.00	F	8.32		2.18	0.00	0.81	0.00	0.81			
1.50 - 1.60	E3	31.00	F	24.66		6.45	0.00	2.40	0.00	2.40			
	E7	32.00	F	12.56		3.28	0.00	1.22	0.00	1.22			
	G2	32.00	F	29.53		7.72	0.00	2.88	0.00	2.88	13.90	1.54	0.00
	D9	23.00	F	13.59		3.55	0.00	1.32	0.00	1.32			
	K1	27.00	F	25.88		6.77	0.00	2.52	0.00	2.52			
	F6	24.00	F	15.00		3.92	0.00	1.46	0.00	1.46			
	B7	25.00	F	5.23		1.37	0.00	0.51	0.00	0.51			
1.60 - 1.70	D4	21.00	F	11.11		2.91	0.00	1.08	0.00	1.08			
	J8	15.00	M		32.27	0.00	5.01	0.00	3.14	3.14			
	F9	15.00	M		31.60	0.00	4.91	0.00	3.08	3.08	15.92	1.66	80.05
	C2	25.00	F	16.26		4.25	0.00	1.58	0.00	1.58			
	J7	15.00	M		35.30	0.00	5.48	0.00	3.44	3.44			
	I7	11.00	S		31.62	0.00	4.91	0.00	3.08	3.08			
	C5	9.00	S		19.52	0.00	3.03	0.00	1.90	1.90			
	H4	10.00	S		16.24	0.00	2.52	0.00	1.58	1.58			
1.70 - 1.80	H8	9.00	S		32.71	0.00	5.08	0.00	3.19	3.19			
	J6	6.00	S		23.49	0.00	3.65	0.00	2.29	2.29	15.86	1.73	100.00
	C3	12.00	S		18.57	0.00	2.88	0.00	1.81	1.81			
	G1	5.00	S		26.03	0.00	4.04	0.00	2.54	2.54			
	H9	4.00	S		26.30	0.00	4.08	0.00	2.56	2.56			
	G6	3.00	S		34.61	0.00	5.37	0.00	3.37	3.37			
	E8	1.00	S		34.85	0.00	5.41	0.00	3.39	3.39			
1.80 - 2.00	I4	0.00	S		50.61	0.00	7.86	0.00	4.93	4.93			
	H7	0.00	S		11.48	0.00	1.78	0.00	1.12	1.12	20.12	1.89	100.00
	L1	0.00	S		26.21	0.00	4.07	0.00	2.55	2.55			
	L2	0.00	S		26.42	0.00	4.10	0.00	2.57	2.57			
	I5	0.00	S		22.34	0.00	3.47	0.00	2.18	2.18			
	G7	0.00	S		31.15	0.00	4.84	0.00	3.03	3.03			
	F2	0.00	S		24.91	0.00	3.87	0.00	2.43	2.43			
2.30 -2.50	E7	0.00	S		40.41	0.00	6.27	0.00	3.94	3.94	14.03	2.30	100.00
	G3	0.00	S		47.55	0.00	7.38	0.00	4.63	4.63			
				382.42	644.19	100.00	100.00	37.25	62.75	100.00			

Appendix D - 2: Partition data for the (+16 - 22mm Blk) particles obtained after 15s & 30s

						+16 -22mm - Blockish																					
						15										30											
Density Range	Particles Used	Sp.gr of Particle	Mass - Particle	Volume-Particle	Height / cm	Float/Sink F/S	Mass Floats	Mass Sinks	Floats wt.%	Sinks wt.%	Floats % of feed	Sinks % of feed	Reconstituted Feed %	Nominal sp. Gr	Partition Coefficient		Float/Sink F/S	Mass Floats	Mass Sinks	Floats wt.%	Sinks wt.%	Floats % of feed	Sinks % of feed	Reconstituted Feed %		Nominal sp. Gr	Partition Coefficient
1.30 - 1.40	J5	1.30	3.73	2.87	32.00	F	3.73		1.82	0.00	1.21	0.00	1.21	1.35	0.00	32.00	F	3.73		1.81	0.00	1.21	0.00	1.21	13.20	1.35	0.00
	AH8	1.31	3.57	2.73	32.00	F	3.57		1.75	0.00	1.15	0.00	1.15			23.00	F	3.57		1.74	0.00	1.15	0.00	1.15			
	H9	1.34	7.87	5.87	32.00	F	7.87		3.85	0.00	2.55	0.00	2.55			32.00	F	7.87		3.83	0.00	2.55	0.00	2.55			
	L4	1.35	4.60	3.41	32.00	F	4.60		2.25	0.00	1.49	0.00	1.49			32.00	F	4.60		2.24	0.00	1.49	0.00	1.49			
	K6	1.35	5.34	3.96	32.00	F	5.34		2.61	0.00	1.73	0.00	1.73			25.00	F	5.34		2.60	0.00	1.73	0.00	1.73			
	AF8	1.37	3.57	2.61	32.00	F	3.57		1.75	0.00	1.15	0.00	1.15			26.00	F	3.57		1.74	0.00	1.15	0.00	1.15			
	L1	1.38	6.60	4.78	29.00	F	6.60		3.23	0.00	2.13	0.00	2.13			31.00	F	6.60		3.21	0.00	2.13	0.00	2.13			
	J8	1.38	5.53	4.01	32.00	F	5.53		2.70	0.00	1.79	0.00	1.79			28.00	F	5.53		2.69	0.00	1.79	0.00	1.79			
1.40 - 1.50	AA4	1.40	6.64	4.74	29.00	F	6.64		3.25	0.00	2.15	0.00	2.15	1.44	0.00	28.00	F	6.64		3.23	0.00	2.15	0.00	2.15	20.58	1.44	8.77
	AC1	1.41	5.25	3.72	25.00	F	5.25		2.57	0.00	1.70	0.00	1.70			31.00	F	5.25		2.55	0.00	1.70	0.00	1.70			
	K3	1.41	7.26	5.15	32.00	F	7.26		3.55	0.00	2.35	0.00	2.35			32.00	F	7.26		3.53	0.00	2.35	0.00	2.35			
	H6	1.43	9.61	6.72	32.00	F	9.61		4.70	0.00	3.11	0.00	3.11			29.00	F	9.61		4.67	0.00	3.11	0.00	3.11			
	A1	1.45	12.86	8.87	32.00	F	12.86		6.29	0.00	4.16	0.00	4.16			31.00	F	12.86		6.25	0.00	4.16	0.00	4.16			
	AB6	1.46	5.58	3.82	26.00	F	5.58		2.73	0.00	1.80	0.00	1.80			13.00	M		5.58	0.00	5.39	0.00	1.80	1.80			
	A2	1.47	9.2	6.26	32.00	F	9.2		4.50	0.00	2.98	0.00	2.98			28.00	F	9.20		4.47	0.00	2.98	0.00	2.98			
	AA1	1.48	7.23	4.89	32.00	F	7.23		3.54	0.00	2.34	0.00	2.34			32.00	F	7.23		3.51	0.00	2.34	0.00	2.34			
1.50 - 1.60	L2	1.50	6.16	4.11	32.00	F	6.16		3.01	0.00	1.99	0.00	1.99	1.54	0.00	29.00	F	6.16		2.99	0.00	1.99	0.00	1.99	16.23	1.54	11.85
	I2	1.51	5.87	3.89	30.00	F	5.87		2.87	0.00	1.90	0.00	1.90			32.00	F	5.87		2.85	0.00	1.90	0.00	1.90			
	AC4	1.52	6.04	3.97	29.00	F	6.04		2.95	0.00	1.95	0.00	1.95			29.00	F	6.04		2.94	0.00	1.95	0.00	1.95			
	AA5	1.52	5.08	3.34	21.00	F	5.08		2.48	0.00	1.64	0.00	1.64			29.00	F	5.08		2.47	0.00	1.64	0.00	1.64			
	AG2	1.55	7.81	5.04	26.00	F	7.81		3.82	0.00	2.53	0.00	2.53			20.00	F	7.81		3.80	0.00	2.53	0.00	2.53			
	L5	1.55	5.60	3.61	27.00	F	5.60		2.74	0.00	1.81	0.00	1.81			32.00	F	5.60		2.72	0.00	1.81	0.00	1.81			
	I7	1.57	7.68	4.89	29.00	F	7.68		3.76	0.00	2.48	0.00	2.48			21.00	F	7.68		3.73	0.00	2.48	0.00	2.48			
	AA9	1.59	5.95	3.74	32.00	F	5.95		2.91	0.00	1.92	0.00	1.92			11.00	S		5.95	0.00	5.75	0.00	1.92	1.92			
1.60 - 1.70	AH2	1.60	5.77	3.61	0.00	S		5.77	0.00	5.51	0.00	1.87	1.87	1.65	54.22	32.00	F	5.77		2.80	0.00	1.87	0.00	1.87	16.51	1.65	37.81
	AB5	1.62	5.93	3.66	21.00	F	5.93		2.90	0.00	1.92	0.00	1.92			15.00	M		5.93	0.00	5.73	0.00	1.92	1.92			
	K9	1.62	7.46	4.60	18.00	M		7.46	0.00	7.12	0.00	2.41	2.41			21.00	F	7.46		3.63	0.00	2.41	0.00	2.41			
	AD1	1.65	4.51	2.73	21.00	F	4.51		2.21	0.00	1.46	0.00	1.46			25.00	F	4.51		2.19	0.00	1.46	0.00	1.46			
	L6	1.65	8.93	5.41	21.00	F	8.93		4.37	0.00	2.89	0.00	2.89			31.00	F	8.93		4.34	0.00	2.89	0.00	2.89			
	I8	1.66	9.37	5.64	19.00	M		9.37	0.00	8.95	0.00	3.03	3.03			14.00	M		9.37	0.00	9.05	0.00	3.03	3.03			
	AK1	1.67	4.00	2.40	20.00	F	4.00		1.96	0.00	1.29	0.00	1.29			13.00	M		4.00	0.00	3.87	0.00	1.29	1.29			
	AE6	1.69	5.08	3.01	19.00	M		5.08	0.00	4.85	0.00	1.64	1.64			21.00	F	5.08		2.47	0.00	1.64	0.00	1.64			
1.70 - 1.80	K2	1.70	13.79	8.11	23.00	F	13.79		6.74	0.00	4.46	0.00	4.46	1.74	55.62	21.00	F	13.79		6.70	0.00	4.46	0.00	4.46	19.30	1.74	48.30
	AC3	1.71	4.31	2.52	13.00	S		4.31	0.00	4.12	0.00	1.39	1.39			23.00	F	4.31		2.10	0.00	1.39	0.00	1.39			
	AI3	1.73	5.33	3.08	21.00	F	5.33		2.61	0.00	1.72	0.00	1.72			17.00	M		5.33	0.00	5.15	0.00	1.72	1.72			
	K8	1.73	7.59	4.39	19.00	M		7.59	0.00	7.25	0.00	2.45	2.45			7.00	S		7.59	0.00	7.33	0.00	2.45	2.45			
	AC5	1.75	7.37	4.21	24.00	F	7.37		3.60	0.00	2.38	0.00	2.38			21.00	F	7.37		3.58	0.00	2.38	0.00	2.38			
	AF5	1.76	5.39	3.06	15.00	M		5.39	0.00	5.15	0.00	1.74	1.74			24.00	F	5.39		2.62	0.00	1.74	0.00	1.74			
	I1	1.78	9.05	5.08	14.00	M		9.05	0.00	8.64	0.00	2.93	2.93			13.00	M		9.05	0.00	8.74	0.00	2.93	2.93			
	I4	1.78	6.86	3.85	4.00	S		6.86	0.00	6.55	0.00	2.22	2.22			0.00	S		6.86	0.00	6.63	0.00	2.22	2.22			
1.80 - 2.00	Z54	1.82	5.27	2.90	2.00	S		5.27	0.00	5.03	0.00	1.70	1.70	1.85	100.00	0.00	S		5.27	0.00	5.09	0.00	1.70	1.70	7.96	1.85	100.00
	Z45	1.83	11.94	6.52	4.00	S		11.94	0.00	11.40	0.00	3.86	3.86			0.00	S		11.94	0.00	11.54	0.00	3.86	3.86			
	Z67	1.90	7.39	3.89	3.00	S		7.39	0.00	7.06	0.00	2.39	2.39			0.00	S		7.39	0.00	7.14	0.00	2.39	2.39			
2.30 -2.50	Z51	2.29	8.94	3.90	0.00	S		8.94	0.00	8.54	0.00	2.89	2.89	2.23	100.00	0.00	S		8.94	0.00	8.64	0.00	2.89	2.89	6.22	2.23	100.00
	Z68	2.21	5.00	2.26	0.00	S		5.00	0.00	4.78	0.00	1.62	1.62			0.00	S		5.00	0.00	4.83	0.00	1.62	1.62			
	Z70	2.20	5.29	2.40	0.00	S		5.29	0.00	5.05	0.00	1.71	1.71			0.00	S		5.29	0.00	5.11	0.00	1.71	1.71			
			309.20				204.49	104.71	100.00	100.00	66.14	33.86	100.00					205.71	103.49	100.00	100.00	66.53	33.47	100.00			

Appendix D - 3: Partition data for the (+16 - 22mm SR) particles obtained after 15s & 30s

+16 -22mm - Sharp pointed prism																											
						15										30											
Density Range	Particles Used	Sp.gr of Particle	Mass - Particle	Volume- Particle	Height / cm	Float/Sink F/S	Mass Floats	Mass Sinks	Floats wt.%	Sinks wt.%	Floats % of feed	Sinks % of feed	Reconstituted Feed %	Nominal sp. Gr	Partition Coefficient		Float/Sink F/S	Mass Floats	Mass Sinks	Floats wt.%	Sinks wt.%	Floats % of feed	Sinks % of feed	Reconstituted Feed %		Nominal sp. Gr	Partition Coefficient
	X22	1.30	2.70	2.08	22.00	F	2.70		2.38	0.00	1.42	0.00	1.42			28.00	F	2.70		2.72	0.00	1.42	0.00	1.42			
	F5	1.35	7.12	5.27	31.00	F	7.12		6.27	0.00	3.74	0.00	3.74			24.00	F	7.12		7.17	0.00	3.74	0.00	3.74			
1.30 - 1.40	H2	1.36	7.05	5.18	32.00	F	7.05		6.20	0.00	3.70	0.00	3.70			32.00	F	7.05		7.10	0.00	3.70	0.00	3.70			
	G4	1.38	6.61	4.79	27.00	F	6.61		5.82	0.00	3.47	0.00	3.47	1.36	0.00	32.00	F	6.61		6.66	0.00	3.47	0.00	3.47	31.04	1.36	0.00
	F9	1.38	6.02	4.36	32.00	F	6.02		5.30	0.00	3.16	0.00	3.16			29.00	F	6.02		6.06	0.00	3.16	0.00	3.16			
	G2	1.39	8.68	6.24	32.00	F	8.68		7.64	0.00	4.56	0.00	4.56			32.00	F	8.68		8.74	0.00	4.56	0.00	4.56			
	H3	1.40	8.58	6.13	32.00	F	8.58		7.55	0.00	4.51	0.00	4.51			31.00	F	8.58		8.64	0.00	4.51	0.00	4.51			
	E9	1.41	12.34	8.75	32.00	F	12.34		10.86	0.00	6.48	0.00	6.48			12.00	M		12.34	0.00	13.54	0.00	6.48	6.48			
1.40 - 1.50	X19	1.43	4.34	3.03	27.00	F	4.34		3.82	0.00	2.28	0.00	2.28			28.00	F	4.34		4.37	0.00	2.28	0.00	2.28			
	H4	1.45	4.56	3.14	22.00	F	4.56		4.01	0.00	2.39	0.00	2.39			21.00	F	4.56		4.59	0.00	2.39	0.00	2.39			
	X21	1.46	3	2.05	32.00	F	3.00		2.64	0.00	1.58	0.00	1.58	1.44	0.00	18.00	M	3.00		3.02	0.00	1.58	0.00	1.58	20.87	1.44	0.00
	F4	1.48	6.14	4.15	26.00	F	6.14		5.40	0.00	3.22	0.00	3.22			28.00	F	6.14		6.19	0.00	3.22	0.00	3.22			
	X4	1.50	7.97	5.31	27.00	F	7.97		7.01	0.00	4.19	0.00	4.19			25.00	F	7.97		8.03	0.00	4.19	0.00	4.19			
	X14	1.51	4.13	2.74	25.00	F	4.13		3.63	0.00	2.17	0.00	2.17			24.00	F	4.13		4.16	0.00	2.17	0.00	2.17			
1.50 - 1.60	Z30	1.52	8.06	5.30	14.00	M		8.06	0.00	10.50	0.00	4.23	4.23	1.52	34.67	29.00	F	8.06		8.12	0.00	4.23	0.00	4.23	12.21	1.52	0.00
	X1	1.54	1.54	1.00	21.00	F	1.54		1.36	0.00	0.81	0.00	0.81			21.00	F	1.54		1.55	0.00	0.81	0.00	0.81			
	X8	1.55	1.55	1.00	25.00	F	1.55		1.36	0.00	0.81	0.00	0.81			24.00	F	1.55		1.56	0.00	0.81	0.00	0.81			
	G7	1.61	4.97	3.09	29.00	F	4.97		4.37	0.00	2.61	0.00	2.61			31.00	F	4.97		5.01	0.00	2.61	0.00	2.61			
	F7	1.64	7.62	4.65	9.00	S		7.62	0.00	9.93	0.00	4.00	4.00	1.65	33.61	0.00	S		7.62	0.00	8.36	0.00	4.00	4.00	20.01	1.65	66.47
1.60 - 1.70	Z23	1.65	5.82	3.53	27.00	F	5.82		5.12	0.00	3.06	0.00	3.06			15.00	M		5.82	0.00	6.39	0.00	3.06	3.06			
	Z36	1.69	4.26	2.52	15.00	F	4.26		3.75	0.00	2.24	0.00	2.24			8.00	S		4.26	0.00	4.67	0.00	2.24	2.24			
	H5	1.76	6.25	3.55	27.00	F	6.25		5.50	0.00	3.28	0.00	3.28			22.00	F	6.25		6.30	0.00	3.28	0.00	3.28			
	F7	1.78	7.62	4.28	0.00	S		7.62	0.00	9.93	0.00	4.00	4.00	1.78	70.39	0.00	S		7.62	0.00	8.36	0.00	4.00	4.00	11.09	1.78	70.39
1.70 - 1.80	G3	1.79	7.24	4.04	2.00	S		7.24	0.00	9.43	0.00	3.80	3.80			0.00	S		7.24	0.00	7.94	0.00	3.80	3.80			
	Z32	1.99	5.46	2.74	0.00	S		5.46	0.00	7.11	0.00	2.87	2.87			0.00	S		5.46	0.00	5.99	0.00	2.87	2.87	24.28		
1.80 - 2.40	Z24	2.06	8.12	3.94	0.00	S		8.12	0.00	10.58	0.00	4.26	4.26			0.00	S		8.12	0.00	8.91	0.00	4.26	4.26			
	Z33	2.17	3.91	1.80	0.00	S		3.91	0.00	5.09	0.00	2.05	2.05	2.18	100.00	0.00	S		3.91	0.00	4.29	0.00	2.05	2.05		2.18	100.00
	Z37	2.19	4.99	2.28	0.00	S		4.99	0.00	6.50	0.00	2.62	2.62			0.00	S		4.99	0.00	5.48	0.00	2.62	2.62			
	Z25	2.24	8.92	3.98	0.00	S		8.92	0.00	11.62	0.00	4.68	4.68			0.00	S		8.92	0.00	9.79	0.00	4.68	4.68			
	Z38	2.29	6.94	3.03	0.00	S		6.94	0.00	9.04	0.00	3.64	3.64			0.00	S		6.94	0.00	7.62	0.00	3.64	3.64			
	Z26	2.32	7.89	3.40	0.00	S		7.89	0.00	10.28	0.00	4.14	4.14			0.00	S		7.89	0.00	8.66	0.00	4.14	4.14			
			190.40				113.63	76.77	100.00	100.00	59.68	40.32	100.00					99.27	91.13	100.00	100.00	52.14	47.86	100.00			

Appendix D - 4: Partition data for the (+16 - 22mm FB) particles obtained after 15s & 30s

+16 - 22mm - Flat																											
						15										30											
Density Range	Particles Used	Sp.gr of Particle	Mass - Particle	Volume- Particle	Height / cm	Float/Sink F/S	Mass Floats	Mass Sinks	Floats wt.%	Sinks wt.%	Floats % of feed	Sinks % of feed	Reconstituted Feed %	Nominal sp. Gr	Partition Coefficient		Float/Sink F/S	Mass Floats	Mass Sinks	Floats wt.%	Sinks wt.%	Floats % of feed	Sinks % of feed	Reconstituted Feed %		Nominal sp. Gr	Partition Coefficient
1.30 - 1.40	C5	1.31	4.72	3.60	32.00	F	4.72		4.79	0.00	2.22	0.00	2.22			31.00	F	4.72		5.37	0.00	2.22	0.00	2.22			
	B5	1.35	5.73	4.24	27.00	F	5.73		5.82	0.00	2.70	0.00	2.70			29.00	F	5.73		6.52	0.00	2.70	0.00	2.70			
	C8	1.35	3.97	2.94	32.00	F	3.97		4.03	0.00	1.87	0.00	1.87			31.00	F	3.97		4.52	0.00	1.87	0.00	1.87			
	D6	1.36	5.72	4.21	27.00	F	5.72		5.81	0.00	2.69	0.00	2.69	1.36	0.00	32.00	F	5.72		6.51	0.00	2.69	0.00	2.69	14.28	1.36	0.00
	C4	1.38	5.12	3.71	32.00	F	5.12		5.20	0.00	2.41	0.00	2.41			30.00	F	5.12		5.82	0.00	2.41	0.00	2.41			
	D5	1.39	5.06	3.64	32.00	F	5.06		5.14	0.00	2.38	0.00	2.38			31.00	F	5.06		5.76	0.00	2.38	0.00	2.38			
1.40 - 1.50	C7	1.40	3.93	2.81	23.00	F	3.93		3.99	0.00	1.85	0.00	1.85			28.00	F	3.93		4.47	0.00	1.85	0.00	1.85			
	D4	1.42	4.19	2.95	31.00	F	4.19		4.26	0.00	1.97	0.00	1.97			32.00	F	4.19		4.77	0.00	1.97	0.00	1.97			
	Y12	1.43	3.12	2.18	27.00	F	3.12		3.17	0.00	1.47	0.00	1.47			21.00	F	3.12		3.55	0.00	1.47	0.00	1.47			
	B8	1.44	6.98	4.85	31.00	F	6.98		7.09	0.00	3.29	0.00	3.29			30.00	F	6.98		7.94	0.00	3.29	0.00	3.29			
	Y32	1.46	3.15	2.16	27.00	F	3.15		3.20	0.00	1.48	0.00	1.48	1.44	28.42	21.00	F	3.15		3.58	0.00	1.48	0.00	1.48	11.55	1.44	12.85
	Y26	1.49	3.15	2.11	18.00	M		3.15	0.00	2.77	0.00	1.48	1.48			0.00	S		3.15	0.00	2.53	0.00	1.48	1.48			
1.50 - 1.60	B4	1.51	6.82	4.52	32.00	F	6.82		6.93	0.00	3.21	0.00	3.21			11.00	S		6.82	0.00	5.48	0.00	3.21	3.21			
	Y21	1.51	3.31	2.19	14.00	S		3.31	0.00	2.91	0.00	1.56	1.56			21.00	F	3.31		3.77	0.00	1.56	0.00	1.56			
	Y3	1.56	4.92	3.15	32.00	F	4.92		5.00	0.00	2.32	0.00	2.32	1.55	21.95	12.00	S		4.92	0.00	3.95	0.00	2.32	2.32			
	E5	1.56	3.46	2.22	19.00	M		3.46	0.00	3.04	0.00	1.63	1.63			28.00	F	3.46		3.94	0.00	1.63	0.00	1.63	14.52	1.55	38.07
	Z15	1.58	4.16	2.63	27.00	F	4.16		4.23	0.00	1.96	0.00	1.96			21.00	F	4.16		4.73	0.00	1.96	0.00	1.96			
	C6	1.58	8.17	5.17	29.00	F	8.17		8.30	0.00	3.85	0.00	3.85			23.00	F	8.17		9.29	0.00	3.85	0.00	3.85			
1.60 - 1.70	Y10	1.61	4.16	2.58	21.00	F	4.16		4.23	0.00	1.96	0.00	1.96	1.64	64.96	26.00	F	4.16		4.73	0.00	1.96	0.00	1.96	13.83	1.64	75.72
	Y33	1.62	4.24	2.62	18.00	M		4.24	0.00	3.72	0.00	2.00	2.00			10.00	S		4.24	0.00	3.41	0.00	2.00	2.00			
	Y1	1.63	6.13	3.76	27.00	F	6.13		6.23	0.00	2.89	0.00	2.89			14.00	S		6.13	0.00	4.93	0.00	2.89	2.89			
	Y2	1.64	4.78	2.91	6.00	S		4.78	0.00	4.20	0.00	2.25	2.25			11.00	S		4.78	0.00	3.84	0.00	2.25	2.25			
	Y30	1.66	2.97	1.79	5.00	S		2.97	0.00	2.61	0.00	1.40	1.40			25.00	F	2.97		3.38	0.00	1.40	0.00	1.40			
	Y13	1.69	7.09	4.20	7.00	S		7.09	0.00	6.22	0.00	3.34	3.34			13.00	S		7.09	0.00	5.70	0.00	3.34	3.34			
1.70 - 1.80	Z7	1.70	5.29	3.11	26.00	F	5.29		5.37	0.00	2.49	0.00	2.49			8.00	S		5.29	0.00	4.25	0.00	2.49	2.49			
	D3	1.71	9.54	5.58	19.00	M		9.54	0.00	8.38	0.00	4.49	4.49	1.73	70.11	12.00	S		9.54	0.00	7.67	0.00	4.49	4.49	19.53	1.73	75.94
	E4	1.71	9.98	5.84	15.00	M		9.98	0.00	8.76	0.00	4.70	4.70			26.00	F	9.98		11.35	0.00	4.70	0.00	4.70			
	Z17	1.72	3.03	1.76	15.00	M		3.03	0.00	2.66	0.00	1.43	1.43			0.00	S		3.03	0.00	2.43	0.00	1.43	1.43			
	E1	1.76	6.53	3.71	17.00	M		6.53	0.00	5.73	0.00	3.08	3.08			17.00	M		6.53	0.00	5.25	0.00	3.08	3.08			
	D1	1.79	7.11	3.97	21.00	F	7.11		7.22	0.00	3.35	0.00	3.35			12.00	S		7.11	0.00	5.71	0.00	3.35	3.35			
1.80 - 2.40	Z4	1.86	4.27	2.30	9.00	S		4.27	0.00	3.75	0.00	2.01	2.01			0.00	S		4.27	0.00	3.43	0.00	2.01	2.01			
	B7	1.88	12.30	6.54	7.00	S		12.30	0.00	10.80	0.00	5.79	5.79			0.00	S		12.30	0.00	9.88	0.00	5.79	5.79			
	Z3	1.97	2.17	1.10	0.00	S		2.17	0.00	1.91	0.00	1.02	1.02	2.10	100.00	0.00	S		2.17	0.00	1.74	0.00	1.02	1.02	26.29	2.10	100.00
	Z10	2.06	3.52	1.71	0.00	S		3.52	0.00	3.09	0.00	1.66	1.66			0.00	S		3.52	0.00	2.83	0.00	1.66	1.66			
	Z14	2.09	7.47	3.57	0.00	S		7.47	0.00	6.56	0.00	3.52	3.52			0.00	S		7.47	0.00	6.00	0.00	3.52	3.52			
	Z13	2.19	4.18	1.91	0.00	S		4.18	0.00	3.67	0.00	1.97	1.97			0.00	S		4.18	0.00	3.36	0.00	1.97	1.97			
	Z5	2.24	5.91	2.64	0.00	S		5.91	0.00	5.19	0.00	2.78	2.78			0.00	S		5.91	0.00	4.75	0.00	2.78	2.78			
	Z6	2.28	5.68	2.49	0.00	S		5.68	0.00	4.99	0.00	2.67	2.67			0.00	S		5.68	0.00	4.56	0.00	2.67	2.67			
	Z1	2.32	10.32	4.45	0.00	S		10.32	0.00	9.06	0.00	4.86	4.86			0.00	S		10.32	0.00	8.29	0.00	4.86	4.86			
			212.35				98.45	113.90	100.00	100.00	46.36	53.64	100.00					87.90	124.45	100.00	100.00	41.39	58.61	100.00			

Appendix D - 5: Partition data for the (+9.5 - 16mm) particles obtained after 15s & 30s

+9.5 -16 mm																											
						15										30											
Density Range	Particles Used	Sp.gr of Particle	Mass - Particle	Volume- Particle	Height / cm	Float/Sink F/S	Mass Floats	Mass Sinks	Floats wt.%	Sinks wt.%	Floats % of feed	Sinks % of feed	Reconstituted Feed %	Nominal sp. Gr	Partition Coefficient		Float/Sink F/S	Mass Floats	Mass Sinks	Floats wt.%	Sinks wt.%	Floats % of feed	Sinks % of feed	Reconstituted Feed %		Nominal sp. Gr	Partition Coefficient
	10	1.31	2.27	1.73	20.00	F	2.27		3.88	0.00	2.14	0.00	2.14			32.00	F	2.27		3.10	0.00	2.14	0.00	2.14			
	11	1.32	1.32	1.00	32.00	F	1.32		2.26	0.00	1.24	0.00	1.24			23.00	F	1.32		1.80	0.00	1.24	0.00	1.24			
1.30 - 1.40	12	1.34	1.58	1.18	27.00	F	1.58		2.70	0.00	1.49	0.00	1.49			32.00	F	1.58		2.16	0.00	1.49	0.00	1.49			
	14	1.35	2.83	2.10	27.00	F	2.83		4.84	0.00	2.66	0.00	2.66	1.35	18.77	31.00	F	2.83		3.87	0.00	2.66	0.00	2.66	16.49	1.35	0.00
	5	1.36	3.13	2.30	31.00	F	3.13		5.35	0.00	2.94	0.00	2.94			29.00	F	3.13		4.27	0.00	2.94	0.00	2.94			
	3	1.37	3.29	2.40	16.00	S		3.29	0.00	6.88	0.00	3.10	3.10			32.00	F	3.29		4.49	0.00	3.10	0.00	3.10			
	9	1.38	3.11	2.25	31.00	F	3.11		5.32	0.00	2.93	0.00	2.93			25.00	F	3.11		4.25	0.00	2.93	0.00	2.93			
	1	1.40	2.39	1.71	32.00	F	2.39		4.09	0.00	2.25	0.00	2.25			29.00	F	2.39		3.26	0.00	2.25	0.00	2.25			
	20	1.42	2.29	1.61	28.00	F	2.29		3.92	0.00	2.15	0.00	2.15			31.00	F	2.29		3.13	0.00	2.15	0.00	2.15			
1.40 - 1.50	16	1.43	1.57	1.10	27.00	F	1.57		2.68	0.00	1.48	0.00	1.48			29.00	F	1.57		2.14	0.00	1.48	0.00	1.48			
	24	1.44	2.51	1.74	22.00	F	2.51		4.29	0.00	2.36	0.00	2.36	1.44	0.00	25.00	F	2.51		3.43	0.00	2.36	0.00	2.36	16.03	1.44	17.31
	32	1.45	3.35	2.31	25.00	F	3.35		5.73	0.00	3.15	0.00	3.15			20.00	F	3.35		4.58	0.00	3.15	0.00	3.15			
	19	1.46	2.95	2.02	32.00	F	2.95		5.04	0.00	2.78	0.00	2.78			15.00	S		2.95	0.00	8.92	0.00	2.78	2.78			
	30	1.47	1.98	1.35	30.00	F	1.98		3.39	0.00	1.86	0.00	1.86			22.00	F	1.98		2.70	0.00	1.86	0.00	1.86			
	33	1.50	1.23	0.82	32.00	F	1.23		2.10	0.00	1.16	0.00	1.16			25.00	F	1.23		1.68	0.00	1.16	0.00	1.16			
	43	1.51	2.60	1.72	32.00	F	2.60		4.45	0.00	2.45	0.00	2.45			32.00	F	2.60		3.55	0.00	2.45	0.00	2.45			
1.50 - 1.60	44	1.52	1.78	1.17	29.00	F	1.78		3.04	0.00	1.67	0.00	1.67			32.00	F	1.78		2.43	0.00	1.67	0.00	1.67			
	27	1.53	1.71	1.12	32.00	F	1.71		2.92	0.00	1.61	0.00	1.61			29.00	F	1.71		2.34	0.00	1.61	0.00	1.61			
	29	1.54	1.46	0.95	22.00	F	1.46		2.50	0.00	1.37	0.00	1.37	1.53	0.00	27.00	F	1.46		1.99	0.00	1.37	0.00	1.37	11.57	1.53	0.00
	46	1.55	1.64	1.06	21.00	F	1.64		2.80	0.00	1.54	0.00	1.54			29.00	F	1.64		2.24	0.00	1.54	0.00	1.54			
	45	1.57	1.88	1.20	32.00	F	1.88		3.21	0.00	1.77	0.00	1.77			25.00	F	1.88		2.57	0.00	1.77	0.00	1.77			
	25	1.60	2.88	1.80	26.00	F	2.88		4.92	0.00	2.71	0.00	2.71			10.00	S		2.88	0.00	8.71	0.00	2.71	2.71			
	60	1.61	2.92	1.81	31.00	F	2.92		4.99	0.00	2.75	0.00	2.75			18.00	S		2.92	0.00	8.83	0.00	2.75	2.75			
1.60 - 1.70	63	1.62	2.14	1.32	14.00	S		2.14	0.00	4.48	0.00	2.01	2.01			29.00	F	2.14		2.92	0.00	2.01	0.00	2.01			
	72	1.63	2.12	1.30	23.00	F	2.12		3.62	0.00	1.99	0.00	1.99			21.00	F	2.12		2.90	0.00	1.99	0.00	1.99			
	54	1.64	2.82	1.72	21.00	F	2.82		4.82	0.00	2.65	0.00	2.65	1.64	31.57	26.00	F	2.82		3.85	0.00	2.65	0.00	2.65	20.50	1.64	26.62
	57	1.65	4.17	2.53	21.00	F	4.17		7.13	0.00	3.92	0.00	3.92			22.00	F	4.17		5.70	0.00	3.92	0.00	3.92			
	62	1.66	1.63	0.98	18.00	S		1.63	0.00	3.41	0.00	1.53	1.53			23.00	F	1.63		2.23	0.00	1.53	0.00	1.53			
	65	1.68	3.11	1.85	18.00	S		3.11	0.00	6.51	0.00	2.93	2.93			22.00	F	3.11		4.25	0.00	2.93	0.00	2.93			
	66	1.70	1.94	1.14	12.00	S		1.94	0.00	4.06	0.00	1.83	1.83			8.00	S	0.00	1.94	0.00	5.87	0.00	1.83	1.83			
	77	1.71	3.46	2.02	15.00	S		3.46	0.00	7.24	0.00	3.26	3.26			21.00	F	3.46		4.73	0.00	3.26	0.00	3.26			
1.70 - 1.80	79	1.73	2.85	1.65	14.00	S		2.85	0.00	5.96	0.00	2.68	2.68			31.00	F	2.85		3.89	0.00	2.68	0.00	2.68			
	80	1.74	2.32	1.33	12.00	S		2.32	0.00	4.85	0.00	2.18	2.18	1.74	100.00	22.00	F	2.32		3.17	0.00	2.18	0.00	2.18	17.56	1.74	53.75
	73	1.75	2.75	1.57	8.00	S		2.75	0.00	5.75	0.00	2.59	2.59			16.00	S		2.75	0.00	8.32	0.00	2.59	2.59			
	74	1.77	2.69	1.52	16.00	S		2.69	0.00	5.63	0.00	2.53	2.53			6.00	S		2.69	0.00	8.13	0.00	2.53	2.53			
	69	1.79	2.65	1.48	0.00	S		2.65	0.00	5.54	0.00	2.49	2.49			0.00	S		2.65	0.00	8.01	0.00	2.49	2.49			
	71	1.80	2.41	1.34	13.00	S		2.41	0.00	5.04	0.00	2.27	2.27			9.00	S		2.41	0.00	7.29	0.00	2.27	2.27			
	76	1.83	3.39	1.85	18.00	S		3.39	0.00	7.09	0.00	3.19	3.19			20.00	F	3.39		4.63	0.00	3.19	0.00	3.19			
1.80 - 2.00	67	1.86	2.60	1.40	14.00	S		2.60	0.00	5.44	0.00	2.45	2.45			8.00	S		2.60	0.00	7.86	0.00	2.45	2.45			
	81	1.91	3.88	2.03	7.00	S		3.88	0.00	8.12	0.00	3.65	3.65			6.00	S		3.88	0.00	11.73	0.00	3.65	3.65			
	68	1.93	1.29	0.67	9.00	S		1.29	0.00	2.70	0.00	1.21	1.21			22.00	F	1.29		1.76	0.00	1.21	0.00	1.21			
	82	1.95	3.65	1.87	0.00	S		3.65	0.00	7.64	0.00	3.43	3.43	1.88	100.00	0.00	S		3.65	0.00	11.04	0.00	3.43	3.43	16.20	1.88	72.82
+2.00	83	2.11	1.75	0.83	5.00	S		1.75	0.00	3.66	0.00	1.65	1.65	2.11	100.00	0.00	S		1.75	0.00	5.29	0.00	1.65	1.65	1.65	2.11	100.00
			106.29				58.49	47.80	100.00	100.00	55.03	44.97	100.00					73.22	33.07	100.00	100.00	68.89	31.11	100.00			

Appendix E

Appendix E contains all the partition curves for the (+22 -31.5mm), (+16 -22mm Blk), (+16 – 22mm SR), (+16 – 22mm FB) and (+9.5 – 16mm) particles that was obtained after 15s, 30s, 60s and 600s of separation respectively.

<u>Appendix E - 1: Dynamic and steady state partition curves for (+22 – 31.5mm) particles</u>

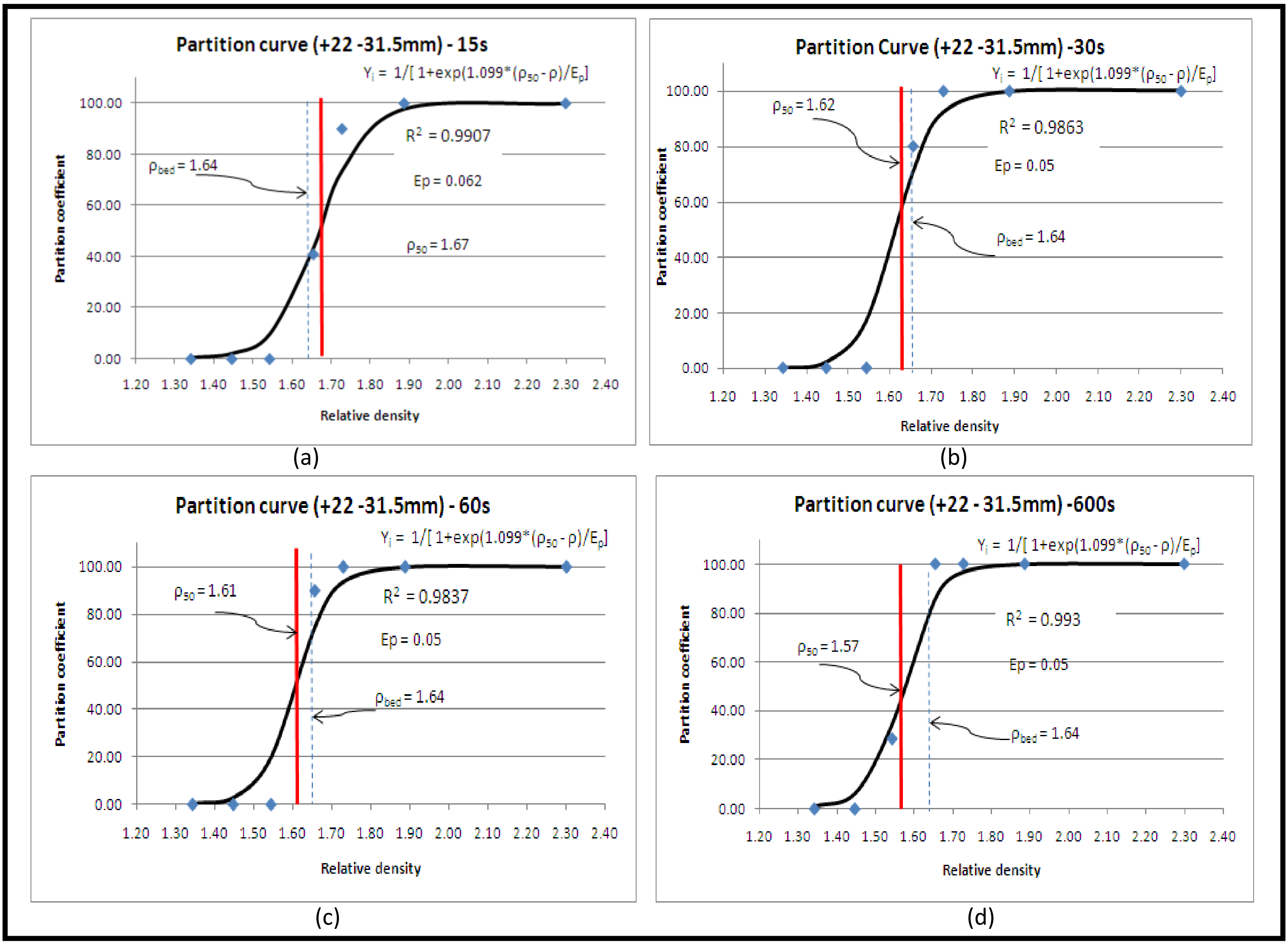

Appendix E - 2: Dynamic and steady state partition curves for (+16 – 22mm Blockish) particles

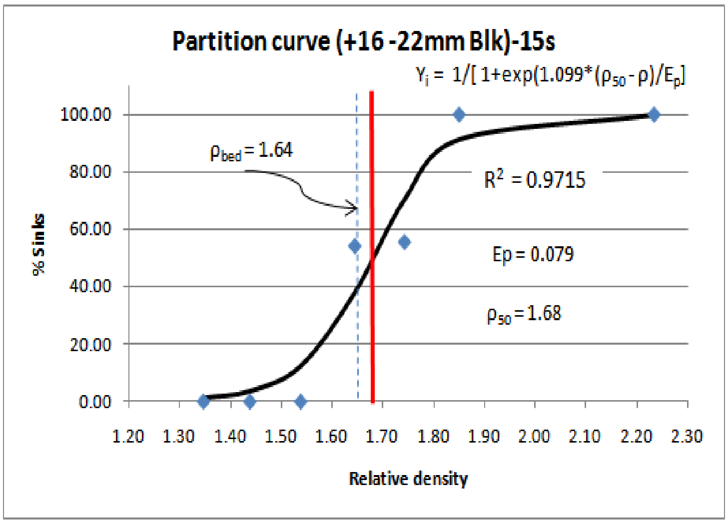

(a)

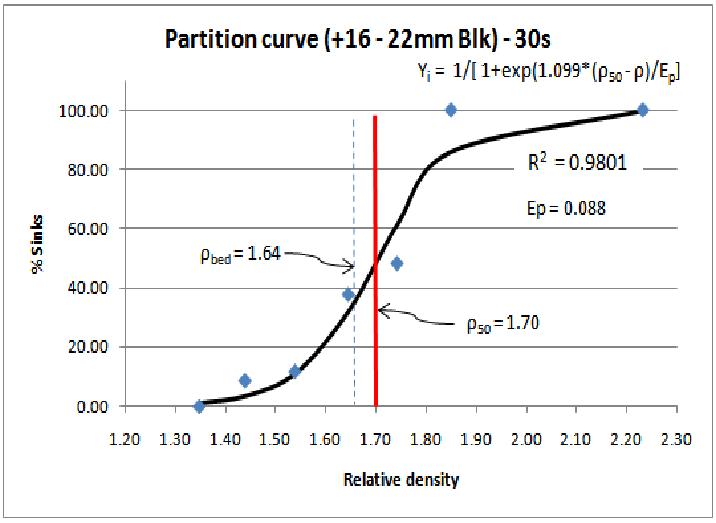

(b)

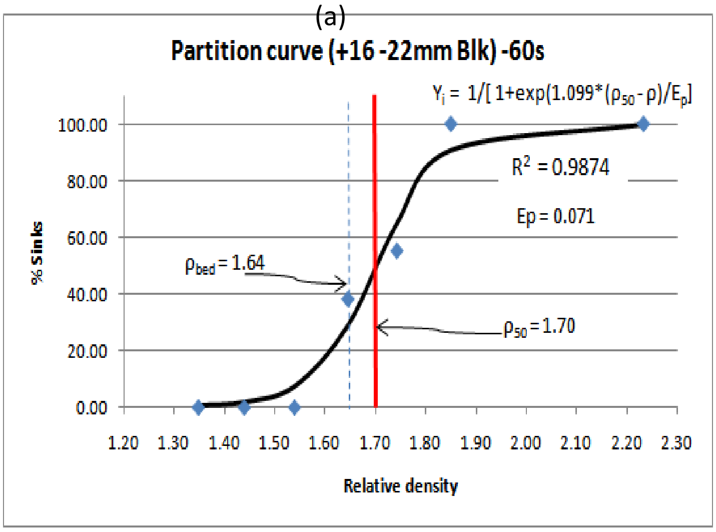

(c)

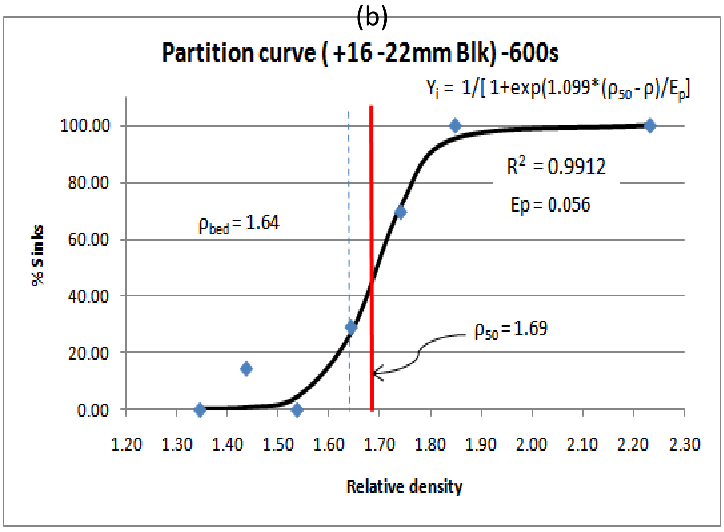

(d)

Appendix E - 3: Dynamic and steady state partition curves for (+16 – 22mm SR) particles

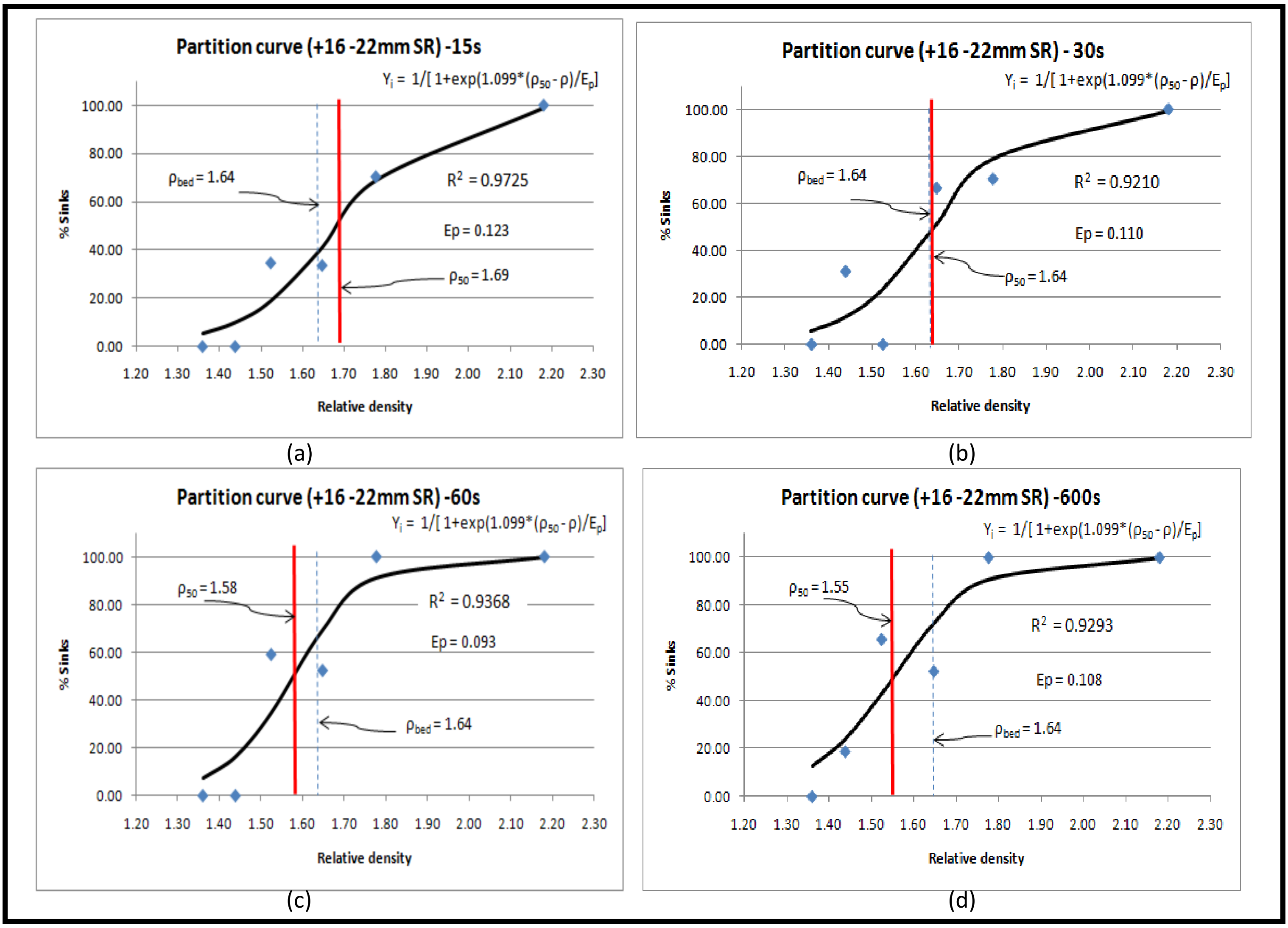

Appendix E - 4: Dynamic and steady state partition curves for (+16 – 22mm FB) particles

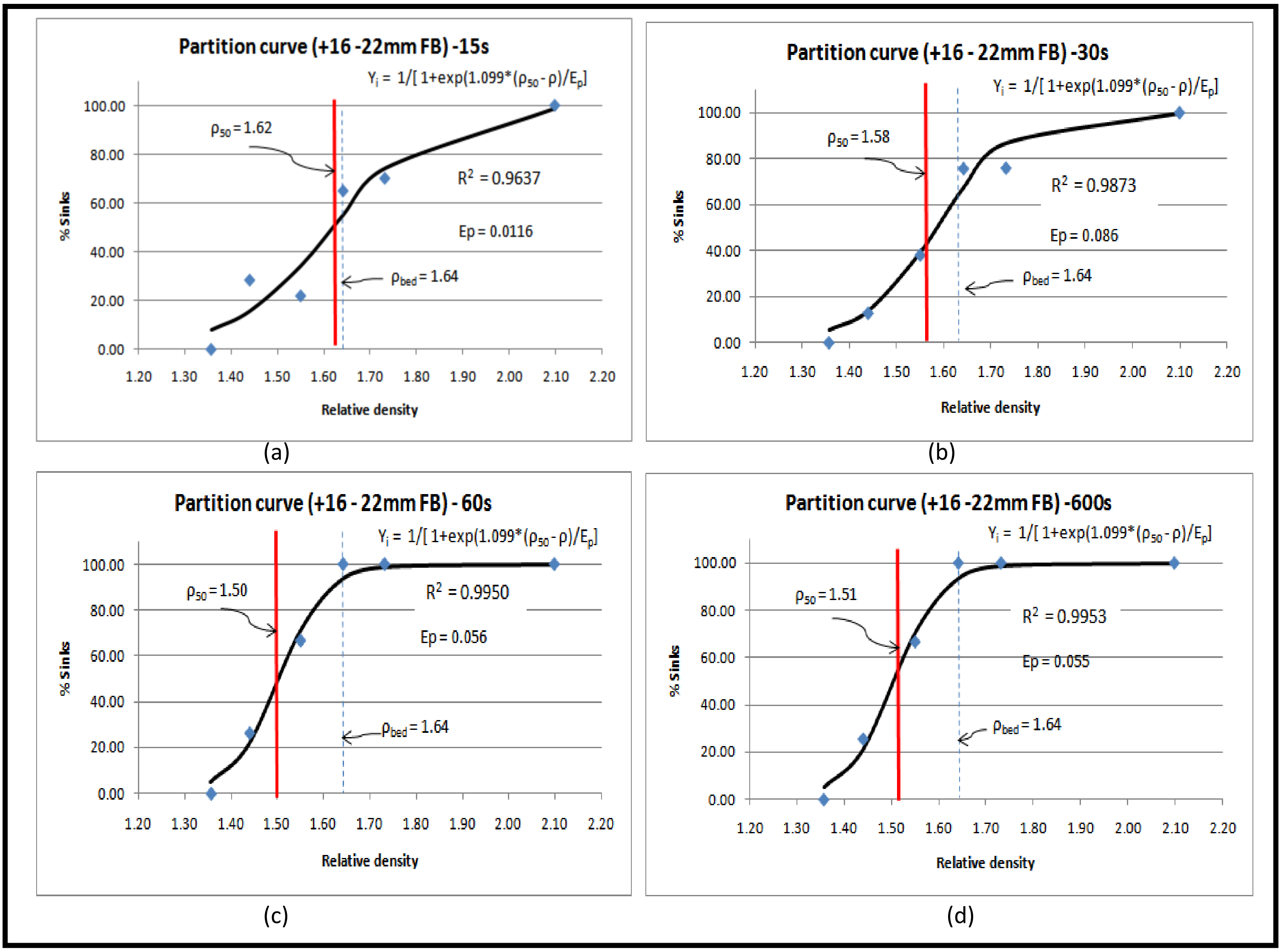

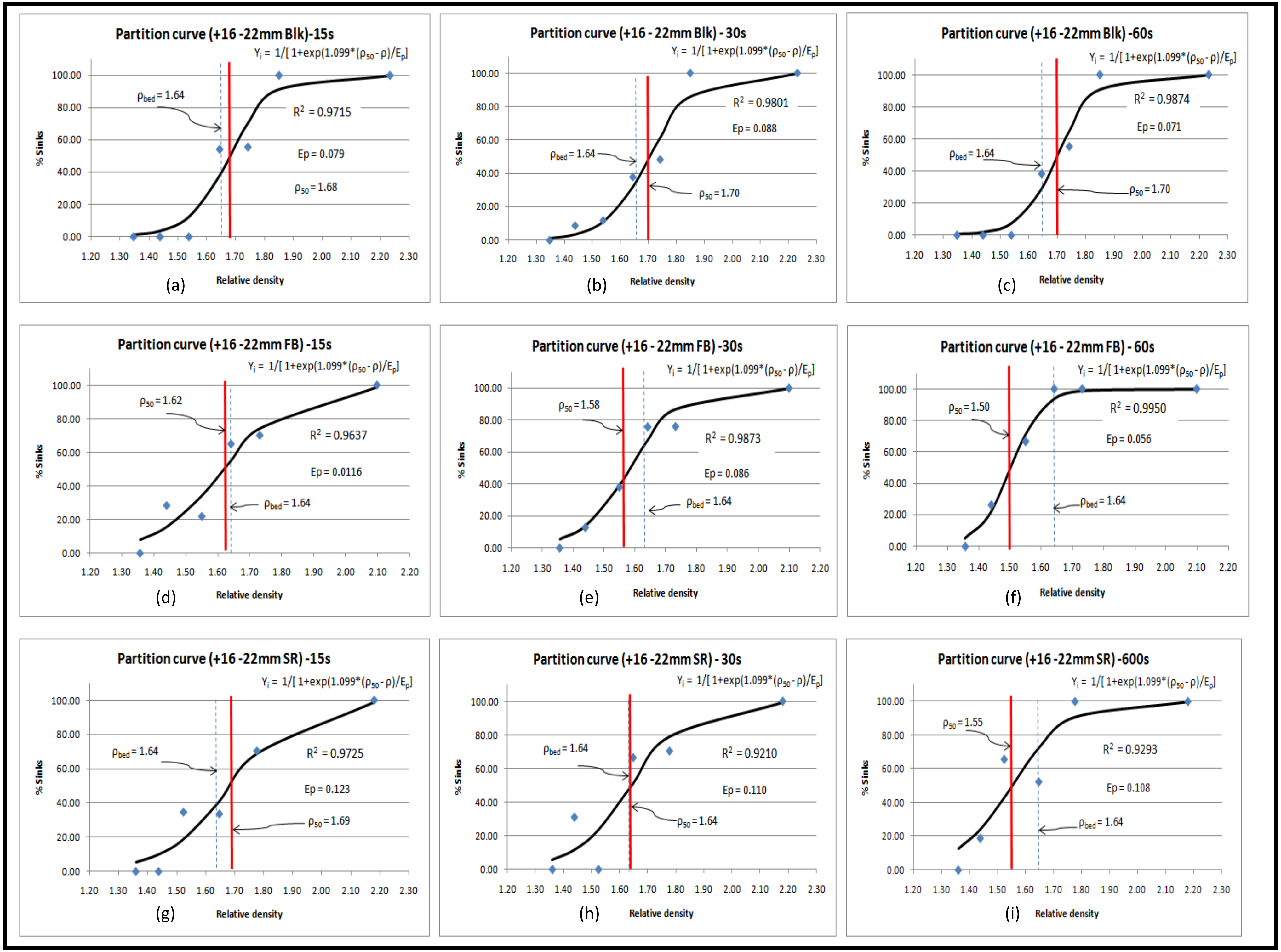
Partition curve (+16 -22mm Blk)-15s
Yi = 1/[1+exp(1.099*(ρ50 - ρ)/Ep]
ρbed = 1.64
R2 = 0.9715
Ep = 0.079
ρ50 = 1.68
% Sinks
Relative density
(a)
Partition curve (+16 - 22mm Blk) - 30s
Yi = 1/[1+exp(1.099*(ρ50 - ρ)/Ep]
R2 = 0.9801
Ep = 0.088
ρbed = 1.64
ρ50 = 1.70
% Sinks
Relative density
(b)
Partition curve (+16 -22mm Blk) -60s
Yi = 1/[1+exp(1.099*(ρ50 - ρ)/Ep]
R2 = 0.9874
Ep = 0.071
ρbed = 1.64
ρ50 = 1.70
% Sinks
Relative density
(c)
Partition curve (+16 -22mm FB) -15s
Yi = 1/[1+exp(1.099*(ρ50 - ρ)/Ep]
ρ50 = 1.62
R2 = 0.9637
Ep = 0.0116
ρbed = 1.64
% Sinks
Relative density
(d)
Partition curve (+16 - 22mm FB) -30s
Yi = 1/[1+exp(1.099*(ρ50 - ρ)/Ep]
ρ50 = 1.58
R2 = 0.9873
Ep = 0.086
ρbed = 1.64
% Sinks
Relative density
(e)
Partition curve (+16 - 22mm FB) - 60s
Yi = 1/[1+exp(1.099*(ρ50 - ρ)/Ep]
ρ50 = 1.50
R2 = 0.9950
Ep = 0.056
ρbed = 1.64
% Sinks
Relative density
(f)
Partition curve (+16 -22mm SR) -15s
Yi = 1/[1+exp(1.099*(ρ50 - ρ)/Ep]
ρbed = 1.64
R2 = 0.9725
Ep = 0.123
ρ50 = 1.69
% Sinks
Relative density
(g)
Partition curve (+16 -22mm SR) - 30s
Yi = 1/[1+exp(1.099*(ρ50 - ρ)/Ep]
ρbed = 1.64
R2 = 0.9210
Ep = 0.110
ρ50 = 1.64
% Sinks
Relative density
(h)
Partition curve (+16 -22mm SR) -600s
Yi = 1/[1+exp(1.099*(ρ50 - ρ)/Ep]
ρ50 = 1.55
R2 = 0.9293
Ep = 0.108
ρbed = 1.64
% Sinks
Relative density
(i)

Appendix E - 6: Dynamic and steady state partition curves for (+9.5 – 16mm) particles

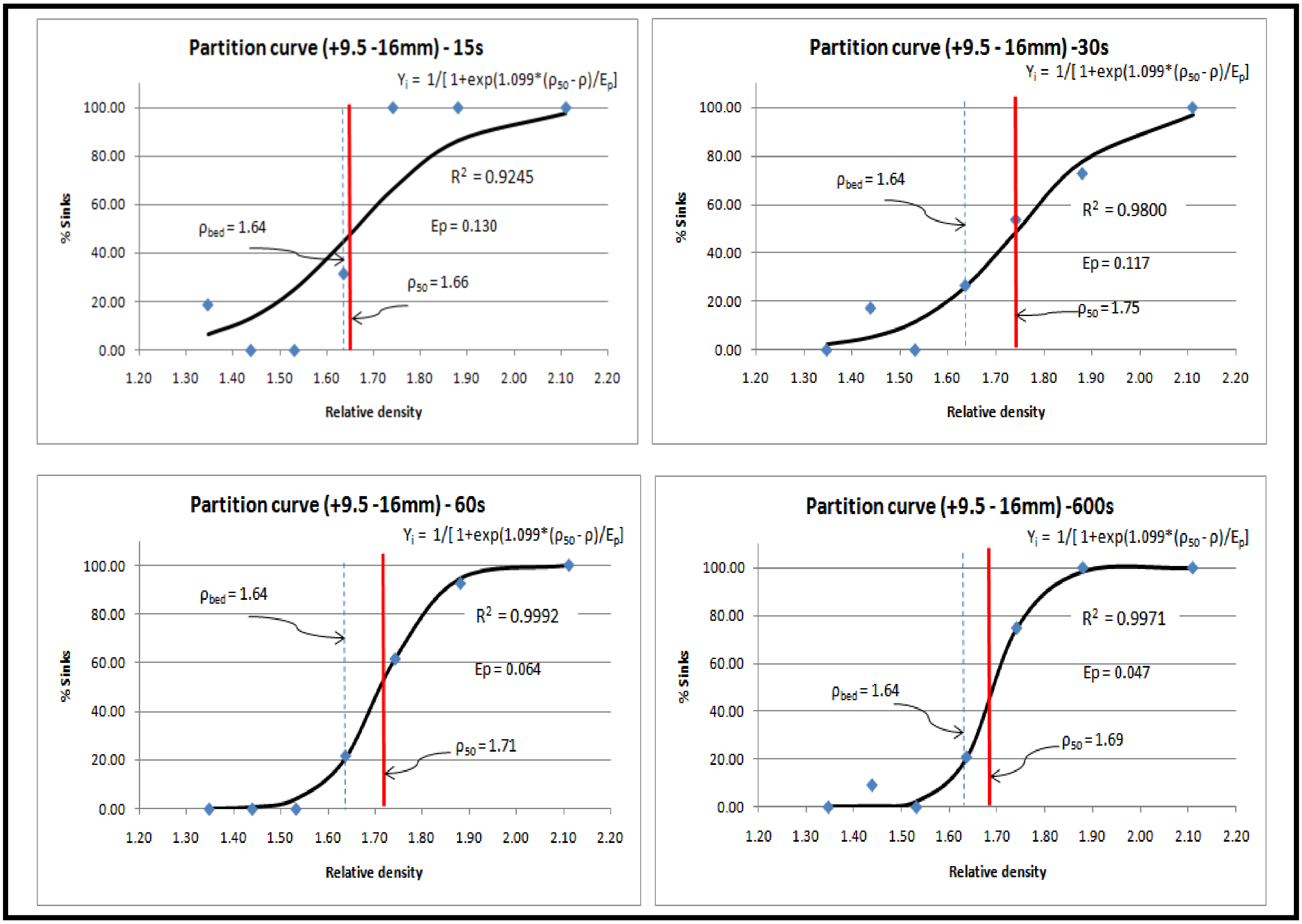

Appendix E - 7: Ep and ρ50 values table for the different particle size ranges and shapes

Time (s)	Particle Size Range											
	+37 - 53mm		+22 -31.5mm		+16 - 22mm Blk		+16 - 22mm SR		+16 - 22mm FB		+9.5 - 16mm	
	Ep	ρ_{50}	Ep	ρ_{50}	Ep	ρ_{50}	Ep	ρ_{50}	Ep	ρ_{50}	Ep	ρ_{50}
15	0.043	1.64	0.062	1.67	0.079	1.68	0.123	1.69	0.116	1.62	0.130	1.66
30	0.050	1.59	0.050	1.62	0.088	1.70	0.110	1.64	0.086	1.58	0.117	1.75
60	0.049	1.60	0.050	1.61	0.071	1.70	0.093	1.58	0.056	1.50	0.064	1.71
600	0.047	1.60	0.050	1.57	0.056	1.69	0.108	1.55	0.055	1.51	0.047	1.69

Appendix F

Appendix F contains the empirical model validation data for the different particle size ranges, shapes and densities.

Appendix F - 1: Empirical model validation data for the (+37 -53mm), (+22 -31.5mm) and (+16 -22mm Blk) particles

						Position of the particle in the bed (bed level -cm)		
Particle Size range	Average Particle diameter (cm)	Empirical viscosity constants (g cm^{-1} s^{-1})	Fluidized bed height cm	Bed density (g cm^{-3})	Specific density of the particle	Experimental cm	Calculated cm	% Error
					1.30	32.0	32.0	0.00
					1.36	32.0	32.0	0.00
					1.40	32.0	32.0	0.00
					1.44	30.0	29.2	2.62
					1.50	22.0	20.4	7.05
+37 -53mm	4.5	2040	32	1.64	1.60	7.0	5.8	16.53
					1.66	-5.0	-2.9	41.57
					1.70	-11.0	-8.8	20.33
					1.74	-14.0	-14.6	4.33
					1.80	-25.0	-23.4	6.52
					1.90	-32.0	-32.0	0.00
					1.95	-32.0	-32.0	0.00
					1.31	32.0	32.0	0.00
					1.35	32.0	32.0	0.00
					1.44	26.0	23.8	8.31
					1.55	15.0	10.7	28.49
+22 -31.5mm	2.7	900	32	1.64	1.70	-10.0	-7.2	28.49
					1.75	-11.0	-13.1	19.19
					1.81	-18.0	-20.3	12.57
					1.86	-28.0	-26.2	6.35
					1.92	-32.0	-32.0	0.00
					2.09	-32.0	-32.0	0.00
					1.30	31.0	30.1	2.90
					1.35	25.0	25.7	2.70
					1.41	23.0	20.4	11.46
					1.48	17.0	14.2	16.67
					1.55	11.0	8.0	27.56
+16 -22mm Blk	1.9	600	32	1.64	1.62	4.0	1.8	55.73
					1.66	-4.0	-1.8	55.73
					1.70	-7.0	-5.3	24.11
					1.75	-9.0	-9.7	8.21
					1.82	-16.0	-15.9	0.40
					1.90	-21.0	-23.0	9.62
					2.20	-32.0	-32.0	0.00

Appendix F - 2: Empirical model validation data for the (+16 -22mm SR), (+16 -22mm FB) and (+9.5 -16mm) particles

Particle Size range	Average Particle diameter (cm)	Empirical viscosity constants ($g\ cm^{-1}\ s^{-1}$)	Fluidized bed height cm	Bed density ($g\ cm^{-3}$)	Specific density of the particle	Position of the particle in the bed (bed level -cm) Experimental cm	Calculated cm	% Error
					1.30	32.0	32.0	0.00
					1.35	31.0	30.5	1.60
					1.41	27.0	24.2	10.39
					1.50	17.0	14.7	13.37
					1.55	11.0	9.5	13.94
+16 -22mm SR	1.9	505	32	1.64	1.69	-8.0	-5.3	34.26
					1.76	-10.0	-12.6	26.23
					1.79	-18.0	-15.8	12.34
					1.99	-32.0	-32.0	0.00
					1.99	-32.0	-32.0	0.00
					2.06	-32.0	-32.0	0.00
					2.17	-32.0	-32.0	0.00
					1.31	25.0	25.8	3.12
					1.36	20.0	21.9	9.37
					1.42	14.0	17.2	22.76
					1.51	15.0	10.2	32.30
+16 -22mm FB	1.9	680	32	1.64	1.56	11.0	6.2	43.19
					1.70	-6.0	-4.7	21.88
					1.76	-8.0	-9.4	17.18
					1.86	-16.0	-17.2	7.41
					1.97	-25.0	-25.8	3.12
					2.06	-32.0	-32.0	0.00
					2.19	-32.0	-32.0	0.00
					1.31	27.0	29.3	8.55
					1.35	27.0	25.8	4.61
					1.40	23.0	21.3	7.32
					1.44	20.0	17.8	11.18
+9.5 -16mm	1.3	280	32	1.64	1.56	14.0	7.1	49.25
					1.62	4.0	1.8	55.59
					1.66	-5.0	-1.8	64.47
					1.70	-8.0	-5.3	33.39
					1.75	-8.0	-9.8	22.12
					1.80	-13.0	-14.2	9.31
					1.86	-21.0	-19.5	6.96
					1.95	-29.0	-27.5	5.06
					2.19	-32.0	-32.0	0.00